Cranfield University

Colin Clarke

Development of an automated identification system for nanocrystal encoded microspheres in flow cytometry.

Cranfield Health

PhD Thesis

August 2008

Cranfield University

Cranfield Health

Analytical Science and Informatics

Doctor of Philosophy

August 2008

Colin Clarke

Development of an automated identification system for nanocrystal encoded microspheres in flow cytometry.

Supervisor: Dr C.Bessant

August 2008

This thesis is submitted in partial fulfilment of the requirements of the Degree of PhD.

Quantum dot encoded microspheres (QDEMs) offer much potential for bead based identification of a variety of biomolecules via flow cytometry (FCM). To date, QDEM subpopulation classification from FCM has required significant instrument modification or multiparameter gating. It is unclear whether or not current data analysis approaches can handle the increased multiplexed capacity offered by these novel encoding schemes. In this thesis the drawbacks of currently available data analysis techniques are demonstrated and novel classification methods proposed to overcome these limitations. A commercially available 20 code QDEM library with fluorescent emissions at 4 distinct wavelengths and 4 different intensity levels was analysed using flow cytometry. Multiparameter gating (MPG) a readily available classification method for subpopulations in FCM was evaluated. A support vector machine (SVM) and two types of artificial neural networks (ANNs), a multilayer perceptron (MLP) and probabilistic radial basis function (PRBF) were also considered. For the supervised models rigorous parameter selection using cross validation (CV) was used to construct the optimum models. Independent test set validation was also carried out. As a further test, external validation of the classifiers was performed using multiplexed QDEMs solutions.

The performance of MPG was poor (average misclassification (MC) rate = 9.7%) was a time consuming process requiring fine adjustment of the gates, classifications made on the dataset were poor with multiple classifications on single events and as the multiplex capacity increases the performance is likely to decrease. The SVM had the best performance in independent test validation with 96.33% accuracy on the independent testing (MLP = 96.12%, PRBF = 94.38%). Furthermore the performance of the SVM was superior to both MPG and both ANNs for the external validation set with an average MC rate for MLP = 6.1% and PRBF = 7.5% whereas the SVM MC rate was 2.9%. Assuming that the external test solutions were homogenous the variance between classified results should be minimal hence, the variance of correct classifications (CCs) was used as an additional indicator of classifier performance. The SVM demonstrates the lowest variance for each of the external validation solutions (average $\sigma^2 = 31479$) some 50% lower than that of MPG. As a conclusion to the development of the classifier, a user friendly software system has been developed to allow construction and evaluation of multiclass SVMs for use by FCM practitioners in the laboratory. SVMs are a promising classifier for QDEMs that can be rapidly trained and classifications made in real time using standard FCM instrumentation. It is hoped that this work will advance SAT for bioanalytical applications.

I would like to thank Conrad Bessant for his guidance and invaluable assistance throughput the project.

I would also like to express my gratitude to my colleagues, Clair Gallagher and Sarah Thiolett for their tireless endeavours in the laboratory.

Thanks to Mike Malecha and Selly Saini for their work in the early stages of this work.

Thanks to the members of the Cranfield Bioinformatics Group and Cranfield Health who have assisted me during course of this project.

This work is dedicated to my parents Joe and Breda, and my brothers, Alan, Eoin and David.

ANN	artificial neural network
ASO	allele specific oligonucleotide
ASPE	allele specific primer extension
CCD	charged couple detector
cDNA	complementary DNA
CC rate	correct classification rate
CoeffV	coefficient of variation
CV	cross validation
$\mathbf{cv_{acc}}$	CV accuracy
DNA	deoxyribonucleic acid
ECOC	error output coding
FCM	flow cytometry
FCS	flow cytometry standard
FITC	fluoroscein isothiocyanate
FN	false negative
FP	false positive
FSC	forward scatter
FWHM	full width half maximum
HIV	human immunodeficiency virus
HLN	hidden layer node
HT	heat transfer
IQR	interquartile range
LDA	linear discriminant analysis
LSC	laser scanning cytometry
LVQ	learning vector quantisation
MC rate	misclassification rate
MLP	multilayer perceptron
MPG	multiparameter gating
MS	mass spectrometry
ODE	octadecene
OLA	oligonucleotide assay
OVO	one versus one
OVR	one versus rest
PCA	principal component analysis
PCR	polymerase chain reaction
PLSDA	partial least squares discriminant analysis
PMT	photomultiplier tube
PRBF	probabilistic RBF
QD	quantum dot
QDC	quantum dot corporation
QDEM	quantum dot encoded microsphere
R	sensitivity
RBF	radial basis function
RF	radio frequency
RFID	radio frequency identification tags
RMP	Recurrent multilayer perceptron
RNA	ribonucleic acid
S	specificity
SAT	suspension array technology
SEM	scanning electron microscope
SERRS	surface enhanced Raman spectra
SMO	sequential minimal optimization
SNP	single nucleotide polymorphism
SSC	side scatter
SV	support vector
SVM	support vector machine
$\mathbf{test_{acc}}$	test set accuracy
TN	true negative
TOPO	trioctylphosphine oxide
TP	true positive
$\mathbf{train_{acc}}$	train set accuracy
TSC	the SNP consortium
YAG	yttrium aluminium garnet
$\boldsymbol{\sigma^2}$	variance

Chapter 1: Thesis introduction and overview

1.1 Introduction

The completion of the human genome sequence in 2001 has heralded a new era in the biosciences [1, 2]. In the "post genomic age" a molecular systems biology approach investigates basic dynamics, feedback control loops and signal processing mechanisms underlying cell function through the analysis of genes, proteins and a myriad of other molecules. The knowledge gained through these experiments is expected to impact many areas of biological science from basic research to medical applications. The availability of cost effective, high throughput analytical platforms for the detection of large numbers of diverse biochemical constituents present in a cell is the rate limiting step in large scale population studies where large numbers of samples are required [3]. Continual development of laboratory instrumentation and production of rapid and economically viable "point of care" platforms for genomics and proteomics is essential for the application of such knowledge in research and the clinic [4].

Suspension array technology (SAT) has emerged as a potential successor to the microarray as a multiplexed analysis platform for applications including single nucleotide polymorphism (SNP) genotyping, gene expression analysis and protein assays. For the analysis of deoxyribonucleic acid (DNA) and ribonucleic acid (RNA) encoded microspheres are conjugated to an oligonucleotide, followed by hybridisation to amplified nucleotide. By assigning each microsphere a unique identifying signature hundreds or thousands of analytes can be measured simultaneously and the identity of the target can be determined by "decoding" the micropshere. The level of multiplexing for a

single sample depends on the coding scheme employed. Identification of the microspheres and detection of hybridisation via a reporter can be measured at rapid rates using a flow cytometer (Figure 1).

In comparison to microarrays, suspension array technology is relatively inexpensive, statistically superior, with improved hybridisation kinetics and increased flexibility in array specification [5, 6]. The limitations of sample number for SNP genotyping analysis seen with microarrays are therefore negated. Commercial suspension technology platforms such as the Luminex system utilise a dual organic dye microsphere encoding scheme offering 100 spectrally distinct microspheres. Various applications including SNP genotyping, gene expression and protein analysis have previously been reported using this system [7]. However Tsuchihashi suggested that the throughput of the Luminex system is limited in terms of multiplex capacity, and the possibility of increasing the multiplex beyond current levels is limited [8].

Fluorescent nanocyrstals or quantum dots (QDs) when used in optical (fluorescent) encoding increase the encoding capacity and promise to extend suspension array technology to the levels of multiplexing possible with high density microarrays. The inherent advantages of QDs (chapter 2) allow flow cytometers currently available in a wide range of locations including hospitals and universities to be used for detection.

It has been suggested that up to 40,000 QD encoded microspheres are practical [9], the identification of such numbers of multicolour microsphere subpopulations from flow

cytometry data using current methods may not be straightforward. While polychromatic flow (8 or more colours) cytometry is advancing rapidly concerns exist that using standard software tools for data analysis lags behind assay chemistry and instrumentation [10]. Attempts at QDEM classification have previously been made using a modified flow cytometer [11], however the utilisation of existing FCM instrumentation currently found in laboratories is advantageous.

The motivation behind this work is the development of novel data analysis techniques and dedicated software for nanocyrstal encoded microsphere identification in flow cytometry improving on current methods. It is hoped that the methods developed during the course of this work will contribute to the development of suspension array technology as a high throughput analysis platform for genomics and proteomics by providing robust data analysis routines for such experiments. The following page gives a general overview of each chapter contained in this thesis.

1.2 Thesis overview

Chapter 2 provides a detailed description of SAT including fluorescent encoding strategies, micropshere manufacture, detection platforms and applications in genomics and proteomics.

Chapter 3 outlines the fundamentals of flow cytometry instrumentation and acquisition of the data used throughout the thesis. The limitations of current microsphere identification methods are exposed and the case for more sophisticated multivariate classification algorithms presented.

Chapter 4 describes the development and implementation of a supervised learning method, support vector machines. The design and evaluation of the system is discussed and compared to the methods used in chapter 3.

Chapter 5 An alternative learning algorithm was also applied to the dataset for comparison to the support vector machine. Two artificial neural network designs are implemented for comparison to the SVM and the optimum classifier determined.

Chapter 6 discusses the optimum data analysis method and a software program for QDEM classification utilising the optimum final classifier is presented. Finally the implications of this research and future recommendations are also discussed.

Chapter 2: Suspension array technology

2.1 Overview

In this chapter suspension array technology is introduced and the potential of the technique highlighted (section 2.2). Microsphere encoding schemes (section 2.3), manufacture (section 2.4) and detection platforms (section 2.5) are subsequently described. Recent examples of SAT applications in the literature are also discussed (section 2.6), finally the aims and objectives of this research are presented (section 2.7).

2.2 Introduction to suspension array technology

Perhaps the technique that has had the most profound effect on modern molecular biology is the planar microarray allowing the interrogation of tens of thousands of genes, even whole human genome analysis in a single assay. From their beginnings as an electropheretic technique with dozens of targets, microarrays have progressed rapidly through the development of more sophisticated manufacturing techniques, parallel processing and simpler detection methods to the high density microarrays in use today. Complementary DNA (cDNA) microarrays were first applied to quantitative gene expression analysis of two cell states [12] and applications have expanded to include SNP genotyping, protein binding, DNA mapping, protein DNA interaction and epigenetic studies [13].

In nucleic acid analysis, each spot on the microarray (a slide composed of a non-porous substrate such as glass or silicon) contains a target specific capture molecule, e.g. oligonucleotide probe. Hybridisation with fluorescently labelled target moieties is carried

out in chambers allowing control of the assay conditions to optimise complementary sequence binding and minimise non specific interactions. Once the reaction is complete non-specific targets are removed by washing and the fluorescence signal of each spot quantified using a confocal scanner or charged couple detector (CCD) camera [14, 15]. For example, in gene expression studies RNA is extracted from cells, reversed transcribed to cDNA, labelled with two organic dyes and attached to the surface of the microarray. The fluorescent readings from the array are measured and the ratios of the two dyes indicate differential transcript production [13].

Suspension array technology has recently emerged as a viable alternative to the 2D array for a range of applications in genomics, proteomics and drug discovery. In a SAT assay microparticles or microspheres act as solid supports for target specific receptor molecules, analogous to a spot on a microarray. Through precise control of characteristics such as size, shape, and fluorescence each microsphere batch is assigned a unique signal analogous to a barcode for the receptor molecule (section 2.3). In comparison to microarrays where the identification of each target is achieved through spot position on the planar surface (positional encoding), SAT identification is achieved through the measurement of identifying signals of the microsphere supports in solution. The first encoded microsphere based "liquid arrays" were described in the 1970s through the work of Fulwyler and Horan *et al.* [16, 17]. The multiplexing capacity of early microsphere assays was restricted as microspheres were differentiated by particle size (scatter measurements) and therefore applications were limited.

Optically encoded microspheres developed by the Luminex Corporation called the FlowMetrix system [18] increased multiplexing capacity to acceptable levels for bioanalytical applications providing the catalyst for renewed focus on SAT and detection instrumentation (section 2.5). The combination of uniquely encoded microspheres in a single experiment allows a 3D array to be formed free from the constraints of the planar surface leading to significant advantages over microarrays in terms of manufacture, application and detection [19].

In microarray manufacture the number of arrays produced at any one time is limited, microspheres however can be prepared individually at concentrations of up to 10^7 particles/ml from which thousands of individual arrays can be prepared [6]. Each assay is therefore flexible in that modifications to the array can be made simply by adding or removing microspheres. Customisation of SAT experiments is inexpensive as the only additional cost is the capture molecules.

The total sample volume required is also decreased for SAT assays. Fuja *et al.* reported for gene expression analysis only 2μg of RNA was required without amplification of reverse transcribed cDNA, sample volumes for planar based experiments are typically >10 μg [20]. Xu *et al.* also reported a reduction in sample volume required for bead based SNP genotyping, here 1ng of genomic DNA was sufficient for polymerase chain reaction (PCR), substantially less than other multiplexed assays [9].

SAT reaction speed is greater than that of microarrays as reactions are carried out in solution. SAT solution phase kinetics are an order of magnitude greater than that of mass-transport limited kinetics of probes attached to a planar surface. Diffusion of molecules to the surface limit planar arrays, SAT reaction rates have been shown to be greater than that of planar arrays, barring steric hindrance in probe-target hybridisation, with the efficiency approaching that of unbound complimentary oligonucleotides [6]. Furthermore Eastman *et al.* reported that hybridisation for SAT can be completed in 1-2 hours, at least an order of magnitude faster than for microarrays [21].

Table 1 Basic comparison of microarray (150µm diameter spots) to microspheres (2µm diameter). Adapted from [22]. The number of individual microspheres in a SAT assay allows the measurement of a number of replicates for each probe increasing statistical confidence in results over those of microarrays.

	Element surface Area (μm^2)	**Total array Elements**	**Total target area (cm^2)**
Microarray	17691	15000	2.7
Microspheres	12.6	877,000,000	111

While there can be no doubt that microarrays have enabled the rapid acceleration of data collection and interpretation, questions have arisen regarding the quality of these results [23]. Yu *et al.* noted that the number of false positive results, even in microarrays prepared in-situ is often high [24]. With the rapid analysis rate of SAT, 50 to 100 replicates per target per well could be possible providing greater statistical confidence in results (Table 1). Also each microsphere can be analysed individually improving quality control, negating the chip to chip variations associated with microarrays, and increasing the signal to noise ratio [22].

Detection of microspheres using FCM enables even greater gains in throughput in comparison to microarrays. Developments in FCM signal processing, sample handling and delivery have the potential to allow analysis rates of 100,000 particles sec^{-1} [6]. FCM can distinguish between free probes and those bound to particles, thus washing steps can be reduced or discarded completely [23].

Recent applications highlighting the potential of SAT are detailed at the end of this chapter (section 2.6) allowing the reader to become familiar with encoding strategies, bead synthesis (section 2.3 and 2.4) and related instrumentation (section 2.5). A basic overview of general steps of a SAT assay is shown below (Figure 1).

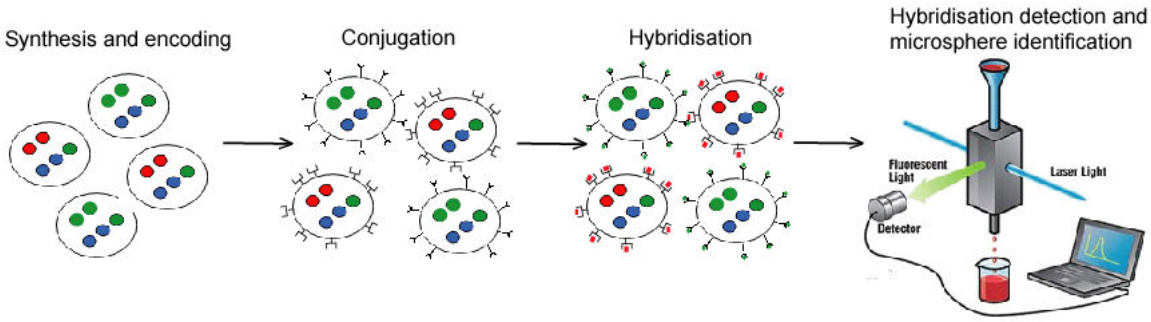

Figure 1 Stages of a typical SAT assay. Firstly, a suitable coding scheme is chosen for the experiment and a number of sets of distinct microspheres are produced. Capture molecules are attached to each microsphere set (e.g. oligonucleotide). The next stage involves the hybridisation of the respective target molecules to the specific microspheres (e.g. PCR amplicons). The presence of the target molecule is confirmed via a hybridization signal, the identity of the micropshere (and therefore target molecule) elucidated using a detection platform (e.g. FCM).

2.3 Encoding schemes

There have been examples of various types of encoding schemes proposed for SAT but by far the most popular is optical encoding. The likely reason for the success of fluorescent encoded microspheres is the suitability for detection with flow cytometry allowing high throughput detection (section 2.5.5 and chapter 3). Optical encoding theory (section 2.3.1) and novel methods for encoding using nanocyrstal flourophores (section 2.3.2) are described. Non optical encoding schemes have also been proposed and are outlined below (section 2.2.3).

2.3.1 Optical encoding

As stated above, the most popular encoding scheme described in the literature is optical encoding via florescent dyes or nanocyrstals. Optically encoded SAT is achieved through controlled internal combinatorial doping with various chromophores at discrete concentrations (hence varying the intensity) for each microsphere and assigning a unique spectral barcode. Decoding of the micropshere signal allows each microsphere target molecule to be identified (Figure 2). Depending on the number of individual emission wavelengths and intensity levels used the multiplex capacity of a particular encoding approach can be calculated as follows:

$$C = N^{m-1} \quad \textbf{(2.1)}$$

Where:
C = number of codes
N = number of intensity levels
m = the number of emission wavelengths

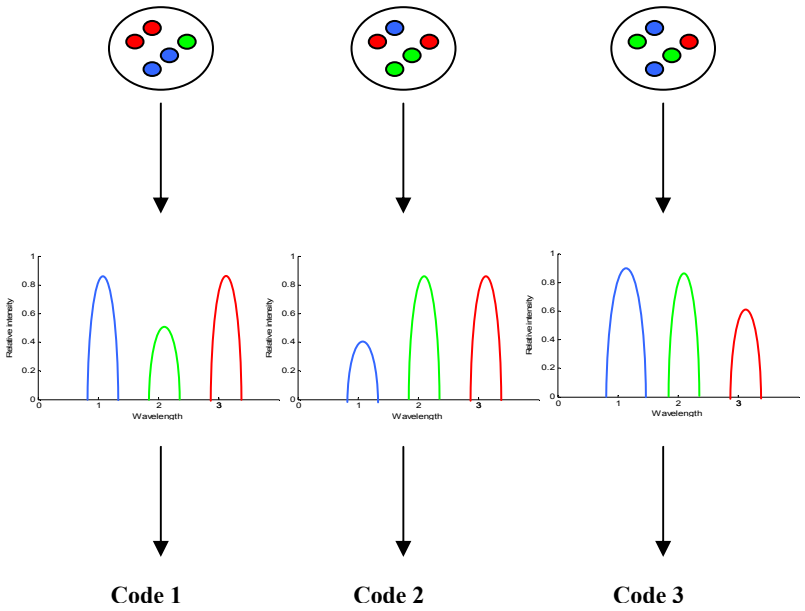

Figure 2 Optical encoding of microspheres. Various emission wavelength flourophores are polymerised within a solid support (microsphere), producing an individual spectral code for each microsphere set. The presence/absence of a target molecule can be determined by decoding each microsphere signal. The multiplex capacity of an encoded library is defined by (Eqn 2.1).

Encoding of microspheres with one or more organic dyes is the most popular form of optical encoding described in the literature. Early applications relied on "homemade" bead sets, however a range of multiplex sets are now commercially available. The Luminex platform represents the most well known example, combining dual organic dyes (emitting at 658nm and 712nm to minimise overlap between commonly used reporters) for its xMAP bead sets along with a dedicated detection system (section 2.5.3). Microspheres of 5.6 µm diameter are encoded over a range of 10 intensities producing up to 100 individual microsphere sets [25].

Beckton Dickenson (BD) Biosciences also produce 7.5 µm diameter beads doped with a single dye (emission @650nm) at various concentrations called the BD Cytometric Array system designed specifically for the FACScan and FACSCalibur flow cytometers (but

also compatible with any cytometer with a 488nm laser) [26, 27]. Several other companies manufacture a range of encoded microspheres including Spherotech, Duke Scientific and Bang's Laboratories. Organic dye based beads have been successful in a range of applications including human immunodeficiency virus (HIV) analysis, thyroid hormone analysis [28] and infectious disease monitoring (section 2.7)[29].

While organic dye based methods have proved useful in a range of applications, the level of multiplexing has not reached the capacity required for post genomic technologies. The narrow excitation wavelengths of organic dyes increase the complexity of instrumentation; as more colours are added to the encoding scheme, additional excitation sources are required prohibiting expansion [8].

2.3.2 Nanocyrstal encoding

Nanotechnology is concerned with the chemical and physical properties of materials with dimensions in the order of magnitude of one billionth of a metre. Nanoscience applies a new philosophy to manufacturing techniques implementing a bottom up approach, starting with a single atom and adding atoms until the design is complete. Researchers are rapidly developing nano-materials that will have a profound impact on all aspects of life over the next decade, none more so than biology and medicine [30]. The first product of the nanotechnology age with applications in the biological sciences is fluorescent semiconductor nanocyrstals or quantum dots. QDs have been under investigation since the 1970s, however their applicability to the life sciences had been limited until recent novel advances in surface chemistry and synthesis methods [31, 32].

QDs are composed of semiconductor materials such as Cd and Se, synthesis is precisely controlled so that the QD dimensions are of the nanometre scale, typically 2-10nm [31]. When a semiconductor material such as CdSe exists at a size less than a critical quantum measurement known as the exciton Bohr radius, the quantum confinement effect occurs altering the electronic and optical properties in comparison to the bulk material. The quantum confinement effect is due to the uncertainty relation that causes the energies of an electron or hole to increase as the wave functions are confined to a smaller space [33]. Electrons are excited from the ground state to an excited state, when returning to the ground state energy is released in the form of photons (fluorescence). The further the electrons are from the ground state, the more energy is released and hence the further into the UV region the QD will emit. The size, and/or composition of the QD is directly proportional to the emission wavelength, so by varying the size or varying the synthesis material of a single QD from the same material a range of different coloured dots can be created [31]. The emission spectra of six sizes of CdSe QD are shown below, the adsorption spectrum is also shown (Figure 3).

At present, organic dyes are the popular choice for fluorescence imaging and detection; however organic dyes have a number of drawbacks including rapid photobleaching, red tailing of peaks, narrow excitation spectra and broad emission spectra. QDs have been the focus of intense research recently due to the inherent advantages of QDs over fluorescent dyes, including size dependant emission wavelength, large excitation spectrum, narrow Gaussian emission spectrum (full width half maximum (FWHM) = 20 – 40 nm) and an extended photo-stable lifetime [31].

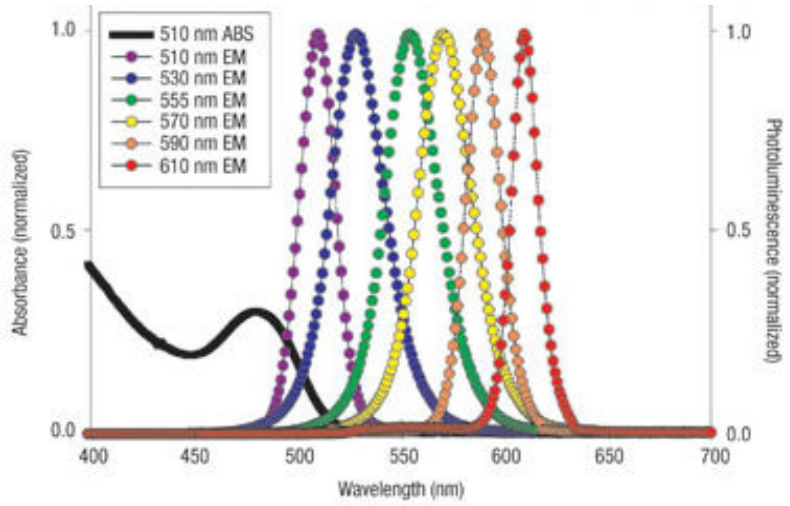

Figure 3 Emission spectra of 6 different QDs. The absorption spectrum of the 510nm emitting QDs is shown in black. Adapted from [34]. In terms of SAT the biggest advantage of QDs over organic dyes is the relatively narrow emission spectrum (20 – 40 FWHM) and broad excitation spectrum which allows excitation of multiple QDs with a single laser.

The current cost of QDs for encoding has been considered a limitation. QD synthesis methods currently produce milligram batches requiring expensive chemicals. In Yu and Peng's synthesis method, 90% of the cost of QD production is attributed to the solvents trioctylphosphine oxide (TOPO) or octadecene (ODE) in which the QDs are 'grown' [35]. Recent work by Asokan's group demonstrated that the organic solvents could be replaced by heat transfer (HT) fluids in the manufacture of CdSe QDs. The findings of the study demonstrated HT fluids were viable alternatives, it was also demonstrated that during the synthesis of smaller QDs the HT fluids were superior. The group concluded that the cost of QD production could be decreased by ~80%, hence this advance should accelerate uptake of QD technology within the community [36].

QDs have the potential to replace organic dyes for optically encoded SAT and QD encoded microspheres are currently gaining popularity for such applications (Figure 4). The broad excitation and relatively narrow emission spectrum of QDs require single laser excitation, decreasing detection instrumentation complexity when additional colours are added to the encoding scheme; furthermore there is reduced overlap between fluorescent emission spectra. The photostability of QDs also allow more reproducible quantitative results in comparison to organic dyes. These advantages significantly increase the multiplex capacity beyond that of organic dyes. Considering Eqn 2.1 (page 12), the use of QDs expand this capacity to that required for large scale genetic analysis, realistically 5-6 colours could be used and 10,000-40,000 unique codes may be produced [37] allowing the multiplexing levels common with high density microarrays to be achieved.

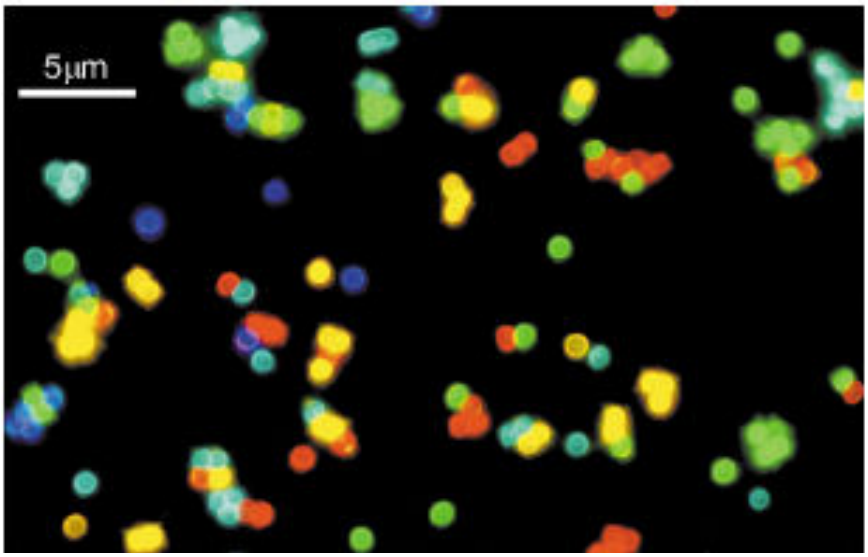

Figure 4 Fluorescent micrograph of CdSe/ZnS QDEM. The microspheres are doped with QDs emitting at 484nm,508nm,547nm,575nm and 611 nm [37].

2.3.3 Non optical encoding schemes

As stated above, the resurgence of interest in SAT was primarily due to fluorescent encoding strategies. While the focus of this work is on optical encoding, alternative coding schemes have been previously demonstrated and are described here for completeness.

Physical encoding relies on the measurement of physical characteristics of particles such as size. The earliest examples of microspheres relied on decoding the scattering properties of various sized microspheres [17]. Benecky *et al.* described the detection of hepatitis B surface antigen using a multiplex bead library distinguishable by particle size through the measurement of scattered light. Identification was possible when each particular bead had 0.1 μm difference in bead size. The group used the sandwich assay format and upon presence of the required antibodies aggregates formed, changing the scatter signal [38]. Particle shape is also employed by 3D molecular sciences; however this encoding scheme is not suitable for high multiplex levels but can be combined with other encoding schemes to increase multiplex capacity.

Raman encoding of microspheres has previously been reported. Such methods rely on the surface enhanced resonant Raman spectra (SERRS) effect to achieve the ultrasensitive measurements required. When a molecule is in close proximity to a fractally rough colloidal metal such as gold or silver and if the incident light is resonant with the molecule and plasmon of the metal, the SERRS effect is observed. The encapsulation of gold particles in silica has been shown to overcome problems with interference between

the molecules and the metal, enhancing the signal by a factor of $10^{13} – 10^{14}$ [39]. Mirkin *et al.* have shown the effectiveness of the technique to be suitable for multiplex analysis of oligonucleotides [40]. The combination of infrared and Raman probes to encode microspheres is also a possibility. Fenniri *et al.* created 24 unique coding signatures through the polymerisation of styrene and alkyl styrene monomers suggesting further use for combinatorial libraries [41]. Doering and Nie state that while these Raman and infrared encoding can be used in a multiplex format they suggest the spectral decoding may be limited [39], however recent work has shown that the discrimination of Raman probes is possible using a modified flow cytometer and principal component analysis (PCA) [42, 43].

Graphical encoding involves the classification of shapes; akin to supermarket barcodes. The creation of microbarcodes has been achieved by fusing blocks containing rare earth glasses (chosen due to narrow FWHM and large quantum efficiency) in a specific pattern on glass ribbons. Each microbarcode could be distinguished using a UV lamp and optical microscope or laser scanning cytometry (section 2.5.1). The authors hypothesised that up to 1 million combinations are possible. To date this method has been demonstrated with an assay to distinguish between human and microbial DNA [44]. Graphical encoding can also be achieving using striped cylindrical metal nanorods or nanobarcodes, formed by the deposition of gold and silver onto mesoporous aluminium films. 100 different strip patterns were created that could be reasonably identified using an optical microscope. Chemical modification of the surface for biofunctionality was also demonstrated [45].

Electronic encoding of microspheres has also been reported. The first example employed a semiconductor radio frequency (RF) device (analogous to radio frequency identification tags (RFID)) enclosed in chemically inert layer. Each of the radio device containers was assigned a unique frequency code and formed the building blocks of the microsphere codes. Decoding of the micro-transponders was achieved using a custom built radio frequency memory retrieval device. These types of codes offer high levels of multiplexing. A major drawback cited is the large size of the microspheres, although research is progressing toward the development of smaller RF devices. Miniature electronic transmitters use an integrated circuit connected to a photovoltaic cell and antenna. Each of the microspheres is decoded using capillary electrophoresis with laser activated code transmission [46].

2.4 Microsphere synthesis, encoding and bio-conjugation

The production of optically encoded beads has three phases; the solid support/microparticle must be manufactured, usually from polymers such as polystyrene, Latex or methylacrylate. The microspheres must also be doped with the dye of choice (organic or nanocyrstal), and the target specific capture molecule attached. Optically encoded microsphere quality depends on a number of factors including the size range, stability, uniformity and the ability to retain the fluorescent dye. It is also important to minimise the surface texture in order to reduce light scatter. Recently there has been an increased focus on the methodology required to create large quantities of microspheres economically.

The drop by drop method as its name suggests produces each micropshere sequentially. A number of different variations of this method can be found in the literature such as the injection of the polymeric solution through a needle, when the polymer leaves the needle and enters the stabilising fluid flowing past the needle tip [47]. Yi *et al.* replaced the needle with a capillary tube (Figure 5) [48], while Takeuchi *et al*. developed a microfluidic device to control droplet formation [49].

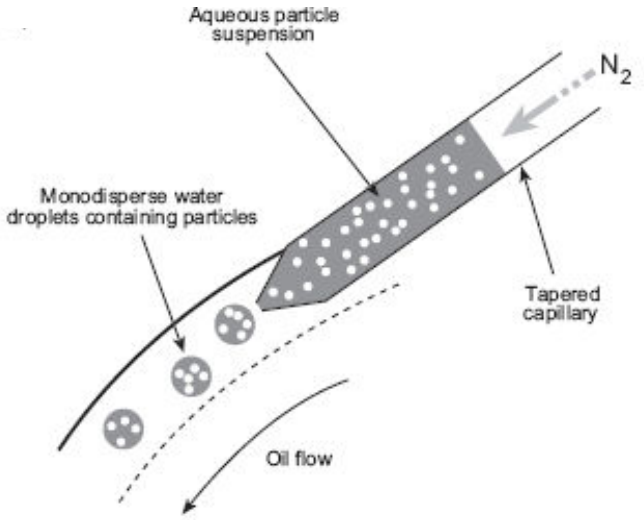

Figure 5 The formation of monodisperse microspheres via drop by drop process [48]. Microspheres are formed upon the ejection of droplets from the capillary tube aqueous phase to an oil based phase where spontaneous formation of microspheres occurs. Variations of this process involve the replacement of the capillary tube with a needle or microfluidic platform.

Microspheres can also be formed simultaneously, using solvent extraction/evaporation principles. These techniques were found to be unpredictable in terms of particle size and homogeneity of the populations. Moreover, simultaneous bead formation using this method is unsuitable for producing large quantities of microspheres economically [50]. Laminar jet disintegration techniques again form microspheres simultaneously; the jet breaks up into uniform droplets due to capillary instability or oscillatory stimulation. These jet based techniques despite perfect size distribution are unable to produce microspheres below 25μm. Martin-Banderas *et al.* overcame this limitation by

application of a flow focussing technique to produce a microjet under controlled conditions [51]. Monodisperse microparticles with excellent size accuracy (~5µm) were produced. The group produced fluorescently encoded microspheres and suggested that the high versatility of the technique could be applied to bead based arrays.

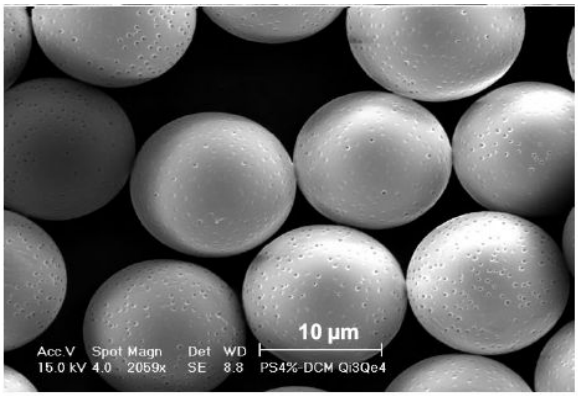

Figure 6 Scanning electron microscope(SEM) image of undoped microparticles produced by the flow focussing method [51]. The surface texture of these microspheres is "golf ball like" which may increase light scattering during detection.

The majority of methods encode the microspheres post synthesis, however it is worth noting that attempts have been made at polymerising QDs directly into the microspheres during synthesis [52]. To date this method has only been achieved using specially designed polymers and QD-ligands, no biological applications have been reported. This method suffers drawbacks from the tendency of colloidal QDs to aggregate within the polymer. The most successful manufacturing methods employ a two stage process, firstly the microsphere are synthesised and flourophores are subsequently added.

There are a number of methods for nanocyrstal encoding of microspheres. The deposition of nanocyrstals onto labelled polystyrene beads has previously been described using the so-called layer by layer method [53]. Polystyrene (PS) beads were used as the solid support, and several layers of QDs were built up in the surface via electrostatic

interactions. The number of monochromatic QD layers was precisely controlled to encode the beads. Once the layer by layer deposition of QDs was complete successful conjugation of anti-immunoglobulin G to the microspheres was achieved [54].

Riegler *et al.* has described a method for encoding involving the immobilization of nanocyrstals within the microsphere interior by demixing two solvents (phase transfer process). The method described involves dissolving the QDs in a beads soluble solvent e.g. toluene, this solution is then added to an immiscible solvent e.g. water. Upon addition of the QDs they are transferred to the polymer phase (a process termed demixing) resulting in the nanocyrstals being incorporated throughout the microspheres via strong hydrophobic interactions. The method is similar to the swelling method (see below); however diffusion plays no part in the process. Using this approach fluorescence was found to be stable, with no surface texture and microspheres were amenable to bioconjugation [47].

Nanocyrstals may also be injected into porous microspheres as described by Nie *et al.* [55]. Initial attempts swelled the microspheres and allowed QDs to diffuse into the internal structure of the microsphere [37], it was noted however that QDs were only absorbed at the surface of the microspheres and they tended to leach from the beads in protein solution and buffer [56]. To overcome these limitations mesoporous polystyrene beads were added to solutions containing precise ratios of various QDs with different emission wavelengths, showing rapid absorption of QDs within the internal porous structure and immobilisation of QDs through hydrophobic interactions. Beads prepared

by this method showed no leakage of QDs when the process had been completed. FCM measurements showed the beads to be 100 times brighter and a observed 5 fold increase in encoding uniformity in comparison to non-porous microspheres. This method has produced by far the best results to date for uniform encoding and signal strength. Cao *et al.* suggested that these polystyrene beads may be stabilised by encapsulating each bead with a layer of silica [57]. The deposition of silica does not effect the bead signal, and increases the stability of the microsphere during the hybridisation step of an assay.

The most popular approach for bioconjugation is the attachment of specific nucleic acid and protein molecules to carboxylated microspheres. Carboxyl groups on the microsphere surface are activated using 1-eythl-3-(3-dimethylaminopropyl)-carbodiimide (EDC) transforming the carboxyl groups to amine reactive sulfo-NHS esters. Conjugation between the carboxyl groups and the amino modified nucleic acids (or protein primary amides) takes place forming an amide bond. A spacer may also be included which in some instances can increase the efficiency of hybridisation [9, 19, 57, 58].

2.5 Detection platforms

2.5.1 Laser scanning cytometry

Laser scanning cytometry (LSC), originally proposed to overcome the limitations of FCM for surgical oncology [59-61], has been proposed as an alternative detection platform for fluorescent microspheres [23]. This technique uses multiple lasers to scan over the imaging surface without the same focusing constraints as fluorescence microscopes. The technique is mostly used in SAT to decode graphical arrays however it

has also been proposed as an alternative to flow cytometry for optical encoding. Coleman *et al.* evaluated the possibility of combining optically encoded microspheres on a planar surface. LSC based optically encoded microsphere measurement however, suffers from a number of limitations. Firstly if the height of the imaging surface is not uniform some microspheres were not in focus thus requiring multiple images to be acquired. Secondly, the microspheres were prone to aggregation on the planar surface possibly due to convection currents which may cause the microspheres to move and aggregate [62].

2.5.2 Microfluidic platforms

Microfluidic devices are capable of high throughput analysis by means of parallel assays, multiplex capacity and automation. The utilisation of microspheres as solid supports with microfluidics is an attractive option. The surface area to volume increase offered by the microspheres improves the sensitivity of such assays due to the higher reaction efficiency. Currently microfluidic platforms approaches are however limited in comparison to FCM in terms of throughput and availability [54].

2.5.3 The Luminex system

The Luminex platform is a flow based system designed specifically for the analysis of dual organic dye encoded microspheres. Luminex has evolved from the FlowMetrix system described by Fulton and co-workers [18], FlowMetrix based microspheres were originally produced as a set of 64 distinct microspheres for a standard cytometer (BD FACScan). The system ran digital signal processing software for real-time analysis of the

microspheres. The main disadvantage of the FlowMetrix microspheres was the fluorescence overlap between the encoding dyes and reporter (hybridisation signal) molecule and compensation was required [63].

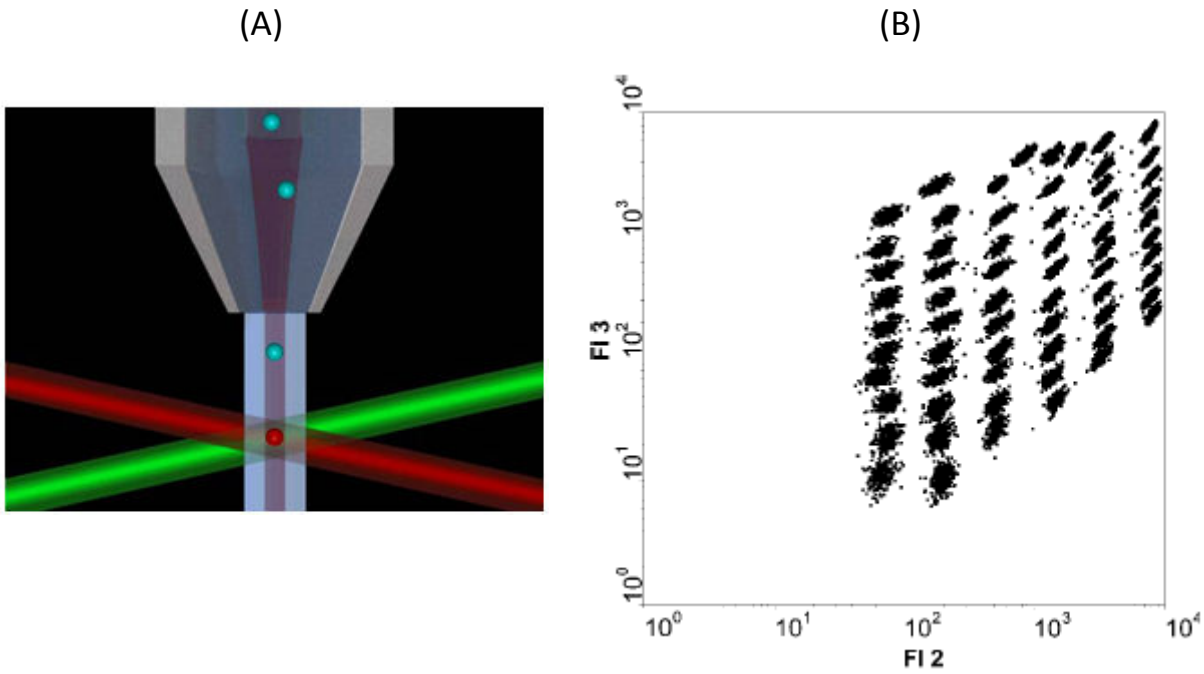

Figure 7 (A) Luminex Flow System showing the dual laser configuration (YAG and red diode) [64]. Microspheres flow past the excitation point individually and spectral responses collected. (B) FL2 and FL3 values for 64 different types of microspheres from the FlowMetrix system. Average of 300 microspheres events per set used [18].

To this end the dedicated flow based bench top system, the Luminex 100, was designed specifically for analysis of FlowMetrix microspheres. The Luminex system employs a 635nm red diode laser to excite the microspheres and a yttrium aluminium garnet (YAG) 532nm laser for improved reporter dye (R-phycoerythrin) excitation in comparison to a 488nm laser. Using this system 100 unique codes can be created. The Luminex platform has been successfully applied in a range of assays including immunoassays [65-69], cytokine analysis [70-75] and nucleic acid analysis [7, 76-82] amongst others.

2.5.4 The Mosaic system

The quantum dot corporation (QDC) one of the main suppliers of commercial QDs developed the Mosaic system (the world's first gene-expression system based on Qbead (QDEM) technology) in collaboration with Matushita/Panasonic. The Mosaic gene expression assay system provided a complete and optimized platform of instrumentation, software and reagents for custom-multiplexed, high-content, and mid-throughput gene expression analysis from cells or tissues. The system contains an inverted epifluorescence microscope equipped with a 405nm laser and CCD detector; multiplex assays are carried out in multiwell plates, using image recognition software to decode the QDEMs. However CCDs suffer from low sensitivities compared to PMTs [23]. In 2006 the QDC was acquired by Invitrogen and since the takeover the Mosaic system seems to have been discontinued for reasons unknown.

2.5.5 Flow Cytometry

Flow cytometry is a well developed technology used for a wide range of analyses. FCM equipment is also available in a large number of locations including hospitals, universities and core laboratories and was the original detection platform for SAT analysis. The detection of QDEMs with FCM offers the possibility of expanding basic single laser FCM analyzer applicability (all QDs are excited by a single wavelength) to genomic and proteomic applications. FCM provides a well developed detection platform for high speed sensitive multiparameter measurements making it ideal for analysis of optically encoded microspheres [83].

In terms of throughput FCM is unmatched. Even basic bench top analysers are capable of making highly sensitive measurements over four or more colours. Flow cytometry in conjunction with sophisticated sample handling techniques can yield a sampling rate of one 96-well plate/min. Using as little as 1µl sample volume, a 100plex assay can be completed in less than a minute 1 min, which translates to 120 million data points per day [6].

This thesis concentrates on the combination of fluorescent encoding of microspheres and flow cytometry for high throughput genomic and proteomic assays. In chapter 3 FCM instrumentation is examined in detail (section 3.3) and the analysis of multicolour QDEMs with an 4 intensity/4 colour encoding scheme is described (section 3.4).

2.6 Applications

Bolstered by recent innovations, SAT is receiving increasing attention for high throughput analysis of genes, proteins and a host of other biomolecular species [19]. The following sections discuss examples of SAT applications in proteomics, SNP genotyping and gene expression. These are by no means the only applications of SAT assays however the following lists focuses on the applications which stand to gain the most benefit from the increased multiplexing analysis offered by fluorescent encoding QDEMs.

2.6.1 SNP genotyping

SNPs are single base substitutions occurring within the general population at a frequency of greater than 1% and accounting for ~80% of the genetic variance between individuals. Located every ~1000 base pairs it is estimated that there are in excess of 3 million SNPs located in the human genome [84]. Mutations, particularly single nucleotide polymorphisms, are thought to play a role in an organisms response to drugs, bacteria, disease, viruses and toxins [3, 85], the understanding of these roles will impact a number of major areas.

SNPs are providing avenues for novel agricultural research to increase rice, wheat and soya bean crop yield, decrease susceptibility to particular diseases and reduce the amount of herbicide applied [86, 87]. Microorganism SNP profiles are also important as demonstrated by recent outbreaks of E.coli as a result of mutations and the resistance of HIV to treatment due to a high frequency of mutation[88].

The application of knowledge gained through SNP identification and relation to phenotype for a population has the potential to revolutionise areas such as medicine and drug discovery by moving away from the "one size fits all" philosophy to a more personalised therapy based on interindividual genetic variations i.e. "the right drug for the right patient" and it is this area known as pharmacogenomics which promises to yield the greatest impact on human life.

Pharmacogenomics aims to elucidate the genetic basis for disease susceptibility, variable drug response (efficacy) and adverse drug reactions (toxicity) [89].To this end the SNP Consortium (TSC) has been formed by the world leading pharmaceutical and academic laboratories to discover and map hundreds and thousands of SNPs with a view to identification of genes related to novel disease markers and drug targets leading to individual drug therapies and diagnostic tests [90].

It is clear cost effective SNP genotyping platforms will be required to profile large numbers of patients and control DNA samples to elucidate the information required in order to draw associations for pharmacogenomic applications. Depending on the study ~5000 tests may be needed to identify functional candidates. When performing a genome scan without prior functional evidence as many as 250,000 – 500,000 loci need to be analysed. The nature of association studies requires multiple testing on the same patient samples. It is estimated that 80% of all haplotypes occur in all populations with only 8% being population specific. Research carried out for the European and Japanese populations have demonstrated the need for 20% more SNPs to cover both populations versus one, research is planned for the African population and the amount of SNPs required to cover all three populations is expected to increase. Moreover the integration of this technology with various other types of 'omic' data is critical in attaining maximum benefit from SNP analysis in medicine and drug discovery [89].

The analysis of single nucleotide polymorphisms has included methods such as single strand conformation polymorphism analysis (SSCP) [91-93], gel length restriction

fragment length polymorphism [94, 95], allele specific oligonucleotide (ASO) hybridisation [96], oligonucleotide ligation assay (OLA) [97] and allele specific primer extension assays (ASPE) [98, 99]. In terms of detection and readout of alleles from the methodologies above, a number of new technologies have been developed for discrimination of signals based on hybridisation or enzymatic cleavage, including mass spectrometry (MS), planar array based platforms [100-102] and SAT. Several studies have reported the suitability of microsphere based assays for SNP genotyping citing rapid data acquisition and excellent sensitivity. SNP assay formats have largely taken the route of OLA or single base chain extension [25]. The first combination of SNP genotyping and multiplexed microspheres was described in 1997 by Fulton *et al.* using 16 sequence specific oligonucleotide probes and demonstrated the sensitivity, precision and speed of the assay format [18].

More recently a number of groups have demonstrated the effectiveness of optically (both organic dye and nanocyrstal) encoded microspheres as a detection platform for SNP genotyping. Ye and co-workers utilised ASPE for a multiplexed SNP genotyping study, with excellent correlation to that of sequencing. The authors also suggested that using a flow cytometer up to 30,000 genotypes could be analysed every eight hours [103], furthermore the group estimated that the cost per SNP is less than $0.20. Single base chain extension has also been detected using fluorescent microspheres. The potential throughput of the assay was estimated as 120,000 genotypes per day, however the cost was slightly higher [104].

Luminex xMAP technology has been used extensively for SNP genotyping; Armstrong *et al*. developed and validated a 32-plex SNP genotyping assay for 8 different genes. Four different ASOs were used for each mutation and employed to detect the allele where the highest fluorescence for each of the four possible microspheres determined the genotype. A direct comparison of results with the TaqMan assay was carried out. The results of the 39 genotypes were found to be in good correlation between both assays [58]. Numerous other examples can be found in the literature for organic dye encoded microspheres used for SNP genotyping including application for basal cell carcinoma [105] and cervical cancer [106].

QDEMs have also been applied to SNP genotyping. The most significant work (and the first to apply QD encoded microspheres to SNPs) to date was carried out by Mahoney *et al.* As a proof of concept the P450 gene family was chosen for study, due to its importance in drug metabolism and difficulty to genotype (due to the high degree of homology between members). QD encoded microspheres were found to highly accurate (100% concordant with DNA sequencing); furthermore the method also had a higher call rate (although it was suggested that this may have been due to PCR amplicons not being purified, suggesting that a PCR purification step maybe avoided when using microspheres). Also noted was the decrease in the DNA concentration required for the assay (1 ng Genomic DNA), substantially less than that required by other assays without direct amplification of the genomic strand. The group also confirmed the advantages over planar arrays stated above. Figure 8 below shows the methodology used [9].

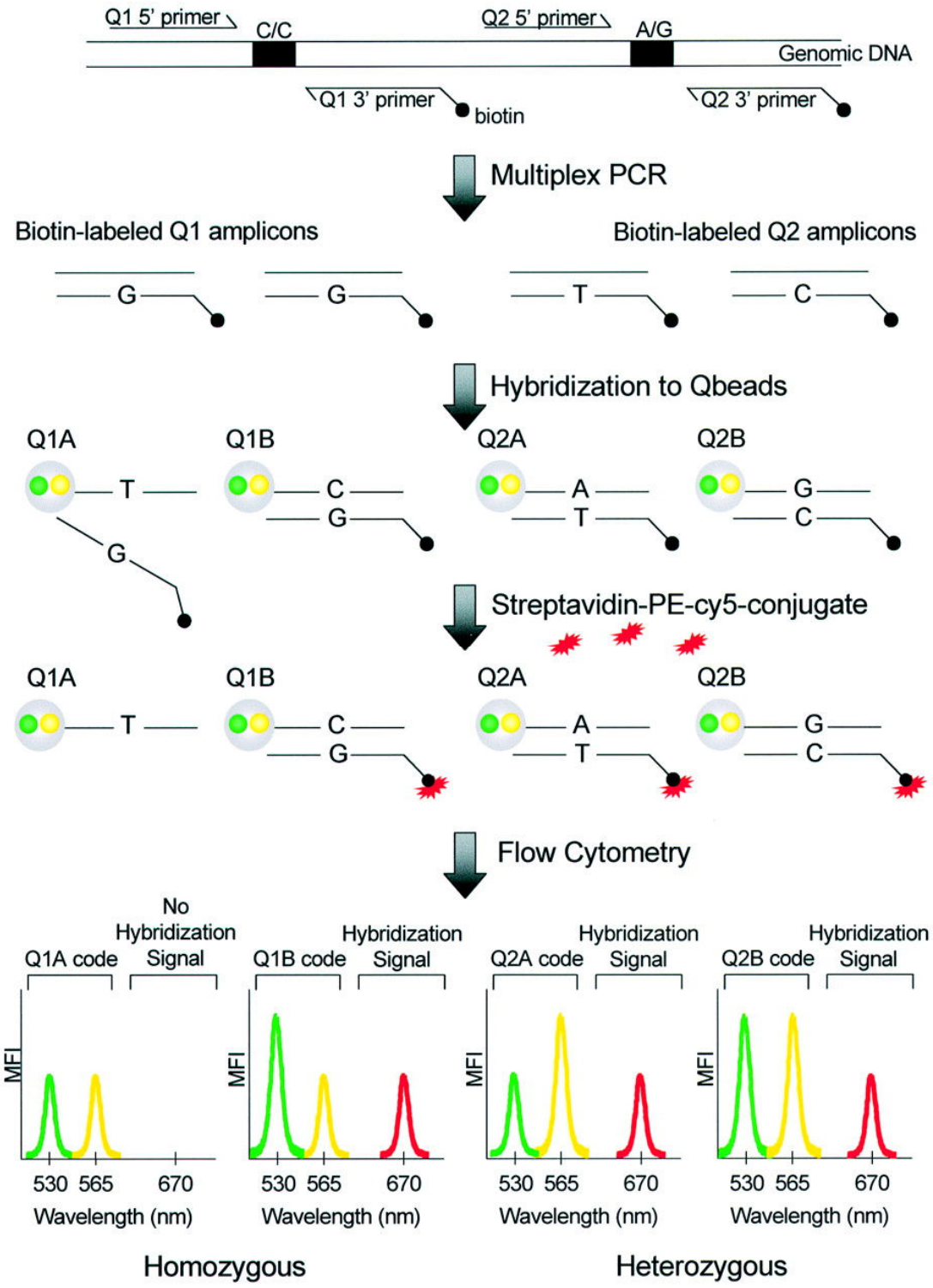

Figure 8 SNP system employed by Xu *et al.* PCR of the genomic DNA is carried out at various SNP loci, biotin labelled amplicons are hybridised to allele specific QD encoded microspheres with unique spectra. The presence of bound target is determined by presence of the reporter signal, streptavidin-PE-CY5. Microspheres are identified using FCM [9].

2.6.2 Gene-expression

To date several reports have detailed gene expression studies using SAT. Fuja *et al.* determined the expression levels of four transcripts, BRCA1, MGB1, DLG1 and ACT1 using SAT. Organic dye based microspheres were conjugated to transcript specific probes by covalent coupling. The results from the study were compared to quantitative real-time polymerase chain reaction (RT-PCR). The authors concluded that the results were concordant with RT-PCR [20] and multiplexed bead assays are a viable alternative to planar arrays for gene-expression profiling. In 2001, the beadsArray™ for the detection of gene expression (BADGE) was carried out on the Luminex platform; a decrease in hybridisation time over other assays was noted. The method also out performed quantitative RT-PCR in terms of multiplexing ability and the amount of RNA required [107].

Increasing the multiplexing levels of gene-expression profiling using SAT is crucial and to this end attention turned to QDEMs. The Mosaic Q1000 system was designed specifically for mid throughput gene expression analysis. In a recent study Eastman *et al.* used 8μm magnetic microspheres for convenience in sample preparation, liquid handling and reduction of the background signal. Specific nucleotides were attached to QDEMs were used to screen ~100 genes (455 are possible with the coding scheme used). Biotinylated cDNA was produced from RNA and hybridised to the microspheres, streptavidin coupled to an infrared emitting QD for hybridisation. The results of the study showed a high agreement with GeneChip microarrays and improved on results aqquired by the Luminex platform [108].

2.6.3 Proteomics

Quantitative proteomics has been suggested as one area where multiplex microsphere libraries may be used to determine the amount and state of proteins in a sample. In comparison to ELISA based techniques which are carried out in microwell plates, microspheres act as the solid support for capture antibodies. The sensitivity of ELISA based assays is in the pg/ml range using high affinity monoclonal antibodies and is easily automated [19]. The large sample sizes required for microplate based methods, led to the application of microarray-type techniques. Capture antibodies are spotted onto glass membranes and glass slides. In terms of protein concentration the best results have been observed using the sandwich assay design. The reproducibility and reliability of microarray based ELISA has not reached the clinical level thus far however and [109] bead based multiplexing assays have been shown to be a viable alternative to slide based methods for highly parallel analysis.

The earliest examples of microsphere based sandwich assays (Figure 9 B) concentrated on the detection of multiple cytokines using the FlowMetrix system. Using this method Carson *et al.* reported that the FlowMetrix assay overcame significant variation from experiment to experiment and also plate to plate variation observed with ELISA assays [110].

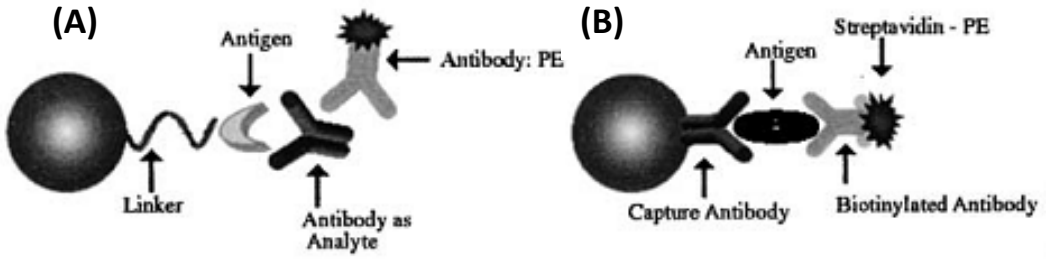

Figure 9 Example of protein SAT assay chemistry and detection. (A) Antigen conjugation for analysis of blood and plasma antibodies. (B) Sandwich assay design. Adapted from[25].

Alternatively the antigen can be conjugated to the beads for the analysis of antibodies in blood and plasma (Figure 9 A). For this assay the antigen is immobilised onto the microsphere and a labelled class or isotope specific antibody is used to report the presence of the analyte [19]. Applications include cryptosporidium antibodies in serum and oral fluids [111] showing good correlation when compared with an equivalent ELISA assay. McHugh *et al.* also applied the technique to the detection of antibodies to cytomegalovirus and herpes simplex virus [112].

Encoded microspheres have also been applied to the study of carbohydrate-protein interactions. An optically encoded microsphere is conjugated to a unique carbohydrate; the microspheres are then incubated on a randomly ordered fibre optic array. The assay allowed for the simultaneous measurement of carbohydrate binding proteins [113].

2.7 Thesis aims and objectives

It is clear that SAT has a great deal of potential in the analysis of genes and proteins for post genomic applications. In order to perform the applications described in the previous sections, particularly SNP genotyping and gene expression analysis at microarray throughput levels an alternative to organic dyes must be found. QDs are an excellent candidate for this role, due to single wavelength excitation and relatively narrower emission peaks. The inherent advantages of QDs over organic dyes allow the multiplexing capabilities of such assays to be extended. Current manufacturing processes have progressed sufficiently enabling the production of bright, stable and reproducible optically encoded microspheres.

FCM was chosen as the detection platform for QDEMs allowing sensitive measurements of multiple fluorescence channels in high throughput. These fluorescent nanocyrstals are naturally extendable to basic FCM bench top systems however the process of decoding highly multiplexed SAT libraries may not be straightforward on current FCM equipment. As the number of unique microspheres increases and additional emission wavelengths are added to the coding scheme the classification of individual microspheres becomes more difficult as the number of fluorescent parameters to consider increases.

This work aims to investigate a number of classification schemes for the identification of QDEMs from FCM data. A commonly used method, MPG is evaluated in chapter 3 followed by the development of supervised learning models. Support vector machines (chapter 4) and artificial neural networks (chapter 5) were selected due to their suitability for multiparameter data, high generalisation ability and previous success in the field (section 4.2.3 and section 5.2.2). The accessibility of these techniques to the community is also of considerable importance as such algorithms are not included at present with FCM software.

The main objectives of this thesis are:

- To determine the optimum classification method for microsphere identification for a QDEM FCM dataset obtained using a flow cytometer representative of those found in research laboratories and the clinic.
- The following techniques were optimised for the data and the most suitable methodology chosen:
    - Multiparameter gating
    - Support vector machines
    - Artificial neural networks
- To develop a user friendly interface to carry out the most suitable method while also providing common FCM software functionality (chapter 6), for the benefit of lab based researchers.

Chapter 3: Flow cytometric analysis of nanocyrstal encoded microspheres.

3.1 Overview

The focus of this chapter is to illustrate flow cytometer instrumentation, describe the acquisition of the datasets used throughout this thesis and to evaluate current encoded micropshere identification methods. The chapter is split into two distinct sections beginning with a brief introduction to general flow cytometry (section 3.2), FCM instrumentation and data processing (section 3.3). The second part of this chapter describes the flow cytometric analysis of a nanocrystal encoded library (section 3.4) and evaluation of a standard classification method - multiparameter gating - for the identification of QDEMs (section 3.4).

3.2 Introduction

Cytometry is loosely defined as measurement of the physical and chemical characteristics of cells. Flow cytometry is the process of measuring these characteristics for a fluid stream of cells or particles (the analyte) flowing through an instrument called a flow cytometer [114]. A flow cytometer enables multiple simultaneous measurements of light scatter and fluorescence at the individual analyte level at very rapid rates. Flow cytometers are subdivided into two categories, analysers and sorters; an analyser measures the properties of each of the cells in the stream, an optional sorting module may be present allowing separation of cells post analysis. (Sorters are not considered here, for further information see [114, 115]).

During measurement a laser beam is passed through a fluid stream containing the population of interest. Excitation of the analyte within the stream (sample core) results in a signal dependant on the properties of the analyte in question. The physical properties of a given analyte can be determined by measuring scattered light of two types. Side scatter (SSC), detected at ~90° to the incident light is proportional to cell granularity and the complexity of a cells internal structure (widely used in the differentiation of cells such as granulocytes). Forward scatter (FSC), is a measurement of diffracted light, measured via a photodiode at a small angle to the axis of the laser beam. Scattering is routinely used as a 'trigger' for cell sorting. Excluding clinical haematology, all FCM analysis employs the use of flourophores. The determination of non-physical characteristics of a cell may be elucidated through labelling with an organic flourophore (e.g. fluoroscein isothiocyanate (FITC)) attached to a carefully chosen primary or secondary antibody. In FCM experiments data is generally presented as histograms or bivariate histograms either as scatter, density or contour plots (see below).

FCM is a well established analysis platform and has applications in a broad range of standard clinical diagnosis and research areas, ranging from DNA histogram analysis to determine ploidy (number of chromosomes in a cell), DNA index S-phase fractions for cancer diagnostics, immuno-phenotyping and of course SAT [116-120].

3.3 Flow cytometer instrumentation

3.3.1 Fluidics system

The flow cytometer fluidics system orders the sample into a stream and transports it through the centre of the excitation or "observation" point. There are two types of fluidic design implemented in modern flow cytometers, the flow cell and stream-in-air. Bench-top cytometers such as the Beckman Coulter EPICS XL use the flow chamber or cell design (Figure 10). All benchtop cytometers employ the flow cell design and are used in conjunction with a laser (or mercury arc lamp source) (section 3.3.2). For an excellent discussion of flow chamber design and stream-in-air flow systems see [121].

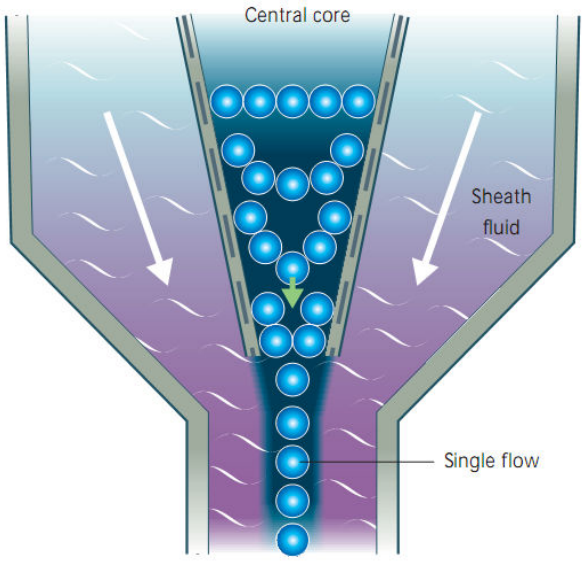

Figure 10 Flow cytometer flow cell, the sample is aspirated from the tube into the fluid stream where it is hydrodynamically focussed to the centre (core). The greater the sheath pressure the more cells pass though the laser at any given time. For micropshere analysis, the sheath fluid pressure is kept low in order to allow each bead to pass through individually [121].

Within the flow cell the sample is injected into a rapidly flowing fluid (sheath fluid). Principles of laminar flow keep the sample core separate from the sheath fluid by

accelerating the particles and restricting them to the centre of the core in a process known as hydrodynamic focusing. The pressure of the sheath and sample fluids is critical; sample pressure must always be greater than the sheath fluid pressure. A pressure regulator controls the sample flow rate by changing the sample pressure relative to the sheath pressure. An increase in the sample pressure increases the flow rate by increasing the width of the sample core allowing more analytes into the stream. However this may lead to more than one cell passing through the excitation point at any given time.

Applications which use a high flow rate during analysis are generally used for qualitative analysis for instance immunophenotyping where ultra-high throughput is desired [122]. Lower flow rates are used for analysis requiring more precise measurements analysis e.g. DNA analysis [123] and SAT applications where a low flow rate is maintained to allow measurement of single microsphere events. During operation the fluidic system must be kept clear of debris and air bubbles to ensure the sample correctly intercepts the laser beam. As the sample core is hydrodynamically focussed toward the centre of the fluidic stream, the position of the sample within the core is a potential a source of excitation intensity variation [121].

3.3.2 Excitation

Sample excitation is primarily achieved with a laser consisting of a cylindrical plasma tube filled with an inert gas such as argon. The primary beam of bench top flow cytometer is at 488nm, although some flow cytometers carry a secondary source usually either a red diode laser at 635nm or a UV mercury arc lamp at 375nm. The wavelength of the laser is monitored and kept constant by means of feedback circuitry. The alignment of

the laser is critical in FCM and must remain focussed on the sample core, in bench-top flow cytometers no adjustment is necessary as the laser is pre-aligned and fixed in position. The beam is directed through a spherical lens which causes the beam shape to become elliptical, before finally entering a focussing lens allowing the beam to intercept the sample core.

Advances in laser technology have produced very stable lasers for flow cytometry in terms of output. Under light stabilized operation modes the laser can maintain an output within ± 0.5% during continuous extended operation. Arc-lamp excitation sources usually have an electronic feed back loop to correct for any instability. For the majority of the arc-lamp lifetime the lamp may maintain ± 0.5% stability however toward the end of its lifetime a larger variation in the intensity of the lamp is often observed [121].

3.3.3 Optics and detection

When a cell is passed through the laser excitation point the emitted side scatter (SSC) and fluorescence signals are routed to the detectors via a system of beam splitters and optical filters. Dichroic mirrors and lenses are used to direct light of a selected wavelength to a particular detector. For example a 560 shortpass (SP) dichroic mirror transmits light of less than or equal to 560nm, longer wavelengths are reflected at 45° from the angle of incidence[121]. In the case of the Epics XL dichroic lenses are used for this purpose, dichroic lenses are used to reflect light shorter than a specified wavelength (Figure 12). Photomultiplier tube (PMT) and photodiode (PD) detectors are the detectors of choice for FCM due to their high sensitivity. Optimisation of the detector for a particular fluorescence signal is achieved through the use of bandpass (BP) filters allowing only a

narrow range of wavelengths to reach the detector (Figure 11). Other filters which may be used with the flow cytometer are short-pass (SP) filters which transmit wavelengths of light equal to or shorter than the required wavelength. Long-pass (LP) filters allow light equal to or longer than the specified wavelength through.

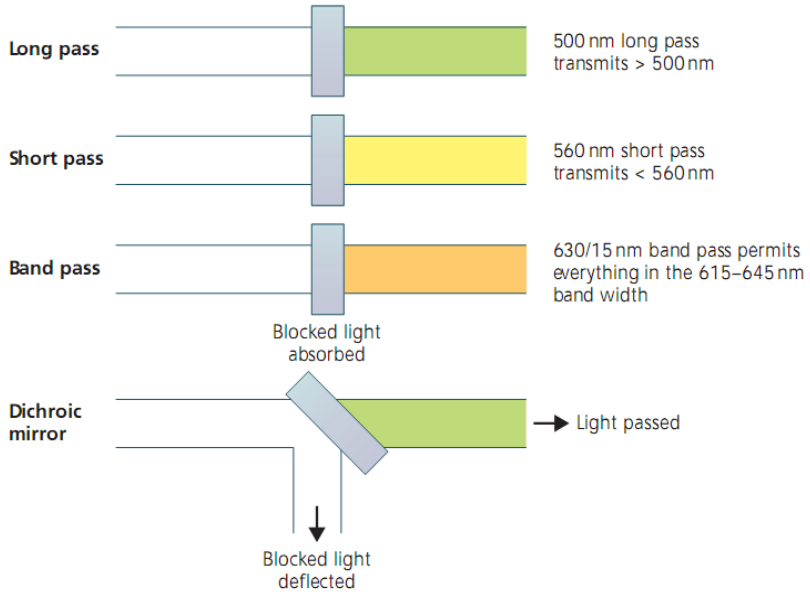

Figure 11 Examples of the filter and mirror that form the optical bench. The optical bench route SSC and fluorescent signals to the PMTs and PDs during FCM.

Optical filters may also contribute to fluorescence, especially those made from glass. Large amounts of light from the excitation source scattered toward the collection optics can induce fluorescence from these filters, interfering with analyte measurements [124]. The performance of the filter system in a flow cytometer is a probability based function and hence there is always a possibility that an excitation photon may enter the detector and be mistaken for sample fluorescence. Careful design of the filter combination is required to minimize this potential source of variation. For example in a high efficiency light collection system, an extra dichroic mirror can be used to decrease the possibility of a 488nm photon entering the detector [125].

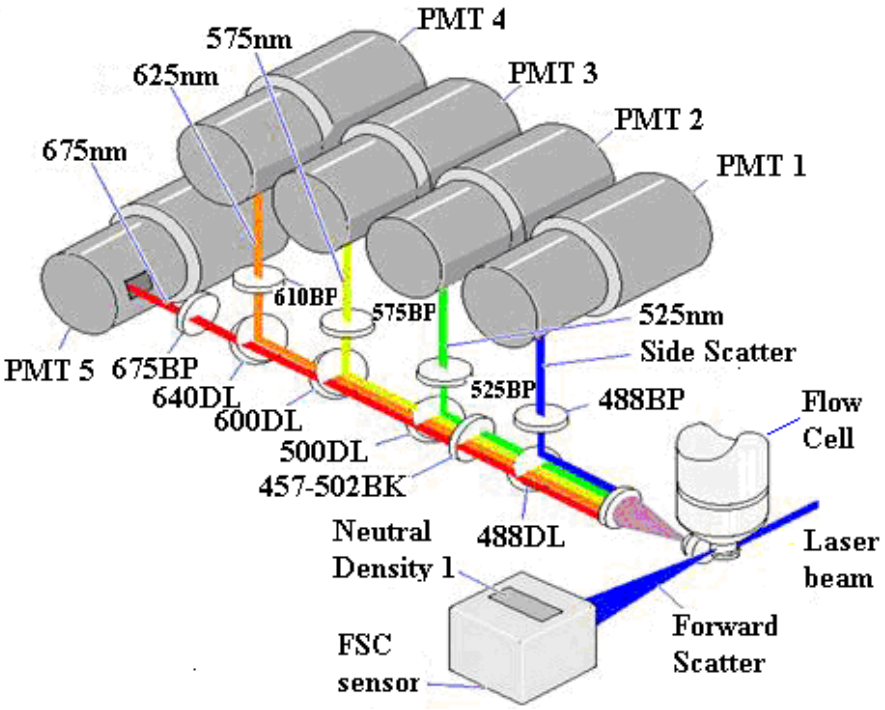

Figure 12 The EPICS XL optical bench FCM configuration was used for all measurements taken during this thesis. Fluorescence is detected at 525nm, 575nm, 620nm and 675nm. Adapted from [126].

The orientation at which the excitation and light collection optics within a flow cytometer are held is termed the *optical bench* (Figure 12). Good design of the optical bench is essential to optimise the total amount of light striking the detector. The linear range of the optics is also important as there exists a dark current which will restrict the range and must be limited through bench design. The high throughput nature of flow cytometry means that each analyte is excited by the laser for a few microseconds, to obtain accurate results the maximum amount of light must be captured. Modern flow cytometers have a light collection efficiency of between 15%-25%, much improved in comparison to older instruments [125]. Good light collection efficiency may also lead to an increase not only in fluorescent light but also background and scattered light. It is desirable to reduce this background noise to a minimum and also to ensure that the increase in fluorescence does not saturate the detector, producing a non-linear response [125].

3.3.4 Electronics

Once light from an analyte is routed to the detector photons are converted to photoelectrons, creating an electrical current. The amount of photons generated by fluorescence emission is small and PMT dynodes amplify the signal through a number of internal gain stages, known as preamplifier gain (PDs generally have no gain and are therefore used for bright FSC measurements). The aim of the FCM electronics system attempts to maximise the signal to noise ratio i.e. only the photons resulting from the interaction of the sample and laser beam are collected. The PMT gain has been described as "the least noisy gain available" in the flow cytometer; therefore adjustment of the PMT voltages is generally preferable over amplifier gain.

Conversion of the detector output current to voltage is achieved using a transimpedance amplifier producing a linear amplification of the signal. Following the restoration of the signal baseline (removal of stray light and dark current), a further programmable amplification stage allows measurements to be controlled by the operator for online histogram adjustment. In order to filter the non-sample signals a discrimination parameter is selected and a user defined threshold is applied. For example during DNA content analysis the discriminator is defined on the DNA parameter e.g. propidium iodide fluorescence, as the analysis measurement of non-nucleated cells is generally of little interest. Only when the signal exceeds this discriminator threshold is the sample event recorded. Following these operations a voltage pulse is produced, the height and area (integral) of the pulses produced are measured. Integration of the pulse width is carried out to account for large analytes in the flow cytometer (i.e. particles that are larger than

the laser beam width). Digitisation of the data is then carried out for conversion of analogue voltages to numeric values using an analogue to digital converter and stored in a flow cytometry standard (FCS) file (section 3.4.2).

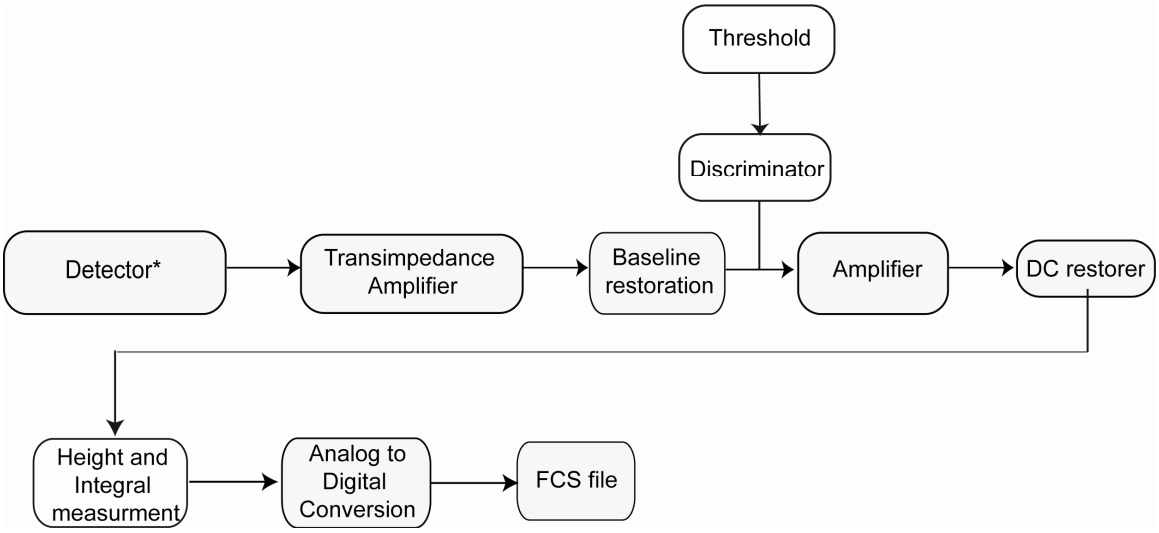

Figure 13 FCM electronics overview. The schematic shows the general FCM signal processing stages from when light enters the PMT detector until the sample measurements are written to FCS files. *PMT detectors also include an internal gain stage.

The final part of signal processing is carried out on a PC for operations such as compensation (user specified correction for overspill between detectors with a correction matrix), linear to logarithmic amplification (conversion of linear signals to log signals for data display is achieved using a log look-up table with the EPICS XL instrument) and data analysis/display (section 3.4.1) can be performed [127]. The sophisticated electronics of modern flow cytometers is unlikely to give rise to significant variation in results [125].

3.3.5 The FCS filetype

The FCS 1.0 format was developed by the Society for Analytical Cytology in 1984, necessitated by the need for a standard file format to allow FCM data acquired on one computer to be used with other types of computer systems. The FCS 1.0 format consisted of a four section file that formed the backbone for subsequent file formats (FCS 2.0 & FCS 3.0). The first section of an FCS file is always the HEADER segment and designates the FSC version of the file. The HEADER segment also contains the 8 byte offset values that defines the remaining file sections. The TEXT segment contains the experimental information including the instrument type, detector ids and acquisition time in the form of keyword value pairs. An example of a common keyword value pair in a FCS file is "$TOT/10000/", the keyword is $TOT and the value is 10,000 – this specifies that a total of 10,000 events were recorded.

The raw data from flow cytometry is stored in the DATA portion in one of four formats, binary, floating point, double precision floating point and ASCII, defined by the $DATATYPE keyword in the TEXT segment. The most common method of data storage is binary integers corresponding to the scatter and fluorescent measurements in columns and events stored in the order at which the analyte passes the laser beam known as a listmode file. In flow cytometry each measurement of an analyte is termed an "event", with the cytometer outputting a $1 \times p$ vector for p parameters (variables) when each QDEM is excited. A dataset is a collection of events from any given analysis, in our case a single QDEM population or a multiplexed solution of QDEMs. The ANALYSIS section is an optional post analysis portion containing the results of data processing and analysis with variables in keyword value format similar to the TEXT section [128, 129].

3.4 Application of a supervised FCM data analysis method for QDEM classification.

This section discusses the suitability of a readily available method for subpopulation classification for the identification of QDEMs from a commercially available library. The acquisition of QDEM data using FCM and the application of MPG are outlined (section 3.4.1 and section 3.4.2). Finally the performance of MPG for QDEM identification is discussed (section 3.4.3).

3.4.1 Multiparameter gating.

The majority of current FCM analysis is dependant on operator interpretation of results from one dimensional histograms or two dimensional scatter plots [121]. These data display methods are routinely used throughout FCM experiments from instrument setup and acquisition to publication [130]. The simplest type of data display for flow cytometry measurements are single parameter frequency histograms (intensity *versus* the numbers of events), which is used routinely in cell cycle analysis. A logarithmic x-axis over a four to five decade log scale allows populations with 10,000 to 100,000 fold differences in intensity to be displayed, e.g. immunophenotype analysis where a high dynamic range is observed. Linear scales are generally used for plotting FSC and SSC measurements.

Bivariate histograms or two dimensional scatter plots are also commonly used to visualise FCM results (three dimensional plots are also possible but seldom used due to the danger of misinterpretation). The relative intensities of the two selected fluorescence and/or scatter parameters specify the *x* and *y* coordinates of the point on a plot - here both

the axes are logarithmically scaled. A limitation of the standard dot plot is that no information is provided as to the proportion of events lying in each subpopulation. An extension of the dot plot allows projection of the density of the subpopulations on the plot to highlight regions based on the concentration of events. Alternatively a contour plot can be produced where lines represent the density based elevation of points. An example of a dual parameter QDEM plot can be seen below (Figure 14) the dots are shaded in relation to the number of events present at each *x y* position.

In flow cytometry the definition of a region around a cluster observed on a bivariate histogram of two parameters is termed a *gate*. Gating is essentially human supervised classification method (expert method) of subpopulation identification in FCM in that the user relies on prior knowledge of the system under measurement to define the regions on a 1D or 2D scatter plot. The definition of a subpopulation across multiple fluorescence detectors is known as multiparameter gating. MPG functionality is available in the majority of FCM software. The process of MPG begins with a series of bivariate histograms; the operator interprets these plots to manually define or "draw" the classification boundaries. In future analyses the gates are applied to unknown samples, events falling within a particular gate are classified with the designated label. The classification of fluorescently encoded beads has previously been achieved using MPG, although the libraries described were less complex than the QDEMs used in this study [131-133]. Each micropshere was analysed individually and a gate defined on each bivariate plot for the population, the process continued until all encoded microsphere regions had been defined.

In the work that follows the MPG method is employed for the recognition of a QDEM library with 20 individually encoded microsphere sets. The coding scheme employs 4 QD colours emitting at 525nm, 575nm, 620nm and 675nm. The concentration was varied over three intensity levels. Each class of microsphere was analysed individually on a standard single laser flow cytometer at 488nm and 1000 events acquired for each type of QDEM. Gates are combined on multiple parameters for each population individually by a flow cytometer operator. Once the gates are defined for each microsphere unknown solutions can be presented and the QDEMs present predicited. A set of microsphere mixtures containing randomly selected QDEMs were prepared to act as an external validation for each of classification methods. Current FCM software does not allow internal testing of gating accuracy as the method relies heavily on user interpretation.

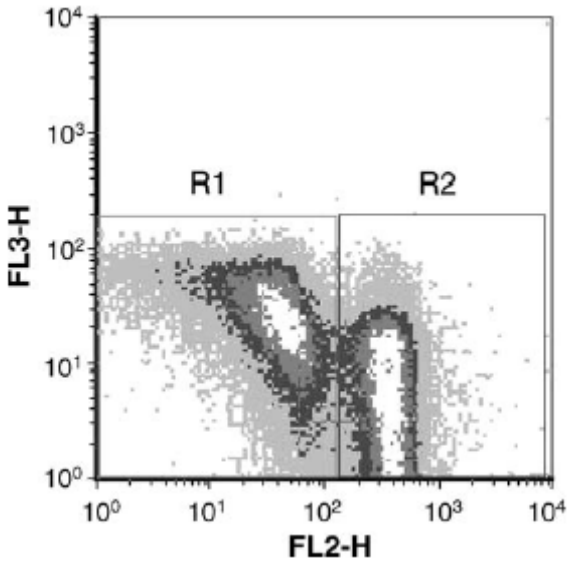

Figure 14 2D gating of nanocrystal microspheres. The complexity of the gating procedure is increased for each colour in the encoding scheme. The microsphere can be classified by their position on the bivariate histogram i.e. class 1 = R1 and class 2 = R2. Adapted from [133].

Note: *An unsupervised clustering algorithm available in the Flojo FCM software suite was also evaluated. However all analyses using this software were unsuccessful in that the identity of clusters could not be established and the number of events per cluster were imbalanced. The details of this study can be seen in appendix 1.*

3.4.2 Materials and methods

A library of 20 carboxyl functionalised 5μM mesoporous methacrylate microspheres (Table 2) containing composition tuneable QDs (Cyrstalplex, Pittsburgh, USA) was analysed using FCM. For more information on QDEM specifications see appendix 3.

Table 2 Specification of each of the 20 QDEM used in this study. The relative intensity of each micropshere is shown at each of the four possible wavelengths.

QDEM Code	QD -Emission Wavelength			
	525nm	575nm	620nm	675nm
QD0000	0	0	0	0
QD0001	0	0	0	1
QD0003	0	0	0	3
QD0010	0	0	1	0
QD0011	0	0	1	1
QD0100	0	1	0	0
QD0101	0	1	0	1
QD0110	0	1	1	0
QD0111	0	1	1	1
QD0202	0	2	0	2
QD1000	1	0	0	0
QD1001	1	0	0	1
QD1010	1	0	1	0
QD1011	1	0	1	1
QD1100	1	1	0	0
QD1101	1	1	0	1
QD1110	1	1	1	0
QD1111	1	1	1	1
QD2100	2	1	0	0
QD2200	2	2	0	0

All data used in this study was acquired in the laboratory by Clair Gallagher. FCM was preformed using an EPICS XL (Beckman Coulter, FL, USA). The instrument was equipped with a 488nm air-cooled argon laser and the standard four colour filter set-up (525BP; 575BP; 625BP; 675BP). The EPICS XL uses digital signal processing (DSP) electronics negating log amplifiers for logarithmic amplification of signals, conversion of linear to log is achieved using a log look-up table. Fluorescence compensation

(mathematical correction for fluorescence crossover between PMTs in FCM) can be accomplished between any pairs of signals from the PMT, which is not possible with flow cytometers employing analogue electronics. Another unique advantage of the EPICS XL is the prism parameter, allowing automatic analysis and display of multicolour data when performing three or four colour analysis [114].

The instrument was calibrated using Flow-Check beads (Beckman Coulter, CA, USA) as per the manufacturer's instructions. All FCM measurements were gated through the FSC and SSC channels and acquired without compensation. 3µl (1mg/ml) QDEM solution was suspended in 297µl of PBS pH 7.8. The solution was sonicated prior to aspiration. Shown below is the flow cytometer detector setup used during analysis (Table 3).

Table 3 EPICS XL detector settings for each of the six measurement parameters.FSC = forward scatter. SSC = side scatter. FL1 = 525nm. FL2 = 575nm. FL3 = 625nm. FL4 = 675nm

	Voltage	Gain
FSC	432	2
SSC	39	10
FL1	623	1
FL2	730	1
FL3	745	1
FL4	876	1

For each QDEM code in the library 1,000 events were obtained and stored in an individual FCS file. All parameter measurements were partitioned into 1,024 channels and recorded as dimensionless intensities. Each detected event is stored a $1 \times p$ vector for p measurement channels. As the identification of the events in each FCS file were known these data are used to construct gates and as training data for the supervised methods in chapters 4 and 5. In order to perform external validation of each of the data analysis methods described in this thesis, additional mixtures of QDEMs independent of the data

used for classifier construction were analysed (Table 4). All MPG was carried out using FCS Express from De Novo software (http://www.denovosoftware.com/).

Table 4 Composition of the multiplexed solutions (QDEMs included are shown). In total there were 10 tests with various QDEM mixtures (chosen at random). This dataset was used as an external validation of the classification methods described throughout the thesis. 500 events per QDEM in solution were recorded.

		Mixture #									
		1	**2**	**3**	**4**	**5**	**6**	**7**	**8**	**9**	**10**
QDEM code	**QD0000**	-	-	-	-	✓	-	-	✓	✓	-
	QD0001	-	-	-	-	✓	✓	-	✓	✓	✓
	QD0003	-	-	✓	✓	-	-	✓	-	-	-
	QD0010	-	-	-	-	-	-	✓	-	-	✓
	QD0011	✓	-	-	-	-	✓	-	✓	✓	✓
	QD0100	-	✓	-	-	✓	-	-	✓	-	✓
	QD0101	-	-	-	-	✓	-	✓	✓	✓	✓
	QD0110	✓	-	-	✓	✓	-	-	✓	✓	✓
	QD0111	-	-	-	-	✓	-	✓	✓	✓	✓
	QD0202	-	-	✓	✓	-	-	-	-	-	-
	QD1000	-	-	-	-	-	✓	✓	✓	-	✓
	QD1001	-	-	-	-	-	-	-	-	✓	✓
	QD1010	-	✓	-	-	-	✓	-	-	-	✓
	QD1011	-	✓	-	✓	-	✓	-	✓	✓	✓
	QD1100	✓	✓	-	-	-	✓	-	-	✓	✓
	QD1101	-	-	-	✓	✓	✓	✓	✓	✓	✓
	QD1110	✓	-	-	-	✓	✓	✓	✓	✓	✓
	QD1111	-	-	-	✓	-	-	✓	✓	✓	✓
	QD2100	-	-	✓	-	-	-	✓	-	-	-
	QD2200	-	-	✓	-	-	-	✓	-	-	-
#Codes		4	4	4	6	8	8	10	12	12	15

Using the external validation set described above requires the determination of the number of misclassifications and allows direct comparison between all classification methods to be drawn. The number of misclassifications for each mixture is calculated as opposed to the number of correct classifications as the identity of each event in the training is not known. While an event may have been classified as a QDEM added to a particular solution, there is no guarantee that the identified class is a true positive (TP). Hence, the number of misclassifications is a more reliable performance measure, as QDEMs included in the mixtures were known and therefore the false positive results can

be calculated. The misclassification rate (MC rate) is calculated as the number of events classified as those not present in a particular mixture as a percentage of total events classified in that mixture.

However, when the number of QDEM types present in a single solution is large the MC results should be treated with caution as the probability of a false positive correct classification increases. To this end the variance of correct classifications was calculated. Assuming that each mixture solution of QDEMs was homogenous, there is expected to be some variation (instrumental and preparation of solutions) between the correct classifications in each mixture solution, a large degree of variation could be indicative of misclassifications between QDEMs present in the mixtures. Therefore, as a further measure of performance the CC variance (σ^2) was calculated as follows:

$$\sigma^2 = \frac{\sum (x - \mu)^2}{N} \qquad \textbf{(3.1)}$$

Where:
x = number of events classified for QDEMs known to be present
μ = mean true positive events
N = total number of classifications for events known to be present

The calculation of the MC rate and CC variance and thus should allow the performance of each classifier to be determined - especially when the number of QDEMs in the mixture is large - to be elucidated more accurately.

3.4.3 Results and discussion

Initial analysis of QDEM FCM data

In total 19,796 events were obtained to characterise the library, only 796 events were obtained from the QD1100 microsphere most likely due to diminished stock solution concentration. Shown below are bivariate plots of the four channels for three QDEM subpopulations (Figure 15). The multiplex test samples were also analysed, 500 events per QDEM in each test were acquired.

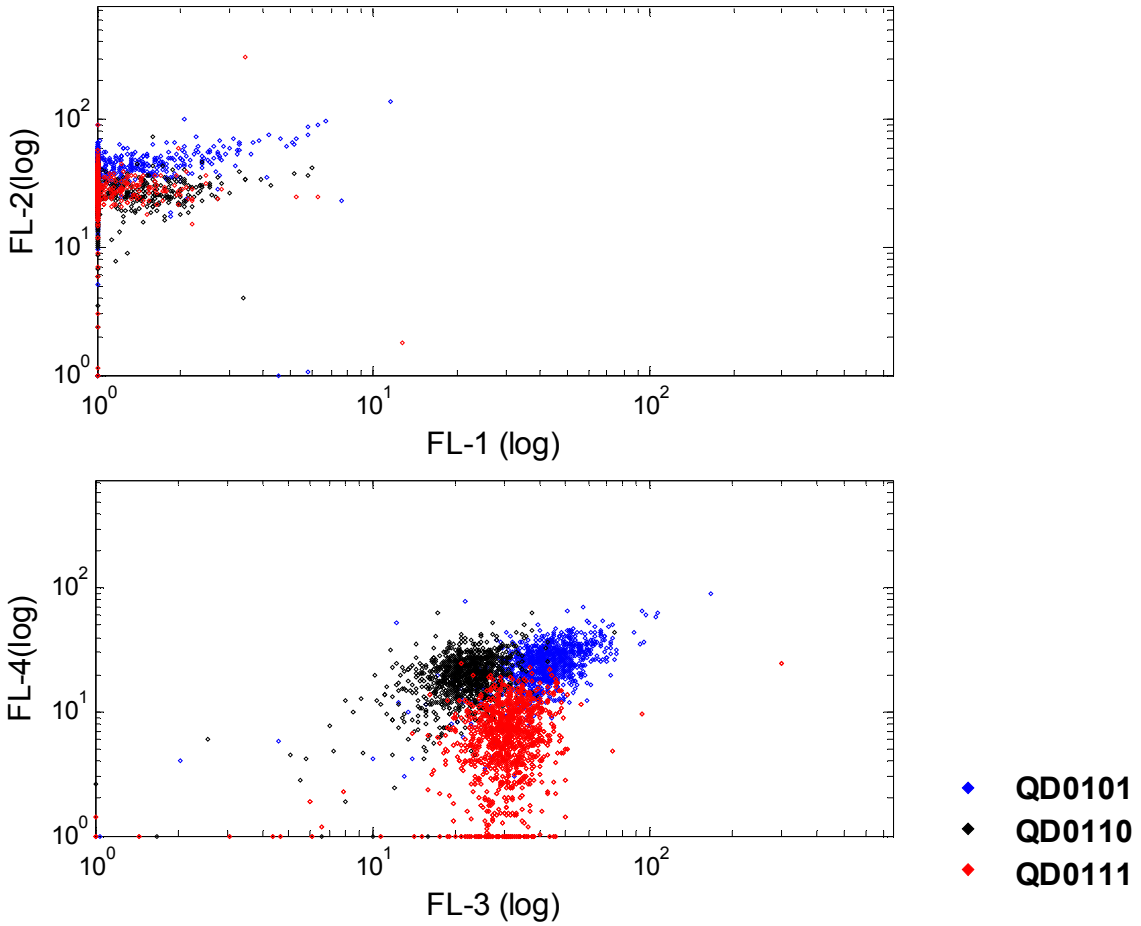

Figure 15 Logarithmic bivariate plots of QD0101 (blue), QD0110 (black) and QD0111 (red).

A high coefficient of variation (CoeffV), a measure of the precision, was observed for each of the populations. While the populations CoeffVs were at the high end of acceptability the QDEMs used in this study are one of the few commercial nanocyrstal encoded libraries available and should stretch the performance of the standard methods and fully test the techniques under investigation in the following chapters.

Closer examination of the data was conducted by means of a boxplot (Figure 16). Boxplotting is an informative display method for multiparameter FCM data. The median fluorescence intensity (MFI) of each flow cytometer channel is shown for each QDEM population. The boxplot also reveals the presence of outliers (events lying beyond 1.5 × IQR of the measurement channel) in each QDEM dataset. Outliers in the results were possibly due to inherent variation in the instrument, run to run contamination and/or errors in microsphere manufacture. The removal of these spurious events would have a beneficial effect on QDEM recognition methods; however the software from which MPG is applied have no means of outlier removal. Chapter 4 describes the implementation of an outlier removal algorithm.

Overspill between parameters for the QDEMs (e.g. the QD1111 boxplot) is evident meaning the fluorescence is not uniform across all detectors. This result was expected as no compensation was applied to the results to correct for overspill. There is little variation in SSC and FSC measurements due to the application of a gate during acquisition to remove possible microsphere aggregates and doublets and damaged beads from the results.

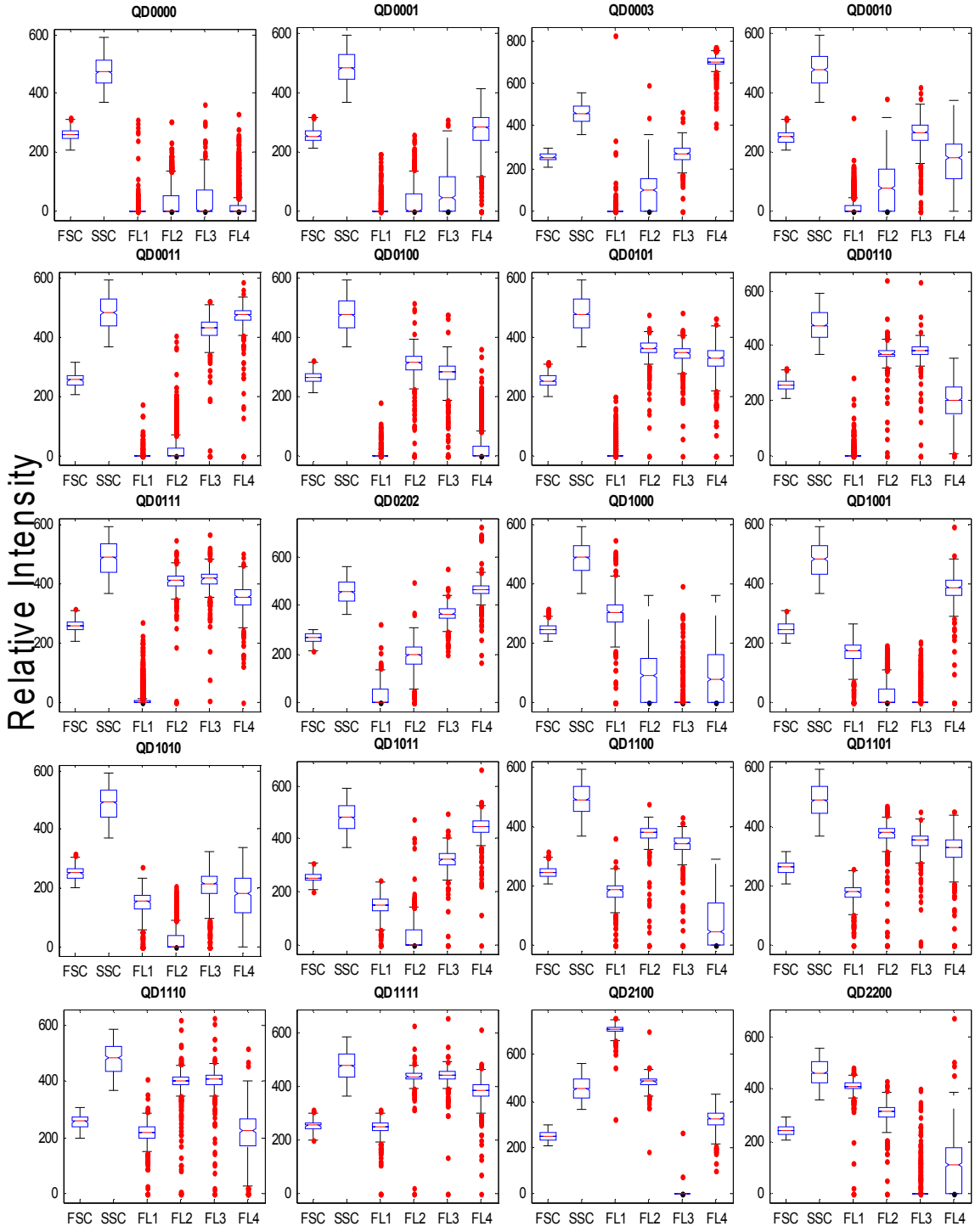

Figure 16 Box and whisker plot of each QDEM FCM population (Table 2). The 25-75th percentile of the data is contained within the boxes; the median is represented by the horizontal axis. Outliers (beyond 1.5 × IQR) are represented by dots. Data is gated on FSC and SSC channels to remove malformed beads and aggregates. (FL1 = 525nm, FL2 = 575nm, FL3 = 625nm, FL4 = 675nm).

Evaluation of multiparameter gating

The first of the classification methods, MPG (section 3.4.1), was employed to differentiate QDEMs from the multiplex testing set (Table 4). A combination gate was defined by manually "drawing" a gate around each of the individual QDEM subpopulations on bivariate histograms and then linking the gates over multiple parameters using Boolean logic (Figure 17). The FCSexpress FCM software suite was used to accomplish this task. To compensate for possible errors in MPG due to outliers the regions were manually tuned to attempt to select the QDEM gates that yielded the lowest misclassification on the training data. Defining the gates required for the QDEM library was a complex, subjective and time consuming process (~45 min), which increases exponentially as the numbers of codes are increased. These concerns would be exacerbated at higher levels of multiplexing with additional QDs and intensity levels. To assess the accuracy of MPG the multiplex QDEM solution data (Table 4) was presented to the combination gates.

Shown below are the number of events recorded for each of the ten tests (an allocation of 500 events per QDEM set), the first point to note about MPG classification results is there are more classifications made on the data than events recorded on the flow cytometer (Table 5). Thus certain events are classified as belonging to two or more populations. Even with painstaking adjustment in order to optimise the gates, the optimum regions for each QDEM were not defined. As stated above the MC rate was used to evaluate the results on the mixture solutions as the actual classes of events were not known.

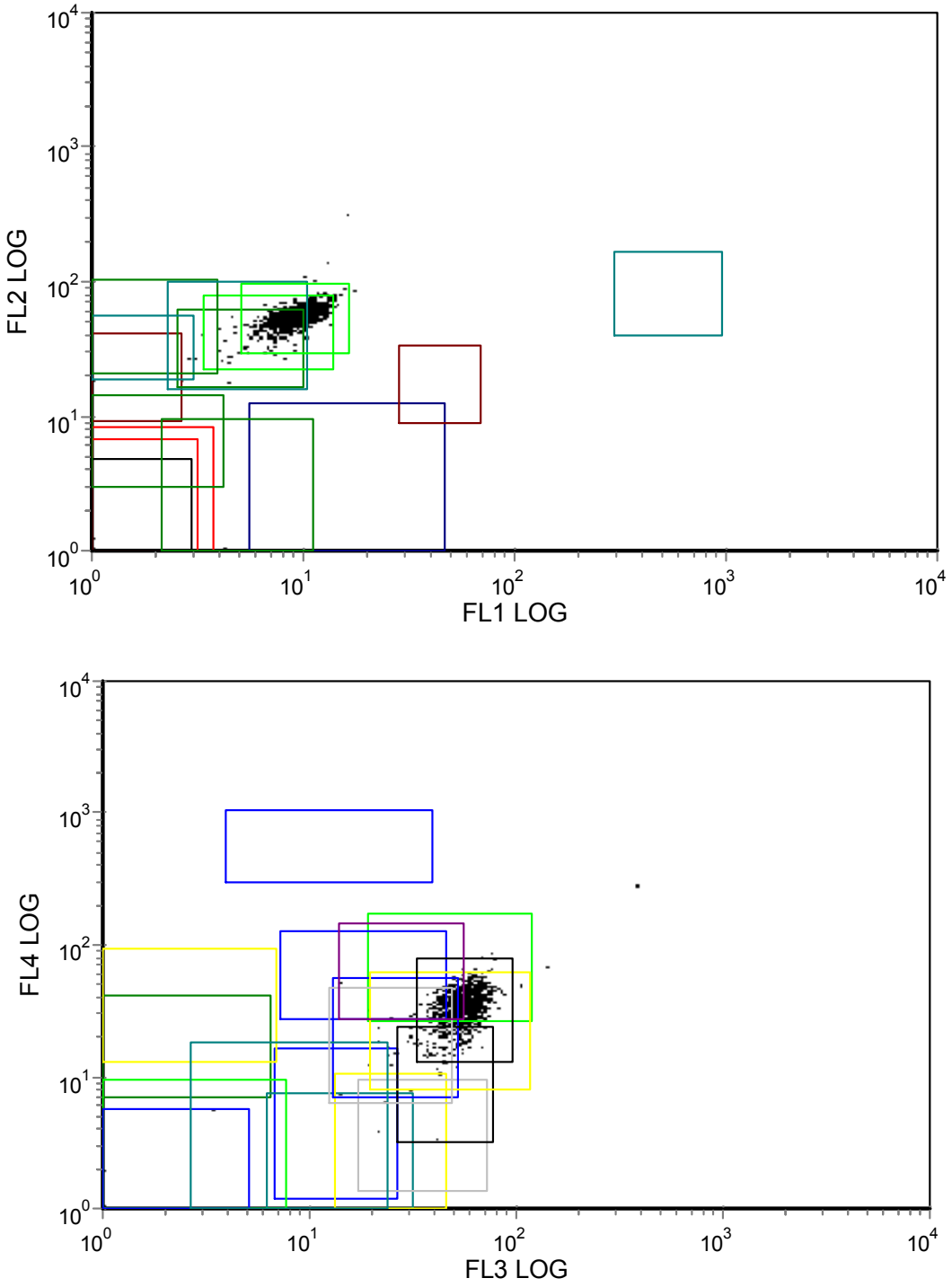

Figure 17 Combination gating of QDEM library. Each of the twenty gates is set individually on each microsphere population. The gates were adjusted to give the best performance on each individual microsphere population. The population is shown above is QD1111, the empty gates were defined the other populations in sequence. Future mixed subpopulation FCM data can then be presented to the gates for classification.

Table 5 FCM analysis of QDEM mixture solutions using MPG. QDEMs present in each mixture are highlighted. The MC rate for each of the mixture solutions is shown and is a more appropriate measure for classifier evaluation in comparison to the correct classifications for reasons outlined above (section 3.4.2). The CC variance was also calculated.

		Mixture #									
		1	**2**	**3**	**4**	**5**	**6**	**7**	**8**	**9**	**10**
QDEM code	**QD0000**	7	25	0	5	**610**	148	10	**599**	**357**	79
	QD0001	0	3	1	1	**232**	**362**	3	**345**	**265**	**535**
	QD0003	0	0	**559**	**608**	0	0	**523**	0	0	0
	QD0010	0	24	0	8	6	38	**489**	10	11	**330**
	QD0011	**558**	3	89	95	0	**568**	0	**363**	**419**	**488**
	QD0100	137	**517**	0	129	**585**	7	11	**446**	126	**410**
	QD0101	223	1	0	174	**1303**	1	**824**	**1069**	**1414**	**1287**
	QD0110	**387**	17	0	**366**	**531**	1	4	**440**	**450**	**420**
	QD0111	172	0	0	122	**1234**	3	**868**	**1090**	**1435**	**1418**
	QD0202	27	7	**210**	**275**	0	33	0	29	35	70
	QD1000	0	145	27	0	0	**551**	**519**	**330**	0	**446**
	QD1001	0	7	0	0	0	5	0	2	**311**	**364**
	QD1010	2	**531**	0	25	1	**510**	61	8	16	**450**
	QD1011	1	**516**	20	**361**	0	**466**	0	**432**	**660**	**510**
	QD1100	**310**	**242**	0	13	270	**444**	40	267	**369**	**357**
	QD1101	137	15	0	**326**	**453**	**615**	**304**	**633**	**589**	**636**
	QD1110	**542**	26	0	128	**533**	**689**	**351**	**943**	**792**	**857**
	QD1111	83	0	0	**484**	91	115	**272**	**702**	**606**	**698**
	QD2100	0	0	**472**	0	0	1	**533**	1	0	4
	QD2200	0	0	**679**	0	0	0	**770**	0	0	0
# QDEM codes		4	4	4	6	8	8	10	12	12	15
#Events		2000	2000	2000	3000	4000	4000	5000	6000	6000	7500
#Classified		2586	2079	2057	3120	5849	4557	5582	7709	7855	9359
#Correct		1797	1806	1920	2420	5481	4205	5453	7392	7667	9206
CC rate (%)		69.4	86.8	93.3	77.5	93.7	92.2	97.6	95.8	97.6	98.3
σ^2		**14565**	**19554**	**39602**	**14806**	**143543**	**10622**	**45276**	**77979**	**158699**	**110174**
MC rate (%)		**30.6**	**13.2**	**6.7**	**22.5**	**6.3**	**7.8**	**2.4**	**4.2**	**2.4**	**1.7**

The MPG method performed poorly on the multiplex testing sets, there was a significant error for each of the first six sets with the worst multiplex mixtures identified as set 1 where 30.6% of events were misclassified. The average MC rate for the 10 tests was 9.7%. However the number of dual classifications was nearly 1900, reducing confidence in the classifications made at higher levels of multiplexing (tests 7 to 10). Furthermore the σ^2 increases for these tests, a high degree of variance between correct classifications

suggest that false positive results are present (Figure 18) and the number of QDEMs in solution masked the performance of gating, (i.e. misclassified events are more likely to fall into a present microsphere gate as additional QDEMs are added). It is more likely that multiplex solutions 1-6 reflect the true performance of the classification method, the average MC rate for these solutions was 14.5%.

3.5 Improving on MPG – the case for research

The limitations of MPG were shown for the identification of QDEMs. The MPG accuracy was questionable for the mixture solutions (Figure 18) with an average MC rate of 9.7% observed. Results on the solutions containing 10 or more QDEMs where the MC rate decreases should be treated with caution as the variance between the correct classification increases.

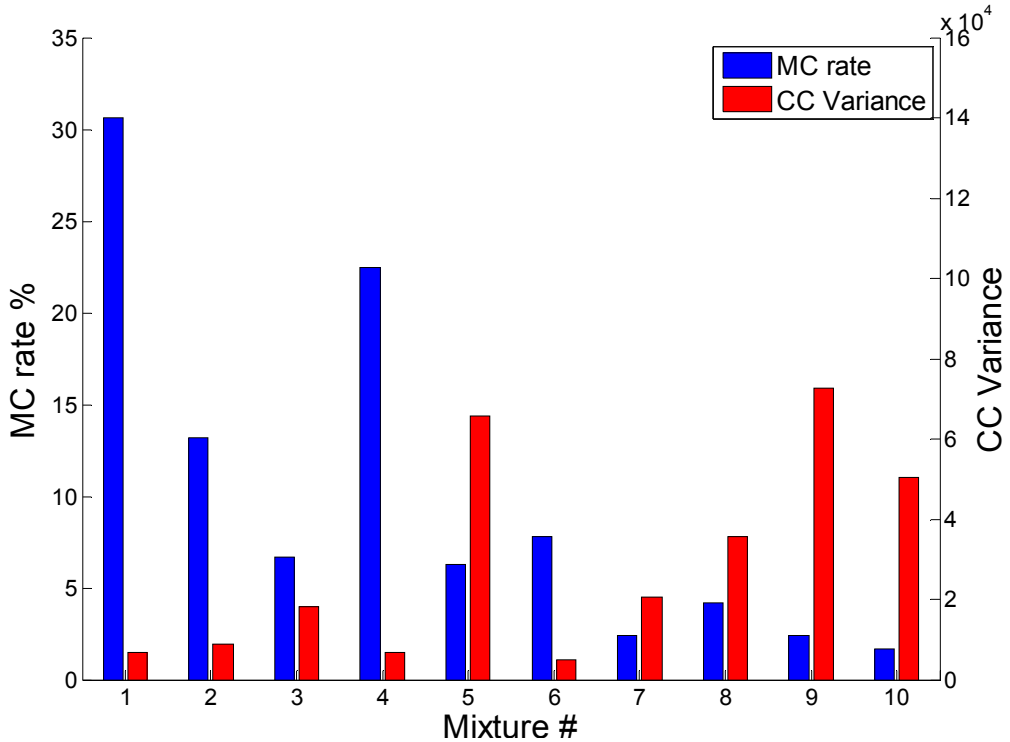

Figure 18 Performance of the MPG for the ten mixture sets. The MC rate of the gating system for each test is shown in descending order. The average MC rate was 9.7%. The CC variance of classifications on solutions containing more QDEMs is increased suggesting misclassifications within these solutions.

Moreover a large number of dual classifications were observed, these were the result of classes lying on the decision boundaries (gates). The technique was also time-consuming, requiring the interpretation of a skilled operator; and there was no assurance that the optimum regions had been defined.

When the number of parameters increases the number bivariate plots required increases exponentially and the interpretation of plots becomes more difficult. The classification accuracy of the MPG would decrease further, moreover MPG be would become even more complex and time consuming. Hence utility of graphical methods such as MPG in polychromatic FCM analysis of QDEMs is limited, and these methods are unsuitable for extension of encoded microsphere populations required for bioanalytical studies. It is on this rationale that this work is based; in the following chapters two supervised learning algorithms are applied to investigate accurate automated discrimination of QDEMs of single events in FCM to improve upon the performance of MPG.

Recently a number of machine learning algorithms for multivariate pattern recognition have been applied for FCM subpopulation identification. The remainder of this thesis describes the construction and evaluation of two popular supervised learning methods, SVMs and ANNs. Such techniques would allow automation and optimisation of the MPG in multidimensional space, and remove the subjectivity of user defined classification boundaries. Moreover these methods would allow the majority of FCM instrumentation present in a wide variety of locations, such as the EPICS XL to remain viable for SAT.

Chapter 4: Support vector machines for the identification of QDEMs from FCM data.

4.1 Introduction

Chapter 3 demonstrated the need for improvement in current methods of QDEM classification. The overall aim of this research was the development of a rapid automated classification method for QDEMs overcoming the limitations of multiparameter gating and unsupervised methods. To this end, multivariate supervised techniques (such as SVMs and ANNs) offer a novel solution worthy of further investigation. In this chapter the theory of supervised learning (section 4.2.1), SVMs (section 4.2.2) and multiclass SVM implementations (section 4.2.3) are described. SVMs are used in a wide range of applications including bioinformatics and biospectroscopy [134-136], and several examples of such methods for the identification of subpopulations from FCM data are presented (section 4.2.4). The methodology for the construction and performance evaluation of an SVM classifier for QDEMs is presented (section 4.3) and the comparison of the SVM to MPG described in chapter 3 discussed (section 4.4).

4.2 Support vector machines

4.2.1 Supervised learning

Supervised learning techniques are trained on previous examples with known classifications thus "learning" the underlying patterns within the data; such models are then applied to previously unknown examples in order to make a prediction. Pattern recognition models construct a classification rule from known examples (*training data*) to recognise unknown examples. Given a training set consisting of input and output pairs, $Z = \{(x_1, y_1), (x_2, y_2), ..., (x_i, y_i)\}$, the aim of training is to produce a function f which maps

the input vectors $x \in X$ to the corresponding class labels $y \in Y$ to allow the prediction of unknown samples. SVM and ANN are examples of popular supervised learning algorithms, the following section details SVM theory while chapter 5 deals with ANNs.

4.2.2 Fundamentals of support vector machines

SVMs are a widely used supervised learning algorithm developed by Vapnik [137]. The popularity of SVMs stems from advantages such as the use of kernels for non-linearly separable data (known as the kernel trick), no local minima, sparseness of the solution, and capacity control (important for good generalisation) obtained by optimising the decision boundary in the margin between classes [136, 137]. SVMs have been shown to outperform similar supervised classification methods such as artificial neural networks and linear discriminant analysis (LDA) in many instances due to a high generalisation ability (ability to classify unknown samples) and robustness to high dimensional data [136].

In terms of classification, for a linearly separable two class problem with class labels +1 and -1, SVMs locate a boundary of separation (hyperplane) to identify the two classes. A generalised hyperplane function is shown below (Eqn 4.1) [138].

$$f(x) = \langle w \cdot x \rangle + b \tag{4.1}$$

Where w is termed the weight vector and b is the bias.

While SVMs share similarities with linear discriminant analysis and perceptrons which also aim to find the separating hyperplane between two classes, the use of simple hyperplanes in LDA and perceptrons is limited as a unique solution does not exist. The best separating hyperplane may not be found as there may be many hyperplanes that separate the data (Figure 19), decreasing the classifiers generalisation ability [136].

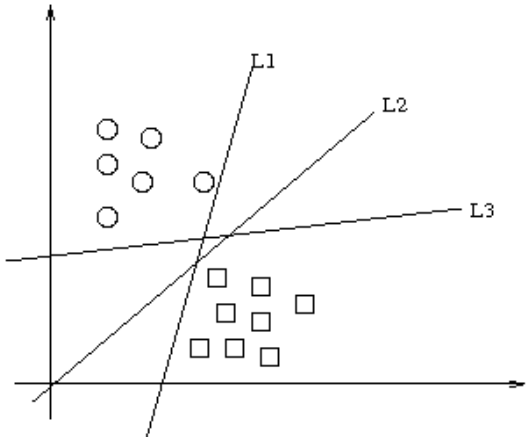

Figure 19 Many hyperplanes can be located for any given dataset. LDA suffers from drawbacks in that the best decision boundary may not be found. SVM overcomes this through optimisation of the maximal margin hyperplane (see below).

SVMs calculate the optimum hyperplane (maximal margin hyperplane) yielding the best generalisation, avoiding overfitting (memorising the training data, thus unseen examples may be misclassified) (Figure 20). The maximal margin hyperplane is determined from X by minimizing the norm of w by means of a constrained optimisation by minimisation of a quadratic function under linear equality constraints (Eqn 4.2) [136].

$$\begin{aligned} &\text{Minimize:} && \frac{1}{2}\|w\|^2 \\ &\text{Such that:} && yi\left(w \cdot x_i + b\right) \geq 1_i \text{ for } i = 1,....n, \end{aligned} \qquad \textbf{(4.2)}$$

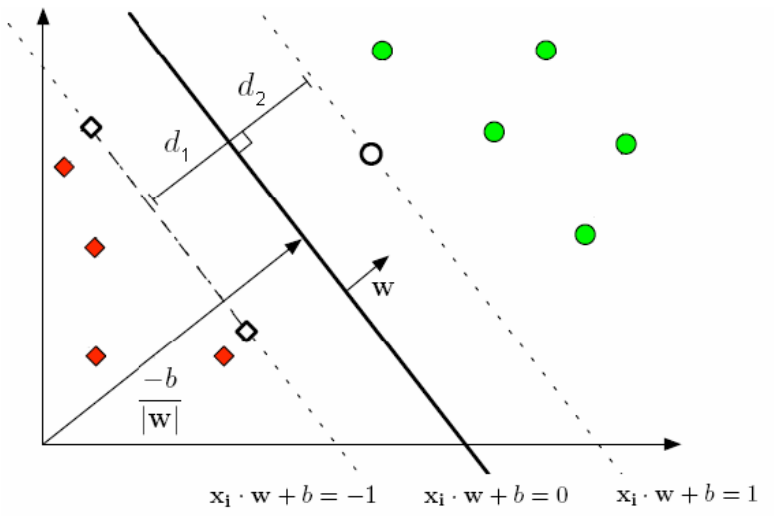

Figure 20 Representation of the SVM solution applied to a linearly separable two class problem. The classes are shown as red diamonds and green circles. The hyperplane is shown as a dark black line. Support vectors (SV) (see below) for each class are shown as blanks shapes.

Location of the maximal margin classifier alone does not take into account the training error of the dataset leaving the SVM susceptible to the effects of noise; as a result more robust margin methods that can tolerate noise, outliers and consider more training points apart from those on the margin were developed. The so-called slack variables and penalty parameter are introduced (Eqn 4.3) allowing the margin to be crossed creating a "soft" hyperplane. The penalty parameter C punishes outliers during the training process and controls the trade off between training errors and model complexity. Slack variables, ξ_i are introduced to allow the margin constraints to be overcome during optimisation to avoid overfitting to noisy data [136, 137].

Minimize: $$\|w\|^2 + C\sum_{i=1}^{n}\xi_i, \qquad \textbf{(4.3)}$$

Such that: $$yi(w \cdot x_i + b) \geq 1 - \xi_i \text{ and } \xi_i \geq 0 \text{ for } i = 1,....n,$$

The resulting decision function is illustrated below (Eqn 4.4), where the constants α_i are called Lagrange multipliers and are determined during the optimisation of the SVM. SV are the support vectors, for which $\alpha_i > 0$, which lie closest to the optimal hyperplane. For the remaining patterns the $\alpha_i = 0$.

$$f(x) = \sum_{x_i \in sv} y_i \alpha_i x_i \cdot x + b \qquad \textbf{(4.4)}$$

The above hypothesis holds only for linearly separable data, many applications in real world analysis tend to be of a non-linear nature. LDA is limited in this regard and failures of the perceptron were exposed by Minsky and Papert in the 1960s [139], leading to the development of multilayer neural networks (see chapter 5).

SVMs however employ kernels to map the data to a high dimensional feature space where the examples become linearly separable and the SVM classification can proceed (Figure 21) [136-138]. Choosing the correct SVM kernel is similar to the choice of ANN architecture and is critical to model performance [136], there are a number of commonly used kernels (Eqn 4.5-4.8) and custom functions can also be written for a particular application. Perhaps one of the main advantages in terms of the application of SVMs is that by using kernels the learning algorithm can be decoupled from the application area. Classification in the high dimensional feature space is not, however without complications, computational expense increases due to the large vectors and high dimensionality may cause overfitting, however SVMs offset any decrease in generalisation ability of the classifier through location of the maximal margin classifier [138].

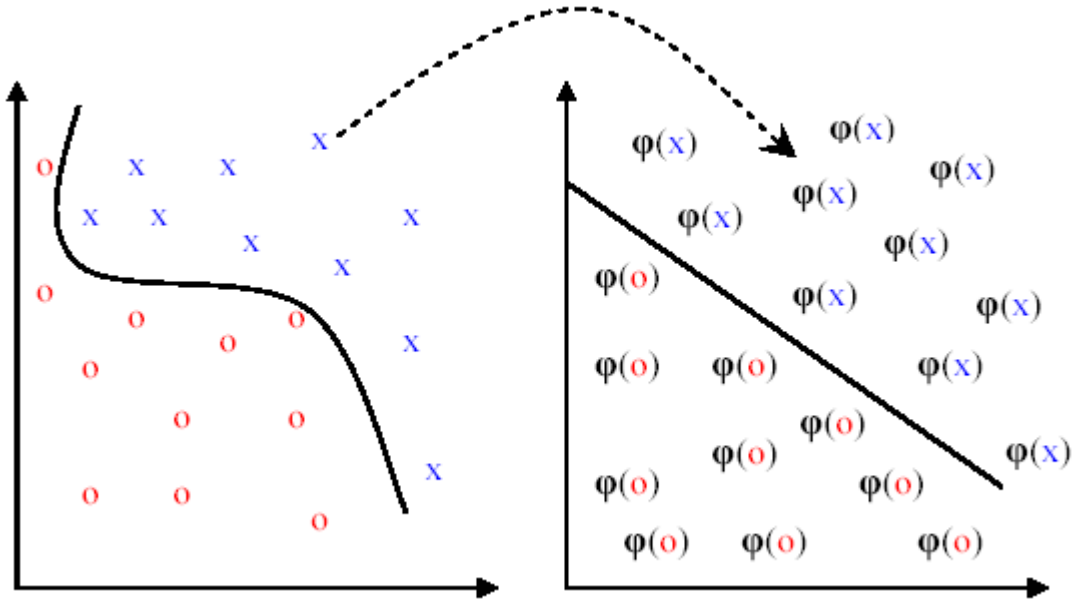

Figure 21 Kernel mapping. The inputs space is projected to the feature space using a kernel. Linear classification is possible allowing non-linear classification where LDA fails.

Commonly used SVM Kernels

Linear Kernel:
$$K(x_i, x_j) = K(x_i^T x_j) \tag{4.5}$$

RBF kernel:
$$K(x,z) = \exp\left\{\frac{|x-z|^2}{2\sigma^2}\right\} \tag{4.6}$$

Sigmoidal:
$$K(x,z) = \tanh(\gamma x.y - \delta) \tag{4.7}$$

Polynomial:
$$K(x,z) = \left(x^T z + 1\right)^q \tag{4.8}$$

4.2.3 Multiclass support vector machines

Thus far only binary SVMs capable of separating two classes from one another have been considered; however a classification system for QDEMs requires the identification of multiple classes. Various approaches have been utilised for extension of the SVM formulation to all classes such as the Vapnik and Weston approach which aims to solve the multiclass problem using a single optimisation [140], [141], binary trees and fuzzy logic methods are also suggested in the literature but so far all have had limited success due to time consuming implementation, the requirement of *a priori* knowledge and the use of clustering or vector quantisation algorithms to determine classifier hierarchy [142, 143]. For multiclass problems several methods exist that combine binary SVM classifiers to create multiclass SVMs. The most popular schemes are the one versus rest (OVR), and the one versus one (OVO) method using majority voting and pairwise coupling [140, 144]. In this thesis only the OVR and OVO methods are employed, it is important to note several other methods exist but the methods outlined above have had the greatest success [145].

The OVR approach and OVO are two common methods of error output coding (ECOC) [146]. When combining binary SVMs an ECOC scheme is used to combine classifier outputs to yield the final prediction. For a K-class problem; when a pattern is classified an output vector is produced by the SVM, this output vector consists of the output from K classifiers and the vector is subsequently mapped to the predicted label. Majority voting (cumulative number of classifications by each SVM) is the basis of class decision; the class which receives the most "votes" is the final class decision for the sample.

The OVR approach is one of the earliest and most widely used multiclass methods [147] and aims to construct K classifiers (one for each class). A hyperplane is formed so that the class under consideration is separated from K-1 classes (all other classes) (Figure 22). A majority type vote is applied to classify the new point, i.e. the outputs of each decision function are employed as the sole measure of class association. (Eqn 4.9)

$$class = \arg\max_{i=1,2,\ldots,K} \left(w_i \cdot x + b_i \right) \tag{4.9}$$

A limitation of the this method is the assumption that each of the classifiers are equally reliable which is not always the case in multiclass problems, and research is ongoing to assign each classifier a reliability measure [148]. Also an imbalance in the number of examples for each class in the training data can compromise the performance of OVR SVMs [147].

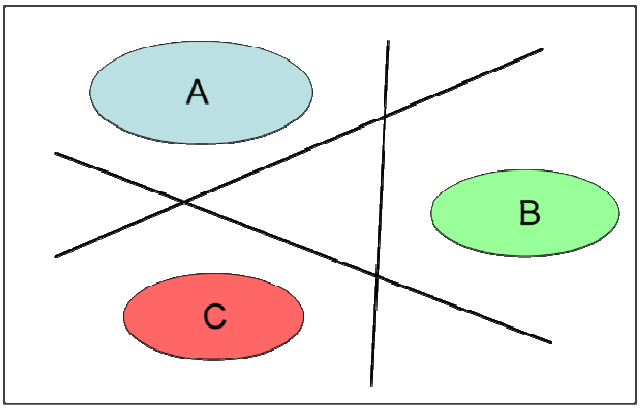

Figure 22 Illustration of the OVR approach. The hyperplanes for separation of each class from the rest are shown. Adapted from [143].

OVO multiclass SVMs create a classifier for each pair of classes resulting in $K(K-1)/2$ classifiers (Figure 23); each classifier is trained to separate between any two classes (i, j). The result is a $K \times K$ matrix where the classification is made by simply summing each row of the matrix for which the sum is maximal (Eqn 4.10):

$$class = \arg\max_{i=1,\ldots,K}\left[\sum_{j=1}^{K} fij\right], \tag{4.10}$$

Where, fij is the signed confidence measure for the ij'th classifier [146]. While the number of individual classifiers is greater than the OVO method, the individual training problems are significantly smaller and may also save on training time. Furthermore the runtime execution of the OVO multiclass SVM is decreased as there is less overlap between classes and individual SVMs require a smaller number of SVs for discrimination. However as stated above the output of different binary classifiers may not be directly comparable as classes may be of different sizes and or less separable from the rest of the data.

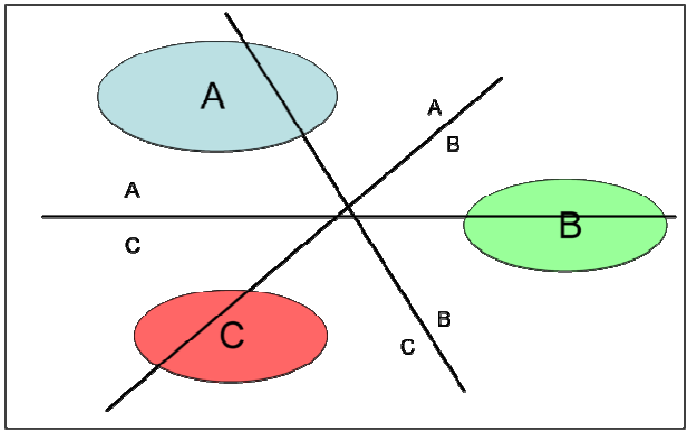

Figure 23 Illustration of the one versus all approach. An SVM is formed for each pair of classes. Adapted from [143].

4.2.4 Previous examples of SVM and flow cytometry data

Interest is growing for pattern recognition techniques in the FCM community as a result of increasing numbers of FCM parameters (more complex analysis), concerns over subjective gating [149] and the advent of flow based post-genomic assays [5]. There are a number of examples reported in the literature for the automated analysis of FCM data with SVMs improving upon traditional FCM data analysis in clinical diagnostics and research. Toedling *et al.* recently demonstrated the use of SVMs in the clinical setting. A radial basis SVM was constructed to automate the classification of leukemic cells from acute lymphoblastic leukaemia patients and compared to a traditional gating method performed by a skilled analyst. The SVM required no control sample group from healthy patients. There was a 99.06% agreement between analyst and SVM; moreover sensitivities of 99.78% and specificity of 98.87% were reported.

The classification of various types of white blood cells was demonstrated by Adjouadi *et al.* Samples from normal and abnormal patients could be identified with 95% and 86.67% accuracy respectively [150]. Quinn *et al.* described the use of a SVM for the identification of cellular viability and lineage in bone marrow cells. In this instance the optimum classifier was found to be an RBF ANN, the SVM misclassified 9.4% ± 2.8% in comparison to MPG; and 6.4% ± 1.3% for the neural network [151]. Analysis of highly variable complex phytoplankton data with SVMs has also been shown to be an effective data analysis method. RBF SVMs were utilised for the recognition of 60 species with a mean accuracy of 90% for each species, outperforming an RBF ANN by 13% [150, 152, 153].

4.3 Materials and methods

4.3.1 SVM training data preparation

The dataset for this study consisted of 1,000 FCM events, for each spectrally unique QDEM, excluding QD1100, of which there were 796 events. The data set described in the previous chapter 3 is therefore a 19,796 × 6 matrix (two scatter intensity and four fluorescence intensity measurements [FSC, SSC, FL1@525nm, FL2@575nm, FL3@625nm and FL4@675nm]), and forms the training data for the SVM. QDEMs were analysed individually and the identity of each event in the training data was known, allowing the application of supervised learning methods for classification. See chapter 3 for more information on acquisition of the training data.

Each of the 20 LMD files containing the training data was imported into MATLAB. Mild and extreme outliers resulting from inherent FCM variation and/or variation in QDEM manufacture were removed beyond 1.5 times the interquartile range (IQR) of each parameter [154], reducing the training set by 1,242 events (6.27% of the total events). The effect of removing the mild and extreme outliers from the training dataset was determined.

Building an SVM classifier has three main phases; parameter selection, training and independent test set validation. The training data and corresponding class labels were randomised and divided to form the *cv_set* (25%), *train_set* (50%) and *test_set* (25%) providing independent data for each of the respective phases (Figure 24). The datasets were then converted to sparse data format files for input to the LIBSVM program (section 4.3.2).

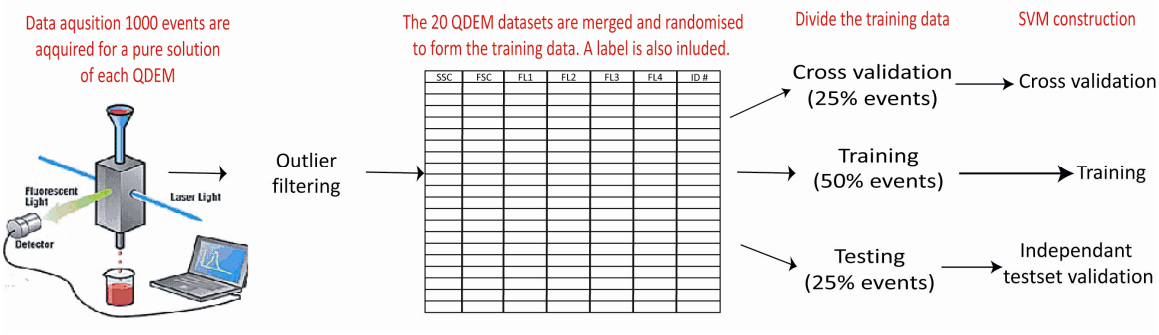

Figure 24 SVM training data preparation. Each QDEM solution is measured individually and combined with the class labels for each QDEM to form the training data. The data is randomised and split to form the datasets for parameter selection, training and testing. An identical procedure is used in chapter 5.

Note: *The MATLAB code for data import, removal of the outliers and conversion to LIBSVM format are available on the CD accompanying this thesis.*

4.3.2 SVM implementation

To implement the SVM algorithm the freely available stand alone package LIBSVM, based on sequential minimal optimisation algorithm (SMO), by Chang and Lin [155], featuring multiclass classification and probability estimates was used. LIBSVM returns probability estimates for each classification based on pair-wise coupling, the class with the highest pair-wise probability is returned as the predicted class [156]. SVM construction and prediction was preformed on a Linux server, with AMD 64 X2 4400+ (dual core) and 4 GB RAM.

4.3.3 SVM model selection and training

Training an SVM model begins by choosing a kernel and varying the SVM settings to return the most suitable model. The generalisation properties of SVMs are governed by a set of meta-parameters (i.e. penalty parameter C) and kernel specific parameters (i.e. RBF γ parameter). The process by which the optimal values are chosen is known as model

selection [157]. A grid based parameter search was carried out to locate the optimum SVM kernel and parameters for the *train_set*. The accuracy of the SVM solution at each parameter setting was assessed using *n*-fold cross-validation, CV has been demonstrated to yield an almost unbiased estimate of the generalisation ability of a model, and most representative of the performance [158].

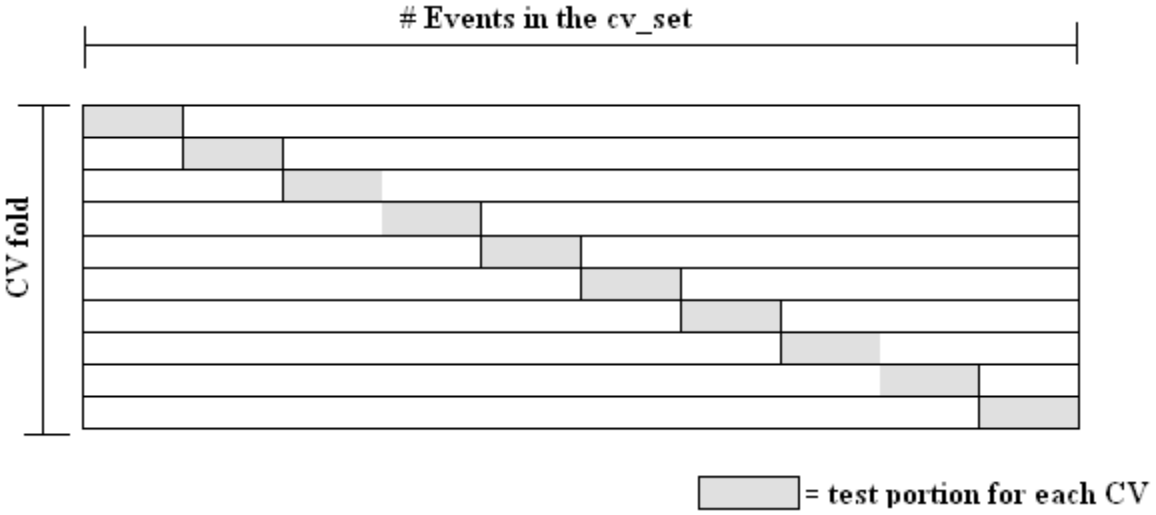

Figure 25 Graphical representation of *n*-fold CV. A ten fold CV method was used to select the optimum parameters for the SVM.

During the CV procedure the *cv_set* was split into ten subsets. During the first pass, data from splits 1-9 are used to train a SVM. The 10th part is used to test the performance of the model (Figure 25). The process continues until all of the data splits are the test set. An average of the performance of each pass, the CV accuracy (cv_{acc}) expressed as a percentage of correct classification was calculated. The settings which yield the maximum cv_{acc} are chosen to construct the final classifier. The accuracy of the model upon the *train_set* ($train_{acc}$) and *test_set* ($test_{acc}$) (section 4.3.4) was calculated in order to choose the best model.

CV was carried out using the Linear and RBF kernel to create linear and non-linear solutions for QDEM classification. For the linear kernel the penalty parameter, C, is varied, however with the RBF kernel C and the width of the RBF function, γ, is also varied in order to construct the optimum SVM. The penalty parameter was varied from 1×10^{-6} to 10 with the linear kernel and RBF kernel. The γ parameter was also varied for the RBF kernel from 1×10^{-4} to 50. The effect of removal of outliers was investigated, and the OVR and OVO multiclass SVM designs were also compared. Once the best solution was determined, the *train_set* was used to train the appropriate SVM model.

4.3.4 SVM validation

An independent validation of the SVM was carried out using the previously unseen *test_set*. From the *test_set* predictions a confusion matrix was plotted to determine the performance of each individual class [159]. A confusion matrix allowed the behaviour of each individual class within the entire classification model to be observed. The well known indicators accuracy, specificity and sensitivity/recall (see below) were calculated from the independent *test_set* confusion matrix for each QDEM class. Firstly accuracy is defined as the probability that a random event will be classified correctly (See Eqn 4.11). Specificity can be defined as the probability of correct negative prediction (See Eqn 4.12). Sensitivity can be defined as the probability of correct positive classification (Eqn 4.13). Both sensitivity and sensitivity are calculated for each individual class considered by the model.

$$Accuracy = \frac{TP + TN}{(TP + TN + FP + FN)} \quad \textbf{(4.11)}$$

$$Specificity(S) = \frac{TN}{TN + FP} \quad \textbf{(4.12)}$$

$$Sensitivity(R) = \frac{TP}{TP + FN} \quad \textbf{(4.13)}$$

Where:

TP = True positives - the number of QDEMs labelled correctly.

FP = False positives - the number of QDEMs incorrectly labelled.

TN = True negatives - number of QDEMs correctly predicted not to be the specified QDEM.

FN = False negatives - number of QDEM predictions that were classified as negative but were actually positive [160, 161].

These performance measures are more likely to reflect the actual performance (and overfitting risk) when applied to examples not seen in the training set. As a further measure of the SVM, the classifications on the multiplex testing sets described in the previous chapter were presented to the classifier. The multiplex test solutions were acquired independently of the training data reveal the ability of the SVM to discriminate multiple QDEMs in a single solution acting as an external validation of the model. The resulting MC rate for these external testing set were calculated for the direct comparison to MPG described in chapter 3.

Note: *See the CD accompanying this thesis for MATLAB code to construct confusion matrices and calculate the performance indicators.*

4.4 Results and discussion

The following section describes the results obtained during the construction and evaluation of an SVM for QDEM recognition. The optimum kernel and SVM parameters are selected for the dataset (section 4.4.1 SVM parameter selection, the effect of outlier removal on SVM performance is investigated (section 4.4.2), and the OVO and OVR SVM multiclass methods compared (section 4.4.3). The selected model performance is further demonstrated through independent test set validation (section 4.4.5) and an external validation with the multiplex tests (section 4.4.6). Finally the SVM is compared to the MPG method outlined in chapter 3 (section 4.4.6).

4.4.1 SVM parameter selection

The primary step in model selection was the identification of the most suitable kernel. From the outset it was observed that the polynomial and sigmoidal kernels had a higher computational expense and classification rates were poor (~30% less than linear and RBF kernels), therefore parameter selection for only the linear and RBF kernels was conducted to construct the optimum model for classification of the QDEM dataset in both linear and non-linear SVM modes. CV was performed for each SVM parameter combination to determine the optimum settings for the model. The train and test accuracies were also calculated as additional indicators. In the case of SVM linear kernel the penalty parameter C was varied from 1×10^{-6} to 10. RBF SVM parameters were also examined in the same manner as the linear kernel; *C* was chosen first and varied over the same range as the linear kernel. Once *C* had been identified, the width of the RBF function (γ) was varied from 1×10^{-4} to 50.

Table 6 SVM model selection. The cv_{acc}, $train_{acc}$ and $test_{acc}$ of each kernel and SVM parameter setting. The best model settings for the linear and RBF kernel are highlighted.

Kernel	Parameters		cv_{acc}(%)	$train_{acc}$(%)	$test_{acc}$ (%)
	C	γ			
Linear	0.000001	----------	5.80	25.80	24.92
Linear	0.00001	----------	6.10	52.19	50.77
Linear	0.0001	----------	5.88	36.53	36.69
Linear	0.001	----------	6.74	78.84	78.30
Linear	0.01	----------	63.45	92.54	92.04
Linear	0.1	----------	94.97	95.83	96.08
Linear	**1**	----------	**96.58**	**96.72**	**96.33**
Linear	2	----------	96.07	96.83	95.38
Linear	5	----------	95.79	96.64	96.10
Linear	8	----------	96.11	96.90	95.88
Linear	10	----------	95.92	96.87	95.77
RBF	0.000001	1	5.47	52.03	52.75
RBF	0.00001	1	5.84	39.4	39.13
RBF	0.0001	1	5.71	51.23	52.04
RBF	0.001	1	5.62	39.9	40.66
RBF	0.01	1	5.71	55.63	55.15
RBF	0.1	1	27.02	85.81	85.92
RBF	1	1	18.21	87.36	86.93
RBF	2	1	89.43	95.25	95.38
RBF	5	1	95.25	96.48	96.13
RBF	8	1	95.92	96.7	96.08
RBF	10	1	95.75	96.58	95.57
RBF	5	0.0001	8.19	77.35	75.87
RBF	5	0.001	67.09	92.71	92.75
RBF	5	0.01	94.76	96.19	96.01
RBF	5	0.05	96.48	96.34	95.98
RBF	5	0.1	96.55	96.49	95.70
RBF	5	0.5	96.44	96.85	95.24
RBF	5	1.5	96.29	97.67	95.38
RBF	**5**	**2**	**95.32**	**97.56**	**96.16**
RBF	5	2.5	95.64	97.95	95.92
RBF	5	5	94.58	98.51	95.64
RBF	5	8	94.84	98.88	95.12
RBF	5	10	94.76	97.21	95.01
RBF	5	12	93.61	99.29	94.58
RBF	5	15	92.02	99.38	94.35
RBF	5	20	91.44	99.62	94.35
RBF	5	30	87.17	99.82	94.17
RBF	5	50	78.28	99.96	89.99

The linear kernel demonstrated the best performance with cv_{acc} (96.58%), $train_{acc}$ (96.72%) and $test_{acc}$ (96.33%) with penalty parameter C = 1 (Table 6). Beyond C = 1 the cv_{acc} and the $test_{acc}$ decrease slightly and the $train_{acc}$ increases slightly (Figure 26). It has been shown that after a certain point increase of the penalty parameter when using the linear kernel does not increase the performance of the model [162]. Total training time was ~3.5 min (average of ten SVMs).

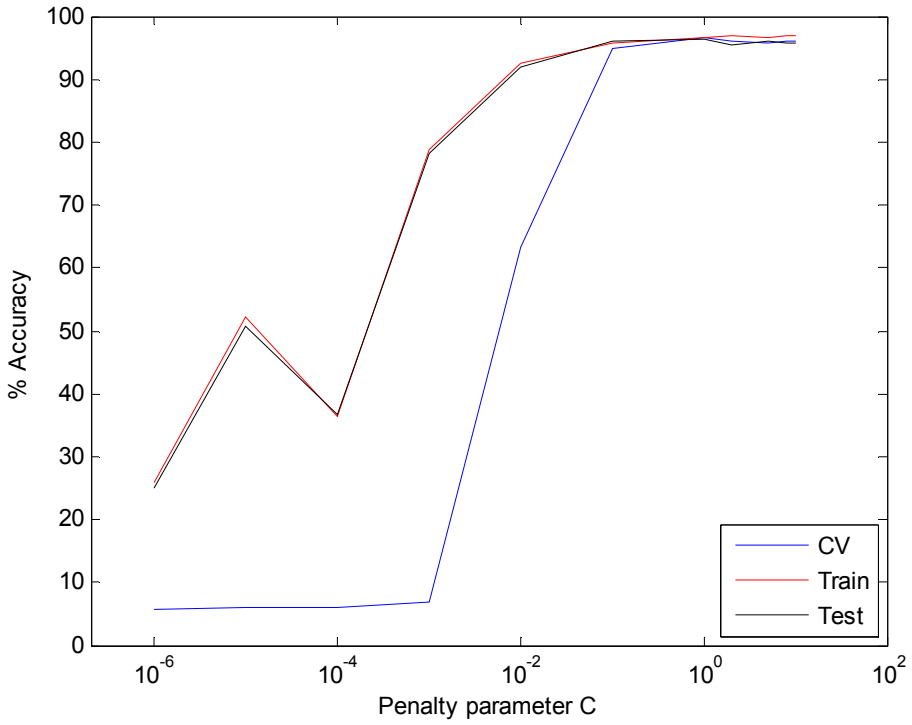

Figure 26 Linear SVM Kernel where C is varied from 1 × 10^{-6} to 10. The result of model prediction of each subset of the training data is shown. C = 1 was selected as the optimum value for the linear SVM. The accuracy of the model remained constant at cv_{acc} = 96.8%, $train_{acc}$ = 96.72% and $test_{acc}$= 96.33%.

In comparison, the optimum RBF kernel had a cv_{acc} (95.32%), $train_{acc}$ (97.56%) and $test_{acc}$ (96.16%) with C = 5 and γ = 2 (Table 6). When the RBF γ was increased above 10, overfitting was evident with the training error approaching 0, moreover the CV accuracy decreases below 95% and the test error begins to decrease reaching a minimum of 89.99%, at which point it was decided not to increase γ any further (Figure 27).

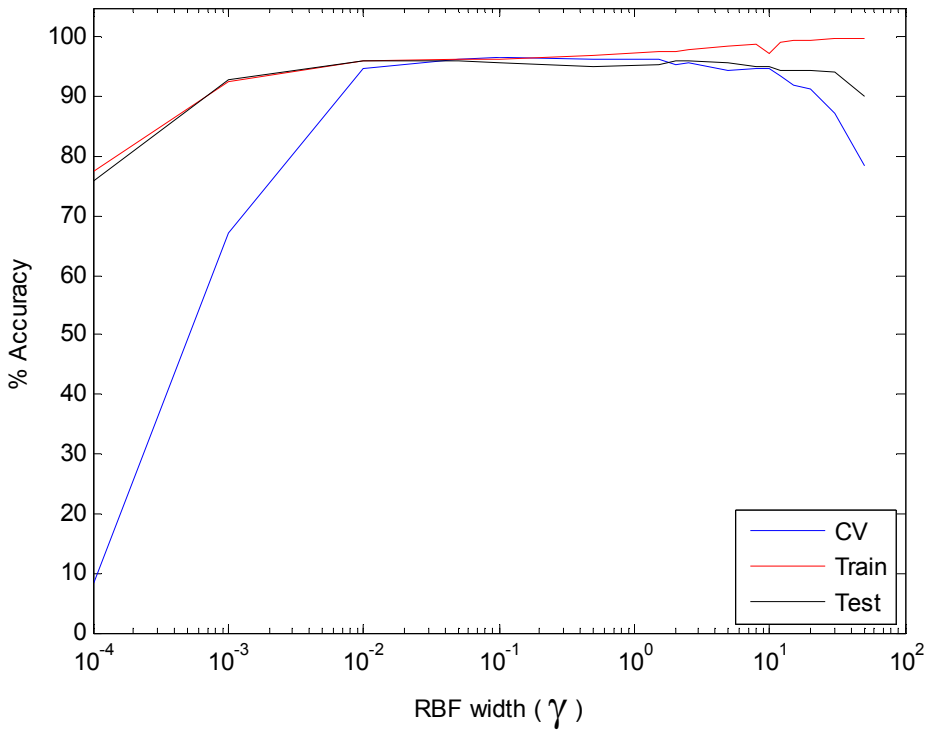

Figure 27 RBF SVM Kernel, C = 5 (Table 4) (the optimum penalty parameter), γ is varied between 1 × 10^{-4} to 50. The resulting of model prediction of each subset of the training data is shown. Overfitting is evident beyond γ = 10 the CV and test accuracies decrease, the training accuracy increases. The optimum RBF accuracies were cv_{acc} = 95.32%, $train_{acc}$ = 97.6% and $test_{acc}$ = 96.16%.

The classification rates of the two SVMs are very similar. The RBF SVM can approximate both linear and non-linear problems and has been shown to have performance comparable to the linear kernel; therefore achieving similar results for both SVMs is not surprising. While LDA or partial least square discriminant analysis (PLSDA) could have been used for this dataset, maximal margin optimisation and the option of non-linear extension to the classification scheme in the future gives the SVM advantages over both methods. The training time for the RBF kernel was slightly greater requiring ~5mins in comparison to ~3.5mins for linear SVM training. As new QDEMs are added to the model the training time is expected to increase (using the OVR multiclass design the number of binary SVMs increasing the training time would increase exponentially (section 4.4.3)).

The RBF kernel required a greater number of SVs (2230) compared to the linear kernel (944) to define the SVM decision boundaries. An increase in the numbers of SVs increases the computational cost of the SVM model during prediction. For QDEMs analysed in a high throughput format, FCM is capable of detection rates of 1000 events per second, the number of calculations required for single event classification are 44% less for the linear kernel. The number of SVs is proportional to the complexity of the separating hypersurface. The authors of the LIBSVM package advise that the linear kernel be chosen following Occam's razor, the simplest model is best, and the model with the fewest SVs was chosen (i.e. the linear kernel with the lowest geometric decision surface complexity) [163].

Therefore a SVM incorporating a **linear** kernel, with $\boldsymbol{C = 1}$ was found to yield the highest CV accuracy with the shortest training time and fewest support vectors. These settings were used in the construction SVMs to determine the suitability of outlier removal and the comparison between OVO and OVR. However application of the RBF must not be discounted for future studies as increases in the coding complexity QDEMs may require a non linear kernel. The performance of the RBF kernel demonstrates the flexibility of SVMs for pattern recognition tasks.

4.4.2 Outlier removal suitability

The suitability of outlier removal process for SVM training by means of the IQR was determined by constructing an SVM for training data with and without outliers and determining the accuracies on each training data split. The number of outliers removed for each class is shown below (Figure 28).

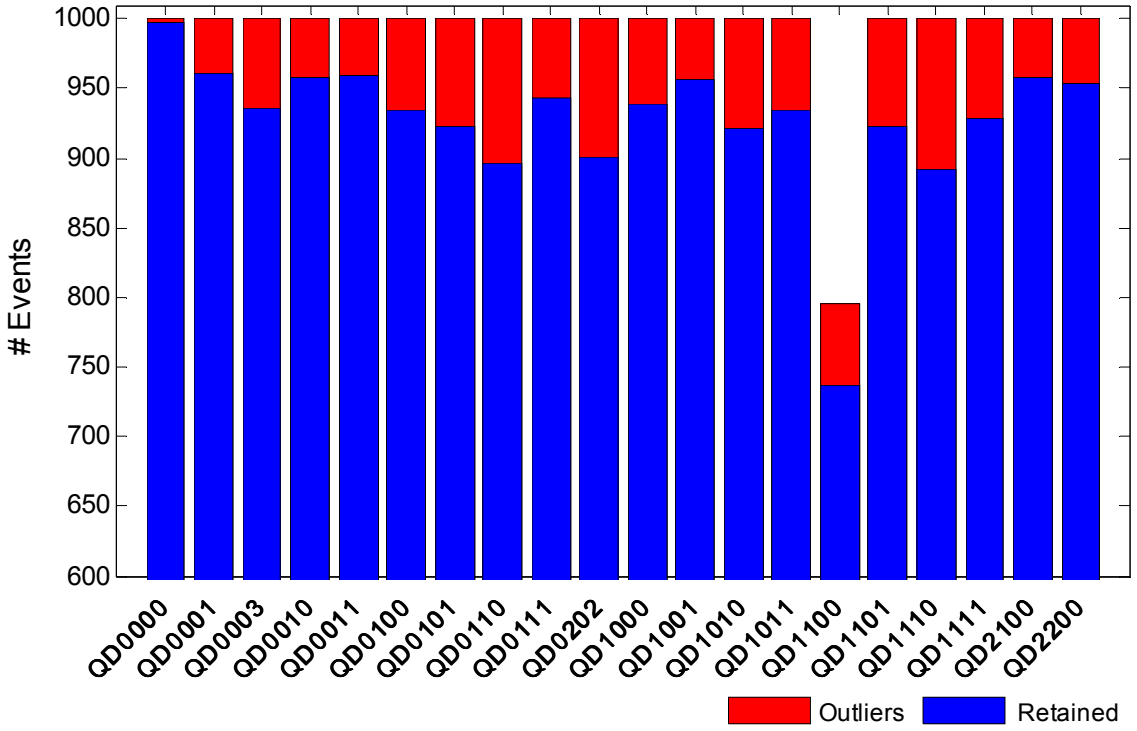

Figure 28 Post acquisition outlier removal for each QDEM. A total of 1242 events were removed. The remaining events were retained to form the training data.

Following outlier removal an increase in the cv_{acc} from 91.10% to 96.58% was observed, moreover the number SVs required to separate the 20 classes decreased from 2145 to 944 reducing model complexity and increasing the classification speed of the SVM (Table 7). The test set accuracy increased by 3.31%. The removal of outliers from the training data is a reliable method which does not affect the generalisation ability, hence outlier filtered training data is used for the remainder of this thesis.

Table 7 Suitability of outlier removal using the optimum SVM configuration. An SVM was trained and tested for the QDEM dataset before and after the removal of outliers.

	#Samples			Kernel	*C*	cv_{acc}(%)	False Positives (test)	$test_{acc}$(%)
	Training	Test	CV					
+Outliers	9900	4948	4948	Linear	1	91.10%	345	93.02%
-Outliers	9277	4638	4638	Linear	1	96.58%	155	96.33%

4.4.3 Evaluation of multiclass SVM designs

To determine the optimum multiclass SVM design, a comparison of the suitability of the OVR and OVO methods (section 4.2.2) for the QDEM dataset was investigated. Cross validation, training and testing were performed and the cv_{acc}, $train_{acc}$ and $test_{acc}$ calculated for both multiclass designs (Table 8).

Table 8 Comparison of the OVR and OVO multiclass SVM methods. The CV, train and test accuracy for each SVM are shown.

	cv_{acc} (%)	$train_{acc}$ (%)	$test_{acc}$ (%)	#SV
OVR	75.24	89.44	89.52	8107
OVO	96.58	96.72	96.33	944

The OVO method clearly out performs these methods and therefore it was decided to use OVO for the SVM. The literature suggests that OVO has a greater performance and the results here support those assertions [145]. A drawback of both the OVO and OVR method is that for any given sample the significance of each classification is weighted equally, while it is impossible to know the classifiers significance, certain classifiers are redundant and can be removed with a so-called mixture matrix [164].

The final design of the classifier was an OVO multiclass SVM employing the linear kernel, with a penalty parameter C = 1, trained and evaluated on outlier filtered FCM data. The performance of the model had cv_{acc} = 96.58%, $train_{acc}$ = 96.72%, and an independent test validation; $test_{acc}$ = 96.33%. These results demonstrate the potential of the SVMs for QDEM recognition in FCM.

4.4.4 SVM performance with increasing QDEMs

The effect of increasing the number of QDEMs per SVM was also investigated as a possible measure of the capacity of this approach when the future numbers of QDEMs increase. The effect of adding classes to the model was assessed beginning with two QDEM populations. To avoid class bias in the evaluation (where the most or least separable classes are considered), 10 individual classifiers were constructed containing *n* random classes for each QDEM number considered and the average cv_{acc}, $train_{acc}$ and $test_{acc}$ calculated (Table 9).

Table 9 Evaluation of the effect of addition of QDEMs on test set accuracy. An individual SVM was constructed for each test.

#QDEM	cv_{acc} (%)	$train_{acc}$ (%)	$test_{acc}$ (%)
2	99.67	99.68	99.69
3	99.75	99.84	99.78
4	99.55	99.60	99.43
5	99.29	99.39	99.33
6	98.69	98.82	98.44
7	98.43	98.57	98.36
8	98.26	98.59	98.43
9	98.65	98.76	98.59
10	97.68	97.97	97.79
11	97.56	97.84	97.66
12	97.63	97.95	98.05
13	97.75	98.06	97.61
14	97.05	97.48	96.95
15	96.91	97.42	97.04
16	96.98	97.30	97.00
17	96.72	97.05	96.70
18	96.14	96.58	96.48
19	96.23	96.68	96.28
20	96.58	96.72	96.33

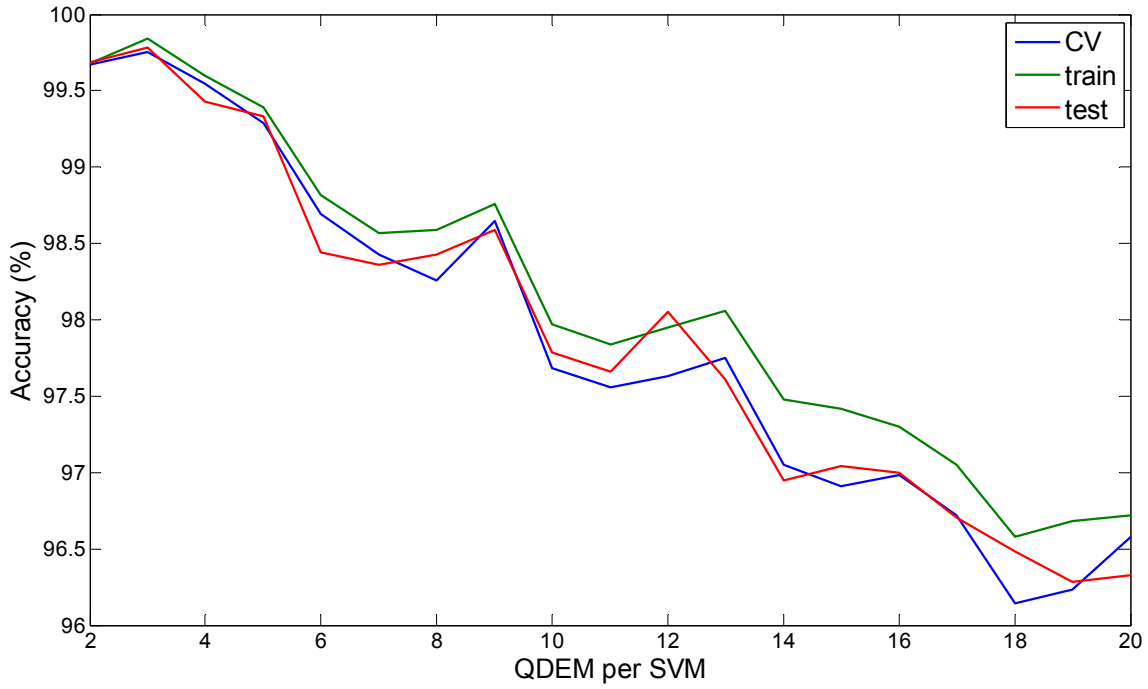

Figure 29 Evaluation of the effect of increasing the number of classes considered by the SVM.

A decrease in the accuracy in the classification of the unseen data ($test_{acc}$ = 3.67%) can be observed between the 2 class and 20 class model. It is thought that the SVM should eventually become independent of the number of QDEM classes as the OVO multiclass design creates an individual set of binary classifiers for each QDEM, therefore complexity (number of SVs) required for each binary classifier does not increase. As the number of QDEMs increases the accuracy would be expected to decrease (as the encoding complexity across the QDEM library is considered) and remain constant. In comparison the addition of classes with the OVR approach would increase the complexity of the decision boundaries as each binary SVM separates a class from all other classes. More QDEM types are required to further investigate the SVM beyond 20 QDEMs and it remains a concern.

In the future if the extension of the SVM methodology to greater numbers of QDEMs incorporating additional colours and intensities proves problematic for the linear kernel, the RBF kernel could be employed. The kernel flexibility offered by the SVM paradigm and OVO is well suited to offset the possible problems associated with increasing the multiplexing ability of an assay.

4.4.5 Independent testing set validation

To further assess the suitability of the constructed model a complete classwise analysis of the SVM was carried out from the results of the independent test validation. By comparing the unseen *test_set* subset of the training data for which each event was known a test accuracy of 96.33% was acquired. In order to determine which QDEMs were misclassified a confusion matrix was constructed from the *test_set* classifications. Each element in the confusion matrix represents the number of microspheres in the test set whose actual label is the row and the predicted label is the column, the TP, FP, TN and FN can be can be calculated from the table. Standard quality indicators of specificity and sensitivity were used to evaluate each QDEM class performance in the SVM (section 4.3.4). The number of SVs required for the discrimination of each class is also shown. See appendix for the full SVM confusion matrix for the QDEM library a summarised version is presented here (Table 10).

Note: *The SVM assigns a label to the class returning the highest pair-wise probability, by rejecting classified events below a threshold of P = 0.5 the MC rate can be further reduced (see below). The pairwise probability of the testing set classification was not taken into account at this stage.*

Table 10 Independent test Set validation, true positives (#TP), specificity (S) and sensitivity (R) are shown. See appendix 1 for the SVM confusion matrix. Test set accuracy = 96.33%. The number of support vectors (#SVs) is shown for each class. The least sensitive class is highlighted.

	ID	#TP	S (%)	R (%)	#SV
1	QD0000	233	99.8	92.8	68
2	QD0001	223	99.6	94.9	65
3	QD0003	260	99.9	100	10
4	QD0010	210	99.8	94.5	65
5	QD0011	234	99.7	97.9	25
6	QD0100	225	100	97.4	22
7	**QD0101**	**216**	**99.9**	**89.3**	**121**
8	QD0110	211	99.9	92.5	102
9	QD0111	229	99.6	93.4	85
10	QD0202	205	100	98.0	36
11	QD1000	241	100	99.5	19
12	QD1001	222	99.8	99.1	19
13	QD1010	212	99.6	95.9	48
14	QD1011	210	99.6	99.5	22
15	QD1100	164	99.4	93.1	60
16	QD1101	226	99.9	97.8	77
17	QD1110	218	100	93.5	87
18	QD1111	254	100	97.3	35
19	QD2100	223	100	100	6
20	QD2200	224	100	100	15

The lowest sensitivity observed was for QD0101(R=89.3%) and resulted from a degree of confusion between QD0101, QD0110 (R= 92.5%) and QD0111 (R=93.4%). The confusion between these classes may have been due to the 620nm QD not being centred over the 625nm emission filter for optimum performance. The remaining QDEM classes perform well with sensitivity of >90% for the entire 19 classes. The microsphere QD0000 was expected to have a higher sensitivity (R = 92.8%) as this microsphere had no emission. The cause of the low sensitivity is not known, one possibility is that a small amount of blank QDEMs were present in the remaining QDEM solutions leading to misclassification in the independent test set validation. All QDEM classes returned excellent specificity (S > 99%).

As stated previously QD1100 had the fewest instances in the training set containing lower concentration of QDEM in the stock solution. The specificity and sensitivity of these QDEMs was 99.4% and 93.1% respectively, suggesting that the imbalance in the number of events for each QDEM has no effect on SVM performance.

4.4.6 Performance on the multiplexed testing sets

While the performance on the training data was excellent, an additional test was conducted to see how the SVM would perform using multiple QDEMs in a single solution (Table 11), forming an external validation of the model. No outlier filtering was carried out on these results (the IQR filtering method only works with single population QDEM datasets) so it was assumed that these datasets would contain similar noise to the pre-filtered training data. Post classification removal of these outliers was accomplished using the prediction pairwise probability provided by LIBSVM.

For the reasons outlined in section 3.4.2 the success of the SVM was measured by calculating the MC rate and σ^2. The table shows the number of classified events belonging to each QDEM. Events were rejected as unclassified results when the pairwise class probabilities were ≤ 0.5, resulting in between 0.1 and 5.2% rejection for each of the tests. The MC rate was calculated for each of the 10 multiplexed test sets (simply the number of false positives divided by total events remaining after probability filtering). Test four yielded the highest number of misclassifications at 6.4%.

Table 11 Prediction of unknown events from test samples using SVM classifier. The number of misclassifications (p ≤ 0.5) is shown for each QDEM (See Table 2 for test set composition).

		Test#									
		1	**2**	**3**	**4**	**5**	**6**	**7**	**8**	**9**	**10**
QDEM code	**QD0000**	7	20	0	5	**554**	94	7	**570**	**340**	52
	QD0001	0	0	1	1	**318**	**448**	4	**398**	**298**	**563**
	QD0003	0	0	**568**	**618**	0	0	**533**	0	0	0
	QD0010	4	9	0	9	10	20	**560**	12	15	**419**
	QD0011	**559**	1	22	14	0	**571**	0	**355**	**410**	**475**
	QD0100	8	**530**	0	11	**426**	3	21	**321**	22	**305**
	QD0101	6	2	0	1	**423**	1	**147**	**277**	**407**	**388**
	QD0110	**497**	12	0	**448**	**709**	1	17	**573**	**625**	**534**
	QD0111	32	0	0	27	**523**	0	**708**	**592**	**762**	**833**
	QD0202	10	1	**231**	**287**	0	5	1	16	18	25
	QD1000	1	14	3	0	0	**467**	**498**	**328**	0	**349**
	QD1001	0	0	0	0	0	1	0	0	**287**	**358**
	QD1010	1	**538**	0	32	1	**522**	5	11	23	**419**
	QD1011	1	**554**	1	**428**	0	**504**	1	**455**	**662**	**490**
	QD1100	**182**	**247**	0	3	80	**231**	5	75	**237**	**222**
	QD1101	1	0	0	**234**	**218**	**318**	**135**	**320**	**319**	**338**
	QD1110	**653**	26	0	83	**554**	**677**	**415**	**909**	**726**	**723**
	QD1111	16	2	1	**697**	25	24	**501**	**600**	**532**	**641**
	QD2100	0	0	**683**	0	0	0	**778**	0	0	0
	QD2200	0	0	**487**	0	0	11	**574**	14	0	10
# QDEM codes		4	4	4	6	8	8	10	12	12	15
#Events		2000	2000	2000	3000	4000	4000	5000	6000	6000	7500
#Classified		1978	1956	1997	2898	3841	3898	4910	5826	5683	7144
Rejected (%)		1.1	2.2	0.1	3.4	3.9	2.5	1.8	2.9	5.2	4.7
#Correct		1891	1869	1969	2712	3725	3738	4849	5698	5605	7057
CC rate (%)		95.7	95.6	98.6	93.6	97	95.9	98.8	97.9	98.7	98.8
σ^2		**41684**	**21660**	**36801**	**32584**	**23520**	**19653**	**43722**	**33235**	**34551**	**27389**
MC rate (%)		**4.3**	**4.4**	**1.4**	**6.4**	**3.0**	**4.1**	**1.2**	**2.1**	**1.3**	**1.2**

On increasing the rejection criteria to p = 0.75 the misclassification decreases to 0.2%, while the rejection rate increases to 16.3% of total events (data not shown). The SVM performed well on the remaining test sets with the MC rate below 4.5%. The 15 QDEM had the lowest MC rate demonstrating the ability of the SVM to discriminate between the lowest intensity microspheres (level 1 intensity). For test 3 only multiple intensity ratio

beads were used. The SVM accurately identified the four multiple intensity QDEMs with only 1.4% misclassifications for test 3. The average MC rate for each of multiplex test sets was 2.9% with an average rejection rate of 2.7%. For tests 1-6 the average MC rate was 3.9%. For each mixture set the top predicted QDEMs corresponded exactly to those QDEMs present in the test solution. QD1100 was also predicted at a lower rate in the multiplexed testing, further suggesting that the stock concentration was originally lower. Misclassifications may be due to confusion between classes, detector overspill or instrumental drift. The use of narrower bandwidth emission filters could reduce cross talk between detectors and centering of the FL3 channel at 620nm should decrease the levels of misclassification in the SVM. The variance of the CCs for each multiplex solution were similar, there was no significant increase in the variance when the individual QDEMs in the solution were increased providing a greater confidence in the accuracy of classifications for mixtures 7-10.

4.5 Conclusion

The aim of this chapter was to improve the accuracy of QDEM identification from FCM data reported in chapter 3. In that chapter, a MPG method was used to classify each QDEM by means of selecting regions from a series of 2D plots. The methods suffered from an inability to find the optimum gates for classification due to overlap between QDEM signatures resulting in multiple classifications for a single event and >30% misclassification for the most difficult microspheres to classify. In comparison the supervised learning paradigm of SVMs, has been shown to outperform MPG in every multiplex test (Figure 30). While MPG analysis returned <2% misclassifications for Test

10, 1859 extra classifications were made than events recorded (this was also the case for other tests), moreover there was an increase in the variance of CCs calling into question the validity of the MPG results and therefore the suitability of the technique. The MPG method is also time consuming and as the number of QDEMs increases it becomes more so, moreover the optimum gates may not be found.

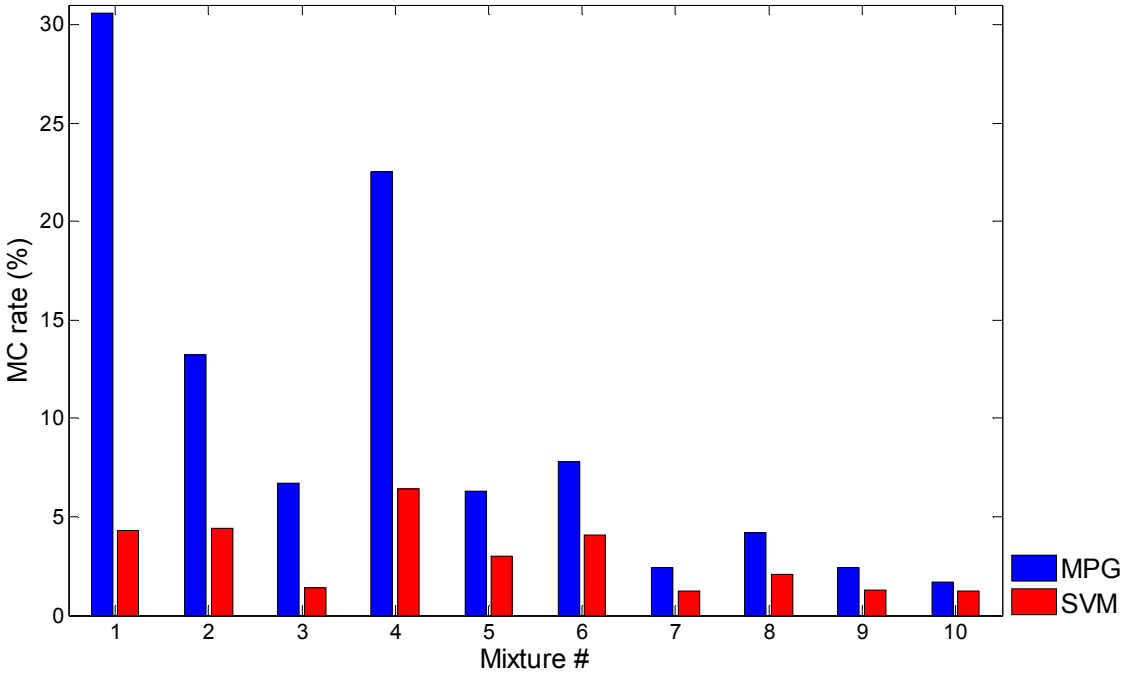

Figure 30 Comparison of MPG (multiparameter gating) and SVM MC rates. The SVM outperforms MPG in all tests. Demonstrating the potential of SVM for the discrimination of QDEMs from SVM and supervised learning algorithms (For a comparison of the variance of CCs see Figure 45).

SVMs have been shown to be a highly accurate means of QDEM analysis, the technique trains rapidly (average training time 3.5mins), moreover the probability of classification can be taken into account and results filtered from the data. SVMs are capable of forming gates in a kernel induced feature space, the algorithm locates the optimum decision boundary between classes by locating the maximum margin hyperplane (section 4.2.1).The SVM reported here has shown excellent specificity (average R = 96.33%), sensitivity (average S = 99.82%), and an overall classification accuracy of 96.33% on

unseen data. Moreover the SVM model preformed well in external validation; demonstrating reduced MC rate for the QDEMs present in each solution in comparison to MPG (Figure 30). The variance of CCs with the SVM model remained relatively constant for the SVM in comparison to those of the MPG across the 10 external validation solutions (Figure 45). Average SVM $\sigma^2 = 31479$ in comparison to $\sigma^2 = 63482$ for MPG.

In comparison to a commercial SAT analysis, the Luminex platform, a classification rate is quoted as >80% [165]. The average 3% MC rate using our SVM model, compared to Luminex misclassification of less than 2%, test 4 had a MC rate of 6.4%, however the Luminex system combines dual organic dyes and a more complex microsphere encoding scheme is used here. Concerns still exist as to the suitability of SVMs for the scaling up of QDEM libraries. The OVO design should be robust and SVM can operate both in linear and non-linear modes which may be advantageous when additional microspheres are added.

SVMs are theoretically well suited to the automatic gating of flow cytometry subpopulations. SVM can be thought of taking the "flow cytometry input space" and using the maximal margin hyperplane to gate the data in a multidimensional feature space to produce optimum classification of QDEMs subpopulations for SAT, the results shown here confirm this.

In the following chapter a comparison between the SVM and another supervised learning algorithm, artificial neural networks is carried out. ANNs have also proved effective for FCM subpopulations in the past thus it is prudent to compare these classification methods to the SVM.

Chapter 5: Development of a neural network based QDEM classification system.

5.1 Overview

Chapter 4 described the successful application of multiclass SVMs to the classification of QDEMs from FCM data. This chapter aims to compare the SVM to artificial neural network classifiers (section 5.2.1). These supervised methods have had reasonable success in FCM (section 5.2.2). Two popular ANN architectures (section 5.3) were constructed using the QDEM data and evaluated using an independent test set validation and external validation for comparison to the SVM classifier.

5.2 Introduction

5.2.1 Artificial neural networks

An artificial neural network is a machine learning technique loosely based on biological nervous systems such as the brain [166, 167]. The origins of ANNs date back to the 1940s, with the description of simplified neurons by McCulloch and Pitts [168], and subsequent development of the perceptron for two class discrimination by Frank Rosenblatt in 1956 [169]. However the failures of the single layer perceptron model in some basic pattern recognition tasks were demonstrated by Minsky and Papert, leading to a decrease in the pace of research lasting until the 80's. The field was revived through the work of Hopkins who demonstrated the use of ANNs for real world applications [170], and the development of the back propagation learning algorithm for multilayer perceptrons [171].

Today neural networks are a computationally efficient, easily constructed, non-parametric method which assumes no *a priori* knowledge of the data under examination and are well accepted in many branches of science and engineering for applications such as pattern classification, function approximation, image processing and many others [166].

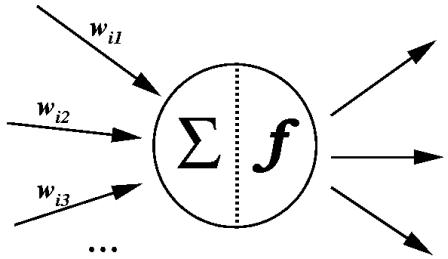

Figure 31 Model of an ANN neuron.

ANNs are composed of a collection of linked processing units (neurons) (Figure 31); each neuron obtains inputs from the external environment and from other neurons in the network. Connections between the processing units are weighted and each input has a weight, w associated with it. The response (output) of each unit is calculated through some function f of the weighted sum of its inputs (Equation 5.1):

$$y_i = f\left(\sum_j w_{ij} x_i\right) \tag{5.1}$$

Where y_i is the output of the neuron. The weighted sum $\sum_j w_{ij} x_i$ is termed the net input to the *ith* unit and is also called net_i. The function f is termed the activation function and governs how the neuron processes input signals to produce an output. The activation function weights the value of the output, often between 1 and 0 or between -1 and 1

depending on the type of activation function used. The activation function introduces non-linearity into the network. Examples of common activation including the step function, Gaussian and the popular sigmiodal activation functions are shown below (Figure 32) [167].

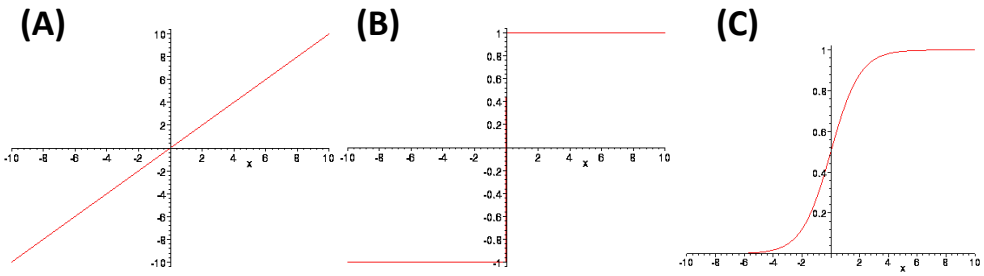

Figure 32 Neuron activation functions. (A) Identity function (B) Step function (C) sigmoid function.

The neurons are divided into processing layers of which there are generally three main types. Firstly an *input* layer which connects the ANN to data environment under study, a *hidden* layer models the data distribution and the *output* layer which delivers the identity of each class. As stated above an ANN is an interlinked structure of neurons; the arrangement of neurons, layers and the connections between them is termed the ANN *architecture* e.g. feed-forward, recurrent or self organising maps (SOM). With the feed forward design the data flow between input and output neurons is only allowed to propagate directly through the network; there are no looped connections. Recurrent architectures can contain connections between the nodes in the same layer or nodes in the previous layers of the network. In the hidden layer of a SOM nodes are arranged into a rectangular or hexagonal lattice, each of which are fully connected to the input layer and define a topographical position.

Combinations of single one-class networks known as ANN ensembles or stacked neural networks (SNN) are also suitable for classification. While some success has been demonstrated, such ensembles suffer from the lack of interaction between single networks during the learning phase and the way the networks are combined increasing the possibility of individual networks not contributing to the classification [172]. Therefore the ANNs employed in this thesis were single networks trained on all classes simultaneously. For a detailed discussion of ANN architectures see [166].

ANN training aims to create a predictive model by configuring a network such that the presentation of a set of input values produces the desired set of outputs. The initial weight vectors for the ANN are chosen randomly and in supervised ANN training the weights are adjusted according to response of data patterns. The updating of weights in an ANN is determined by learning rules, of which there are four basic types, error-correction, Boltzmann, Hebbian, and competitive learning.

While this chapter concentrates on supervised paradigms (section 4.2.1) ANN training can be either supervised or unsupervised. Examples of unsupervised networks include the Kohonen's SOM [167], and Hopfield networks [170]. There also exists a hybrid method where both supervised learning and unsupervised learning are combined, with part of the weights are usually determined through supervised learning, while others are determined through unsupervised learning [173]. The specific characteristics and learning methods of the selected ANNs for this study are detailed below (section 5.3). For an excellent review of training methods for ANNs see [167] and [166].

5.2.2 Previous applications in flow cytometry

To date a number of examples of the application of ANNs to classification of microalgae from FCM data have been reported in the literature [174-177]. Boddy *et al.* previous work illustrates the application of ANNs to FCM for the identification of phytoplankton species from 11-parameter data. Radial basis function neural networks (section 5.3.2) were trained to recognize 35-70 species of phytoplankton. The best performing RBF network could correctly identify 91.5% of phytoplankton after training using gradient descent algorithm [176]. The identification of fungal spores using flow cytometry and artificial neural networks has also been reported previously [178] [179].

Quinn *et al.* has recently described a pattern recognition methodology for the classification of live, apoptotic (programmed cell death) stage and dead cells from FCM data based on ANNs. FSC and SSC measurements relate to cell size and granularity and are indicators of the morphological changes that cells undergo during apoptosis. Lecours dual staining method with 7-aminoactinomycin D (7AAD) and annexin V was utilised to determine cell lineage and the developmental stage. Traditional data analysis was used to set gates to define the intensity threshold for these dyes to locate live, apoptotic and dead cells, cells positive for 7AAD are designated as dead (degradation of the cellular membrane allows access to nuclear DNA resulting in an increase in binding). Cells positive for annexin V but negative for 7AAD are designated as apoptotic, and finally cells with observed negative populations for both dyes are “live”. The gates were defined by an expert panel of analysts resulting in variations between users particularly at the boundaries between populations. Both supervised and unsupervised ANNs were evaluated consisting of multilayer perceptron, radial basis function (RBF), recurrent

multilayer perceptron (RMP), learning vector quantisation (LVQ) and the SOM topologies. A comparison of the ANNs to an SVM was also carried out. It was found that the RBFP, LVQ, and MLP resulted in an error rate of 6.4% ± 1.3. The RBF was determined to be the optimum classifier with an expected error of 4.5% [151]. The misclassification rate of the SVM in this instance was 9.4% ± 2.8%

A study by Kothari *et al.* described the neural network analysis of immunophenotype FCM data for the discrimination of leukaemia subcategories based on lineage and differential antigen expression. The fluorescence data from 170 samples (28 inputs per sample) was used to train the MLP ANN allowing the distinction of leukaemia subtypes, a test set accuracy of 89.7% was observed indicating that such a classification scheme has potential [180]. DNA flow cytometry histogram plots have also been analysed using ANN allowing the identification of high and low leukaemia risk patient groups [181].

Following a review of the literature it is clear that the RBF and MLP classifiers have been the most successful for the identification of FCM subpopulations. It was therefore decided to concentrate on these ANN architectures for comparison to MPG and the SVM.

5.3 Selected ANN architectures

The topology of an artificial neural network describes the patterns of connections between the units and the propagation of data throughout the network. The two most successful topologies employed in the literature for FCM applications follow the feed-forward method. Each ANN classifier constructed in this study had 6 nodes in the input layer (one for each FCM parameter) and 20 neurons in the output layer (one for each

individual QDEM). The following section describes both the MLP and RBF type networks in detail.

5.3.1 Feed forward multilayer perceptrons

As stated above single perceptron neurons have limited ability in classification problems, the combination of perceptrons arranged in layers however is a much more powerful learning technique. MLPs are the most popular ANN described today in the literature. An MLP "may be viewed as a practical vehicle for performing a nonlinear input-output mapping of a general nature" [182]. These highly connective (each neuron is connected to every neuron in the previous layer) feed-forward architectures calculate a weighted sum of their inputs, and pass the activation level through the network to produce the output.

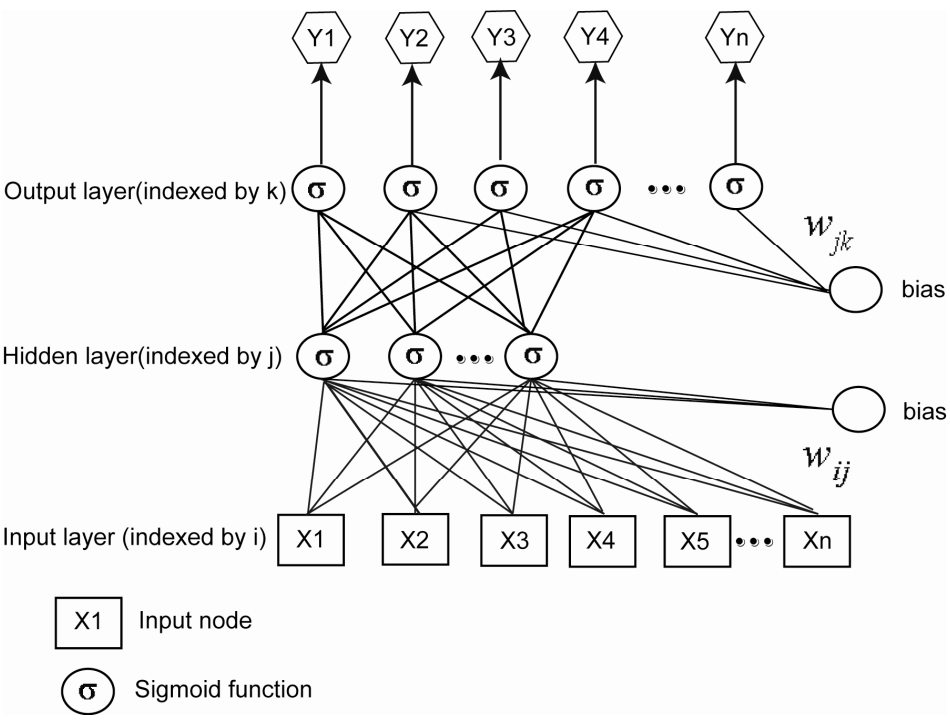

Figure 33 Multilayer perceptron.

For any given layer the neurons receive their input from the previous layer on the input side of their network and their output to the following layer on the output side, there are no interlayer connections (Figure 33). The first layer is known an as the input layer. The input signal is modified by the initial weights w_{jp} and the bias b_1 resulting in an input to the j^{th} neuron in the hidden layer (j =1, 2, 3) of net_j, which is a weighted input of the intensity values [166, 183].

$$y = f\left(\sum_{i=1}^{N} w_i \cdot x_i\right) + b_i \qquad \textbf{(5.2)}$$

The hidden layers are activation functions of the weighted inputs plus a bias, the output of the hidden layer is then distributed to any other hidden layers until the output units are reached. Based on the equation above the output of the j^{th} neuron in the hidden layer is:

$$y_j = f_H\left(net_j\right) \qquad \textbf{(5.3)}$$

The training method employed for MLPs in this work is known as the back propagation algorithm [184, 185]. The network weights are updated with respect to the classification error calculated upon input of the previous training set, the learning rate and the magnitude of the output.

The back propagation algorithm, a type of error correction learning is defined as a gradient descent method to minimize the squared error cost function [166], an error signal is then back-propagated from the output layer to the hidden layer and the network is altered. Back propagation consists of two passes throughout the various layers of the MLP, a forward pass and backward pass. During the forward pass, an input pattern is applied to the nodes of the network, and its effect propagates through the network layer by layer producing an output signal. While the weights remain fixed during the forward pass of the training algorithm, during the backward pass the weights are adjusted in order to reduce the error. The back propagation algorithm is an iterative process, on each iteration or *epoch* the training set is presented to the network. The weights in the network are updated according to the degree of classification error, the magnitude of the output and the learning rate, η. Once a predefined threshold, for example the desired CV_{acc} or a set number of iterations is reached training terminates. A representation of the decision boundaries formed by an MLP is shown below (Figure 34).

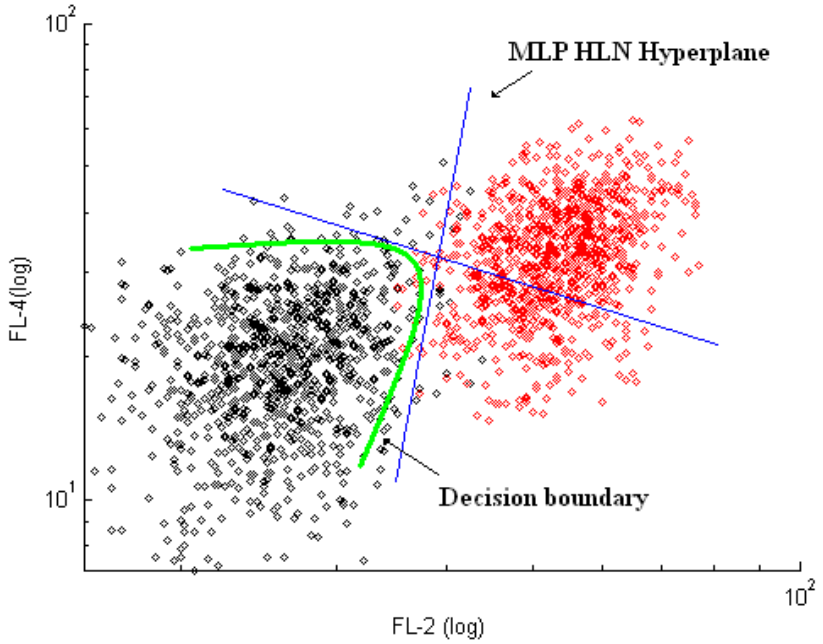

Figure 34 Representation of MLP separation of a two QDEM problem in 2-dimensional space.

5.3.2 Radial basis function networks

RBF ANNs can be considered as a special type of multilayer feed forward network using of a number of locally tuned neurons [186-188]. A RBF is composed of a single hidden layer, with linear output functions (there is also a bias on each output node) and nonlinear transfer functions [166]. There are no weights in the hidden layer, the outputs of the hidden units are in fact calculated using the "closeness" of the input to some positive radially symmetric function (a kernel) [183]. A RBF ANN has a hidden layer of radial units e.g. Gaussian (Figure 35), this single hidden layer is sufficient for any application due to the non-linearity of the radial unit function. While MLP units are defined by their weights and threshold, radial units are defined by the central point and radius. Each node in the hidden layer represents a kernel function and each output node calculates the weighted sum of the hidden layer outputs [188].

The kernel function output is determined by its centre and width, the output is high when close to the centre and decreases rapidly toward zero as the input distance from the centre increases. Gaussian functions are popular in the literature and have been shown to be successful in FCM subpopulation classification [151].

The Gaussian hidden layer function is given by:

$$Z_j(x) = \exp\left(-\frac{\left\| X - \mu_j \right\|^2}{2\sigma_j^2} \right), \qquad \textbf{(5.4)}$$

Where σ and μ are the width and centres of the j^{th} node in the hidden layer. Z_j is the output. A summation of each output node gives the response of the network for a given input.

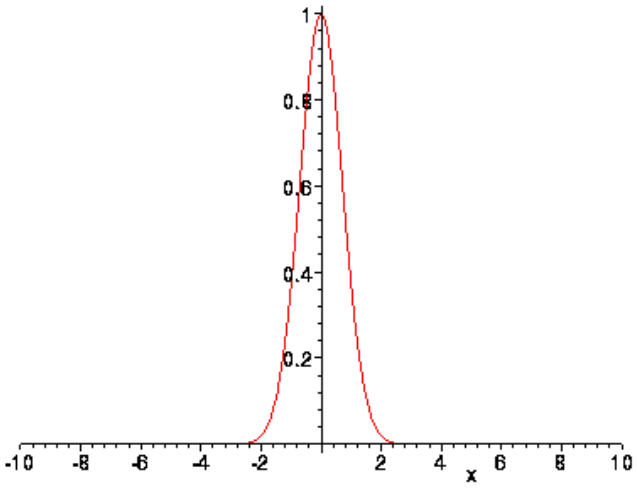

Figure 35 Radial Basis Function: Hidden layer nodes use Gaussians of varying standard deviations to determine the output.

While MLPs classify a given pattern by means of hyperplanes, RBF ANNs divide up the input space by considering the distribution of the data under consideration (Figure 37). Training a RBF ANN is different to the training of MLPs in that there is no updating of the weights after each pass. Training of the RBF hidden node kernel is achieved through the selection of the function centres and widths using a cross validation procedure, finally the hidden-to-output weights are calculated. Selection of the radial function can be thought of as defining the optimum number of basis functions.

The training of RBF neural networks occurs in two separate stages; an unsupervised routine such as K-means clustering can be used to determine the centres of the basis functions [189], for more information see [183]. The second stage involves a simple least mean squares (LMS) optimisation or singular value decomposition to calculate the weights for the output layer of the network [190]. Further improvement in the classification performance of the network has been reported using a gradient descent method to simultaneously adjust the basis function and weights.

For classification problems standard RBF ANNs can encounter difficulties as the output decision is based on distance from the hyperplane. It is preferable to return a probabilistic confidence level for example a softmax probability function may be implemented. An alternative solution is to use a variation of RBF networks called probabilistic RBF. The training algorithm employed is based on Bayesian probability distributions, classified patterns are ranked as probabilities of a match. This ANN has three layers, input, pattern layer and a decision layer (Figure 36).The pattern layer contains a node representative for each class and receives the weight value from the hidden neuron.

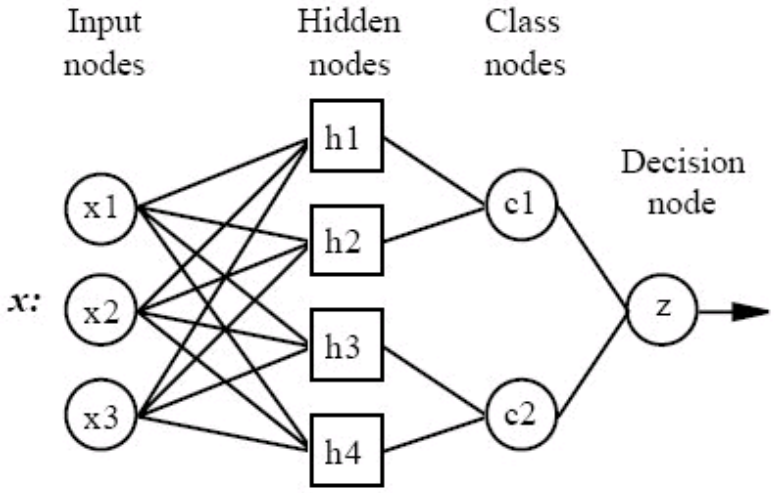

Figure 36 Probabilistic radial basis function ANN. Hidden node layers contain Gaussian functions. Class specific notes compute a weighted sum based on the values of the hidden nodes for each group and the decision layer produces the classification based on the largest vote.

Classification of an unknown sample x is determined from the product of the class kernels and the a priori probabilities. The designated class is that which has the highest discriminatory values [191]. For the Gaussian kernel used in this study the discriminant function is in form of:

$$D_i(x) = \frac{\hat{p}(i)}{M_i} \sum_{j=1}^{M_i} \exp\left(-\frac{1}{2\sigma^2} d^2\left(x, x_j^{(i)}\right) \right), \qquad \textbf{(5.5)}$$

Where $x_j^{(i)}$ is the j th training sample of class i, M_i is the number of training samples of class i and $\hat{p}$ is the mean a priori probability. σ is known as the smoothing parameter.

Class specific votes are then cast for each pattern neuron and proceeds to the pattern layer where the weighted votes are compared and classification based on the largest vote.

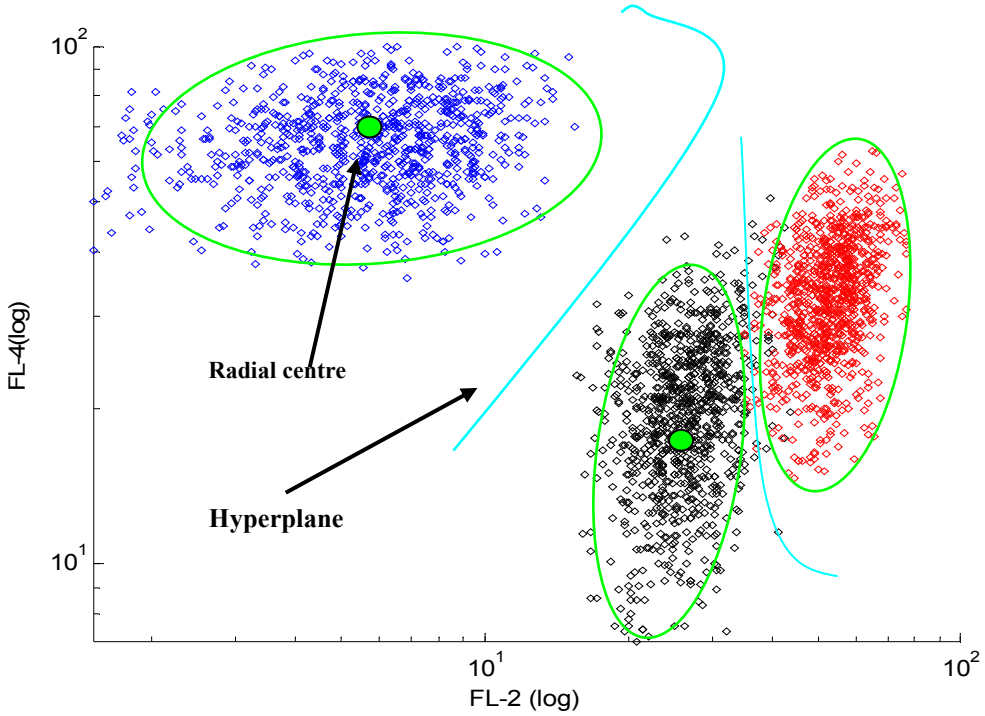

Figure 37 Representation of PRBF separation of a 3 class QDEM problem in 2-dimensional space adapted from [179].

The PRBF ANN has advantages over standard RBF ANNs as the outputs are probabilistic and training time is rapid (transfer of training cases into the radial layer is therefore sub-second). However the advantage of rapid training is balanced by the slow execution time as the model contains all training cases. PRBFs have a single tuneable parameter called the smoothing factor. Careful selection (through CV) of smoothing factor is important, if too small overfitting risk is increased, too large and the classification error may increase [192].

5.4 Materials and methods

5.4.1 Training data

The training data described in section 3.4.2 was supplied to the artificial neural networks. Outliers were removed from the data using the process described previously. For more information on the training data preparation see section 4.5.1.

5.4.2 Multilayer perceptron implementation

The open source DTU toolbox (available from http://isp.imm.dtu.dk/toolbox/ann/) was used to construct the MLP as the nc_multiclass algorithm included in the package allows the output of class probabilities. The algorithm allows the construction of a two layer network, the hidden layer has hyperbolic tangent functions and the output layer incorporates softmax function allowing the outputs for each class to be determined as probabilities [193, 194].

5.4.3 PRBF ANN implementation

The PRBF ANN was implemented using the MATLAB neural network toolbox. The ANN is constructed using the *newpnn* function in MATLAB which adds neurons iteratively to the hidden layer until a specified error value is achieved. For more information see the MATLAB user manual [195].

5.4.4 Cross validation

The parameters of the MLP ANN (number of hidden layer neurons (HLNs)) and PRBF ANN smoothing factor (σ) were selected using a ten fold CV procedure identical to that applied with SVM parameter selection (section 4.5.2).

5.4.5 Classifier testing and external validation

For the optimal ANN designs the number of QDEMs per ANN was varied from 2 to 20 and the cv_{acc}, $train_{acc}$ and $test_{acc}$ were calculated. The $train_{acc}$ of the PRBF network was always 100% (as the training data is copied to HLN (section 5.3.2)). An independent test set validation was carried out using a portion of the training data held back from ANN construction. The effectiveness of each model was determined using the previously described methodology. An external validation of both ANNs was performed on the multiplex testing sets (section 3.5.2).

Note: *The source code for the MLP and PRBF implementation, CV and independent test set validation are available on the CD accompanying this thesis.*

5.5 Results and Discussion

The results of each ANN are shown below for parameter selection (section 5.5.1); training (section 5.5.2) independent test set validation (section 5.5.3). In addition each of the supervised techniques classification rates were monitored as the number of QDEMs per model was increased to determine the capacity of the models for identification of increased coding complexity (section 5.5.4). The multiplex mixture solutions were then presented to the optimum ANN models (section 5.5.5). Within each of the sections comparisons to the multiclass SVM classifier described in chapter 4 are discussed.

5.5.1 ANN parameter selection

Parameter selection for the MLP involved tuning of the HLNs until the optimum number for the data set was found (Table 12 and Figure 38). A Similar cv_{acc} was observed for the 4, 5 and 6 HLN MLPs. Independent test set validation was used to select the model that yielded the optimum generalisation on unseen data. The best $test_{acc}$ = 96.12% was obtained using the 5 HLN MLP and was therefore the optimum MLP design for this dataset.

Table 12 MLP ANN parameter selection. The cv_{acc} of the 4, 5 and 6 HLN MLPs were similar. Independent test validation identified the optimum MLP with 5 neurons in the hidden layer as optimal (highlighted). Average of ten MLPs.

HLNs	cv_{acc}	$train_{acc}$	$test_{acc}$
1	46.50	46.75	45.49
2	87.20	87.50	87.30
3	95.55	95.72	95.17
4	96.45	96.84	95.92
5	**96.72**	**96.95**	**96.12**
6	96.63	96.77	96.01

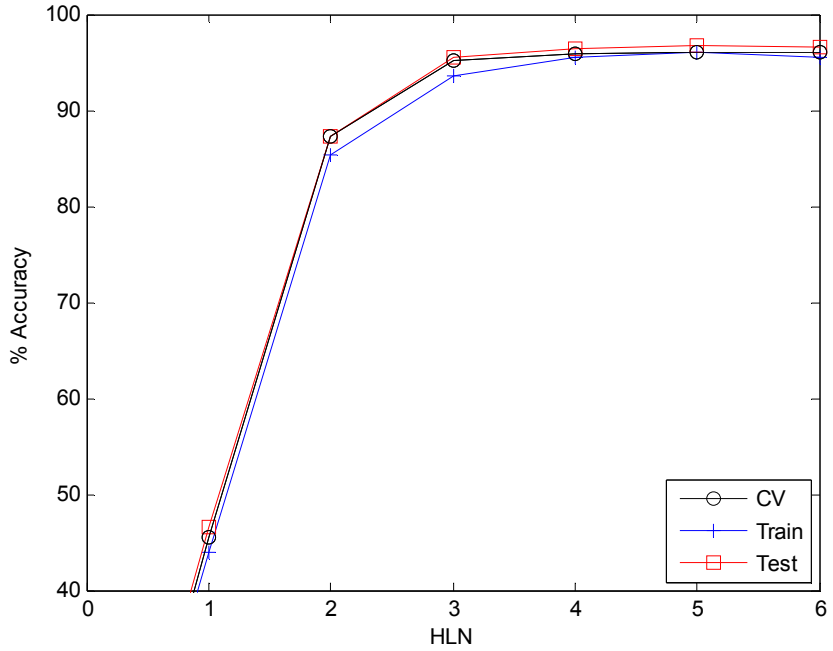

Figure 38 Performance of MLP with the CV, training and testing sets versus HLNs. The optimum number of nodes in the hidden layer was determined to be 5. cv_{acc} = 96.72% for the 5 HLN MLP.

In order to construct the best PRBF network the smoothing factor σ was varied from 1×10^{-6} to 50. The results presented are the average of 10 individual cross validation training and independent test sets (Table 13). The optimum smoothing factor using the PRBF ANN was calculated to be σ = 2.5. The cv_{acc} and $test_{acc}$ for the most accurate ANN were 94.69% and 94.38% respectively. The $train_{acc}$ is not applicable in the case of the PRBF (the training data is copied to the hidden layer therefore $train_{acc}$ will always be 100%).

Table 13 PRBF model selection. The smoothing factor sigma is varied from 1×10^{-6} to 50 and the cv_{acc} and $test_{acc}$ are calculated as an average of ten PRBF ANNs. There is no training error for PRBF ANNs. A QDEM classification based on the ranked probabilities for each class, the class with the maximum posterior probability is chosen (see eqn. 5.5 above).

(σ)	cv_{acc} (%)	$test_{acc}$ (%)	(σ)	cv_{acc} (%)	$test_{acc}$ (%)
0.000001	5.01	4.56	**2.0**	92.06	93.56
0.00001	4.92	5.12	**2.2**	92.68	94.02
0.0001	5.14	5.01	**2.5**	**94.69**	**94.38**
0.001	4.88	5.18	**2.8**	94.14	94.18
0.01	5.16	4.96	**3.0**	93.95	94.10
0.1	5.30	5.24	**4**	94.24	94.20
0.5	5.53	23.40	**5**	94.24	94.70
1	59.79	72.04	**10**	94.42	94.82
1.2	72.89	81.9	**15**	94.70	94.60
1.5	85.04	90.02	**20**	94.30	94.20
1.8	90.47	92.58	**30**	94.57	94.94
			50	94.15	94.18

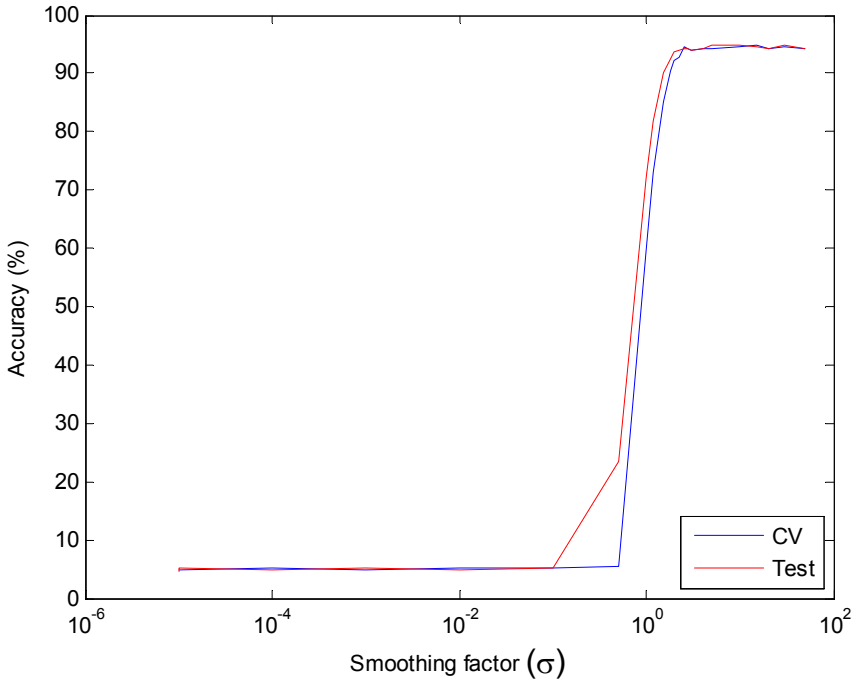

Figure 39 PRBF cross validation results. A ten fold cross validation procedure was carried out for a selection of PRBF smoothing factor from 1×10^{-6} to 50. The optimum accuracy was at σ = 2.5.

The training, evaluation of these classifiers is discussed below and comparisons to the multiclass SVM demonstrated in chapter 4 are drawn.

5.5.2 Training and execution

Training time is an important consideration in the application of supervised learning techniques for SAT application to allow experimental flexibility with respect to the assay targets (chapter 2). Minimisation of the training time would allow QDEM populations for analysis to be changed rapidly. The MLP had the longest training time of the three classifiers (5.75 hours) decreasing the rate at which the classifier can be re-trained on additional QDEM signatures, furthermore significant experimentation is required for MLP optimisation [179]. The PRBF ANN on the other hand has near instantaneous training times, however for large numbers of events the prediction is time consuming and computationally expensive (section 5.3.2). The SVM classifier required ~3.5mins to train; moreover the classification speed was in the order of seconds for thousands of events, therefore the SVM offers a compromise between classification speed of MLPs and the training time of the PRBF.

5.5.3 Independent test set validation

Following presentation of the independent test data to the MLP and PRBF the sensitivity and specificity of each class was calculated (Table 1). See the appendix for full MLP and PRBF confusion matrices. The MLP ($test_{acc}$ = 96.12%) was a more suitable classifier than the PRBF ($test_{acc}$ = 94.12%), the SVM ($test_{acc}$ = 96.33%) outperformed both ANNs.

The SVM had the lowest sensitivity for the QD0101 QDEM (R = 89.3%), resulting from confusion between this QDEM and the QD0110 and QD0111 microspheres. The sensitivity for this code calculated from the MLP was improved by 6.3%. The PRBF sensitivity on QD0101 (R = 86.8%) performed worse than that of the SVM. For the

QD0110 and QD0111 microspheres the identification sensitivity of both ANNs underperformed in comparison to the SVM, therefore while the MLP increased the sensitivity on the QD0101(R = 95.60%) signal, there was a decrease with the QD0110(R = 89.95%) and QD0111(R = 91.73%) in comparison to the SVM. For the remaining microspheres sensitivities of the SVM were greater than that of the ANNs or the difference was small. From the results of independent testing the SVM and MLP yielded a comparable performance on the unseen data; the PRBF was clearly the worst classifier with sensitivities for the QD1110 microsphere greatly diminished (R = 84.1%). In order to further separate the SVM and MLP methods the accuracy of each of the mixture test solutions were compared (section 5.5.5).

Table 14 MLP and PRBF independent test set validation; true positives (#TP), % specificity (S) and % sensitivity (R) are shown. The class with the lowest sensitivity for the ANNs are highlighted.

	QDEM	5 HLN-MLP			PRBF		
		#TP	S (%)	R (%)	#TP	S (%)	R (%)
1	QD0000	245	99.7	92.93	250	99.7	91.1
2	QD0001	193	99.7	92.16	200	99.7	88.9
3	QD0003	236	100	100	236	100	100
4	QD0010	228	99.6	93.49	230	99.0	92.7
5	QD0011	253	99.9	96.25	257	100	94.8
6	QD0100	216	99.9	99.54	221	99.9	97.3
7	QD0101	217	99.6	95.60	239	99.4	86.8
8	QD0110	188	99.5	89.95	197	99.4	85.8
9	QD0111	224	99.7	91.73	222	99.3	92.6
10	QD0202	214	99.7	99.07	215	99.7	98.6
11	QD1000	230	99.9	98.73	234	99.9	97.0
12	QD1001	220	99.9	100	222	100	99.1
13	QD1010	231	99.7	98.00	246	99.7	92.0
14	QD1011	230	99.9	98.70	229	100	99.1
15	QD1100	162	99.7	94.85	166	99.7	92.6
16	QD1101	224	99.9	95.41	229	99.5	93.3
17	**QD1110**	**185**	**99.7**	**88.18**	**194**	**99.5**	**84.1**
18	QD1111	228	99.7	98.71	230	99.6	97.9
19	QD2100	213	100	100	213	100	100
20	QD2200	227	99.9	99.13	228	99.9	98.7

5.5.4 Effect of increasing QDEMs on performance

The capacity of the MLP and PRBF was investigated with respect to the effect of increasing classes. The cv_{acc}, $train_{acc}$ and $test_{acc}$ were determined for each ANN (Table 2). To avoid bias arising from using well separated classes each of the experiments was comprised of *n* random QDEMs in the training data were selected, an average of 10 passes were calculated. The accuracy of the ANNs shows a clear decrease as the number of QDEMs added increase (Figure 40 and Figure 41).

Table 15 ANN performance against the number of QDEM considered by the model.

#QDEM	5HLN-MLP			PRBF	
	cv_{acc} (%)	$train_{acc}$ (%)	$test_{acc}$ (%)	cv_{acc} (%)	$test_{acc}$ (%)
2	100	100	100	99.85	99.68
3	99.9	100	99.94	99.86	99.41
4	98.55	99.38	98.67	99.06	98.93
5	99.10	99.64	99.46	98.24	97.87
6	99.04	99.57	99.26	99.18	98.92
7	98.10	98.94	98.25	98.49	98.24
8	98.99	99.17	98.68	98.77	98.45
9	98.32	98.76	98.42	97.68	97.68
10	98.72	98.28	98.96	96.83	97.31
11	98.21	98.08	98.40	96.20	96.43
12	98.31	98.04	98.48	95.95	95.98
13	98.27	98.04	98.16	95.92	96.18
14	97.08	98.00	97.36	95.66	96.09
15	97.10	97.20	97.08	95.80	95.98
16	96.99	97.20	97.24	95.67	95.60
17	96.94	97.40	97.10	94.80	94.80
18	96.78	97.27	96.96	94.88	94.94
19	96.34	97.01	96.59	94.20	94.39
20	96.06	96.98	96.12	94.27	94.09

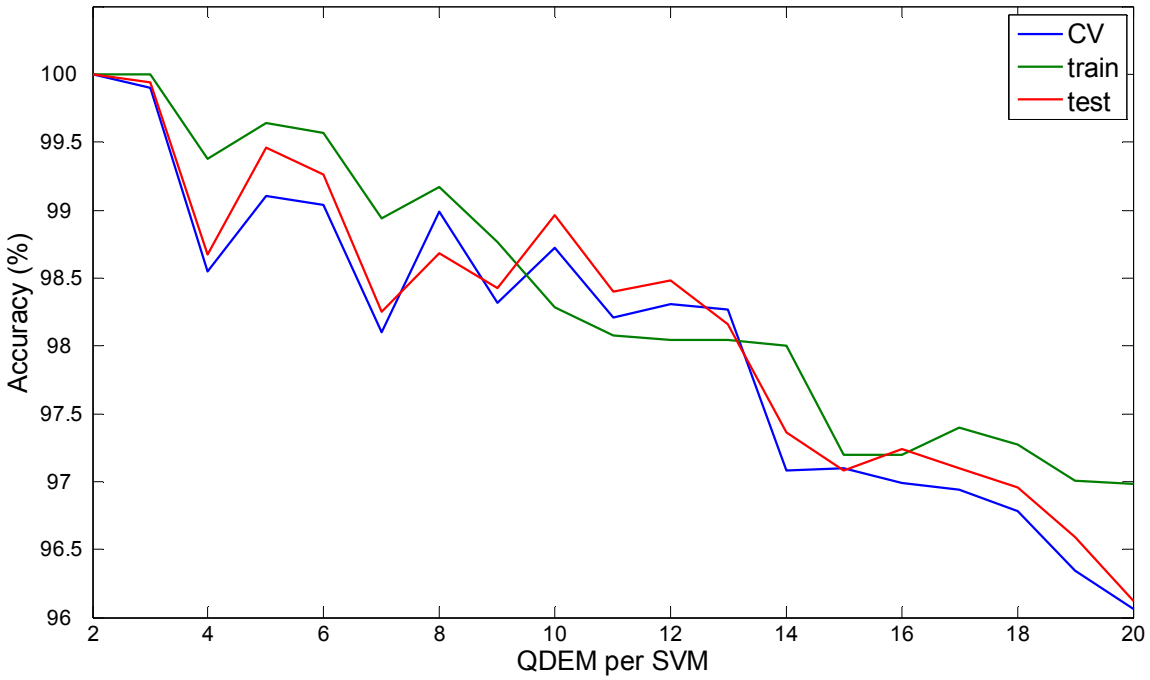

Figure 40 Evaluation of the effect of increasing the number of classes considered by the MLP ANN. PRBF as expected had no train error. There is a steady decrease in both the cv_{acc}, $train_{acc}$ and $test_{acc}$ accuracy.

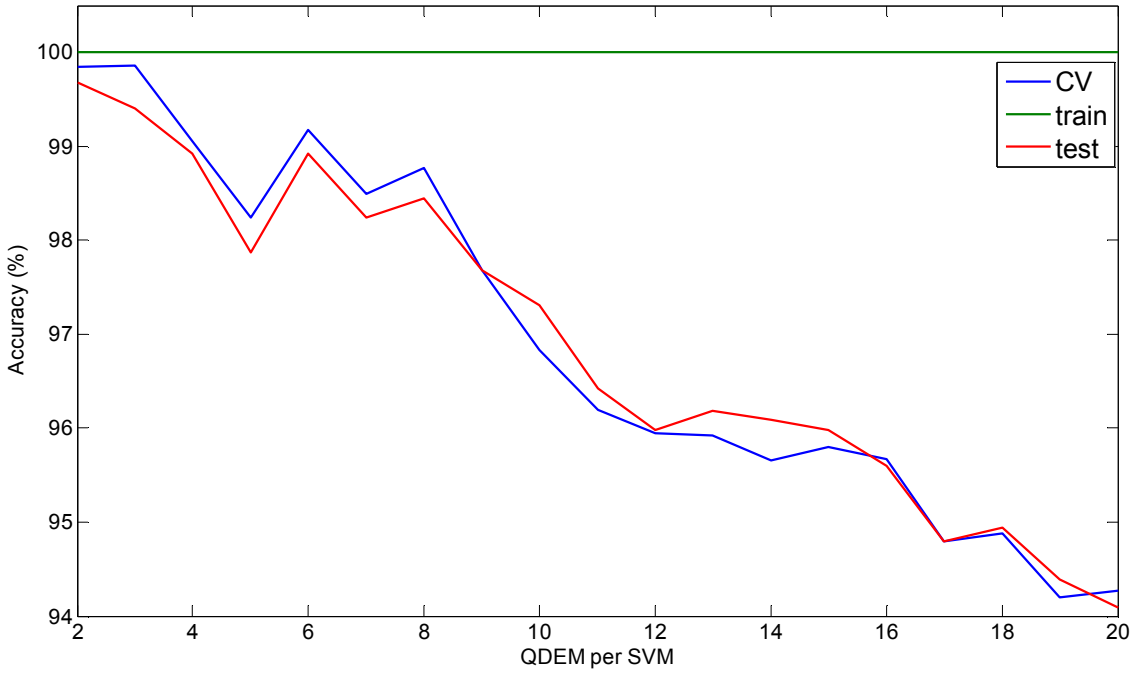

Figure 41 Evaluation of the effect of increasing the number of classes considered by the PRBF. The plot shows that there is an observable decrease in test set accuracy with increasing numbers of QDEMs.

In the future as additional classes are added to the model, the classification accuracy may decrease further, possibly as a result of the single net design; The combinatorial binary classifier of the SVM may offset the decrease in classifier performance. There are attempts within the community to create more efficient ensemble ANNs through the use of ECOC schemes which may prove useful for QDEM in the future.

5.5.5 External validation

External validation was carried out using the multiplex solutions for the MLP (Table 16) and PRBF (Table 17). The MLP incorporates the SOFTMAX function in output layer to allow probability outputs [196] and classified events below $p < 0.5$ are filtered, from the final results, in a similar manner to the SVM. There is no filtering of the classified events using the PRBF ANN as the network outputs are naturally probability based. Once again the MC rate and σ^2 were determined for each mixture solution as described in section 3.4.2. For the SVM the highest MC rate was for the multiplex tests was 6.4% (test 4). The performance of the MLP on this test set has decreased by 7.16% in comparison to the SVM. The FP classifications were mainly observed for the QD0101, QD1010 and QD1110. For the mixture 1 analysis; the solution containing the most difficult to classify microspheres performed poorly, with a MC rate of 20.9%, some 16.6% below that of the SVM. Misclassifications occur mainly with QD0101 and QD1101 microspheres. The SVM outperformed the MLP or the difference was negligible for the remaining multiplex testing solutions. The average MLP MC rate from external validation was 6.1%. The variance of the CCs across the MLP was however poor, again the 7-10 mixtures were large in comparison to the SVM additionally a higher variance for tests 1-6 was observed. The average σ^2 =56698 for the ten mixtures.

Table 16 Prediction of unknown events from test samples using MLP ANN classifier. The total numbers of QDEM classifications ($p \leq 0.5$) are shown for each dataset, the microspheres present in the mixtures are highlighted.

		Mixture#									
		1	***2***	***3***	***4***	***5***	***6***	***7***	***8***	***9***	***10***
QDEM code	**QD0000**	4	13	0	3	**453**	41	3	**475**	**278**	29
	QD0001	1	3	3	5	**389**	**493**	8	**453**	**337**	**585**
	QD0003	0	0	**565**	**610**	0	0	**523**	0	0	0
	QD0010	14	35	3	21	49	63	**579**	58	58	**472**
	QD0011	**551**	0	18	6	0	**548**	0	**348**	**394**	**450**
	QD0100	45	**538**	**0**	38	**457**	4	9	**352**	42	**344**
	QD0101	165	5	2	117	**1191**	2	**848**	**920**	**1204**	**1142**
	QD0110	**331**	1	0	**330**	**410**	0	4	**391**	**436**	**376**
	QD0111	1	0	0	1	60	0	**34**	**92**	**112**	**169**
	QD0202	11	0	**219**	**281**	0	18	8	14	27	40
	QD1000	0	19	2	37	0	**469**	**508**	**343**	42	**403**
	QD1001	0	0	0	0	0	0	0	0	**287**	**341**
	QD1010	1	**642**	0	119	4	**587**	2	50	111	**480**
	QD1011	2	**441**	6	**302**	0	**429**	2	**405**	**581**	**460**
	QD1100	**257**	**252**	0	1	**106**	**281**	32	107	**279**	**293**
	QD1101	148	10	3	**825**	**458**	**599**	**394**	**944**	**844**	**920**
	QD1110	**388**	2	1	54	**286**	**348**	**321**	**782**	**576**	**549**
	QD1111	0	1	1	**132**	0	0	**347**	**50**	**59**	**110**
	QD2100	0	0	**682**	0	0	0	**777**	0	0	0
	QD2200	10	6	**487**	2	10	31	**567**	20	16	24
#Codes		4	4	4	6	8	8	10	12	12	15
#Events		2000	2000	2000	3000	4000	4000	5000	6000	6000	7500
#Classified		1929	1968	1986	2884	3873	3913	4968	5804	5683	7187
Rejected (%)		3.5	1.6	0.7	3.8	3.1	2.1	0.6	3.2	5.2	4.1
#Correct		1527	1873	3906	2481	3750	3754	4898	5555	5387	7094
CC rate (%)		79.1	95.1	98.3	86.0	96.8	95.9	98.5	95.7	94.7	98.7
σ^2		**15608**	**27520**	**38642**	**64829**	**99563**	**12747**	**54661**	**81720**	**102309**	**69385**
MC rate (%)		**20.9**	**4.9**	**1.7**	**14.0**	**3.2**	**4.1**	**1.5**	**4.3**	**5.3**	**1.3**

Interestingly the PRBF showed improvement for test 1 (Table 17). The RBF displayed a MC rate decrease of 11.9%, although there were still 4.7% of events misclassified in comparison to the SVM. The PRBF performance on mixture 5 was poor, returning 16.7% misclassified events, 13.7% and 13.5% worse than the SVM and MLP respectively. The main source of misclassifications in this mixture were due to QD0111 misclassifications (R = 92.6%). A considerable number of errors were also noted on mixture 4 (12.8%) due

to significant misclassifications on QD0010 (R = 92.7%) and to lesser extent on QD1110. The sensitivity of this class was R = 84.11%. The average MC rate for the PBRF external validation was 7.5%.

Table 17 Prediction of unknown events from test samples using PRBF ANN classifier. (See section 3.4.2 for multiplex test compositions). The QDEMs present in each solution are highlighted.

		Mixture #									
		1	***2***	***3***	***4***	***5***	***6***	***7***	***8***	***9***	***10***
QDEM code	**QD0000**	8	18	0	4	**569**	122	8	**582**	**349**	73
	QD0001	0	1	1	1	**298**	**419**	3	**374**	**281**	**532**
	QD0003	0	0	**562**	**604**	0	0	**523**	0	0	0
	QD0010	47	105	24	234	75	159	**1006**	150	380	**901**
	QD0011	**550**	1	28	16	0	**551**	0	**354**	**396**	**454**
	QD0100	24	**530**	0	22	**449**	4	16	**330**	32	**317**
	QD0101	13	1	0	5	**429**	2	**145**	**285**	**395**	**352**
	QD0110	**479**	10	0	**437**	**735**	2	28	**616**	**686**	**554**
	QD0111	27	0	0	28	542	0	**717**	**570**	**762**	**871**
	QD0202	16	2	**225**	**284**	0	21	0	17	31	49
	QD1000	1	10	3	0	0	**446**	**480**	**321**	0	**342**
	QD1001	0	1	0	0	0	1	0	1	**178**	**215**
	QD1010	1	**508**	0	15	3	**492**	18	13	21	**378**
	QD1011	1	**537**	1	**321**	0	**496**	0	**431**	**624**	**462**
	QD1100	**176**	**236**	0	8	**94**	**236**	9	91	**238**	**217**
	QD1101	6	2	0	**247**	**225**	**322**	**156**	**331**	**307**	**367**
	QD1110	**616**	38	0	52	**535**	**671**	**356**	**805**	**703**	**702**
	QD1111	35	0	0	**722**	46	47	**222**	**725**	**617**	**707**
	QD2100	0	0	**682**	0	0	0	**774**	0	0	0
	QD2200	0	0	**474**	0	0	9	**539**	4	0	7
#Codes		4	4	4	6	8	8	10	12	12	15
#Events		2000	2000	2000	3000	4000	4000	5000	6000	6000	7500
#Correct		1821	1811	1943	2615	3334	3633	4918	5724	5536	7371
CC rate (%)		91.0	90.5	97.1	87.1	83.3	90.8	98.3	95.4	92.2	98.2
σ^2		**37788**	**21033**	**37485**	**36414**	**25872**	**17992**	**80262**	**30915**	**41614**	**47338**
MC rate (%)		**9**	**9.5**	**2.9**	**12.8**	**16.7**	**9.2**	**1.6**	**4.6**	**7.8**	**1.8**

The average variance for the multiplex tests for the PBRF was $\sigma^2 = 37671$. An increase is observed in test 7-10 suggesting that there is an increase in the number of misclassifications between QDEMs present in the mixture.(For a comparison of the variances for each of the classifiers see Figure 45)

The MLP is the most suitable ANN classifier and performs comparably to the SVM in independent test set validation in terms of accuracy. The SVM however outperforms the MLP in external validation, moreover the SVM sensitivities for the most difficult to classify microspheres were superior. Additionally for the SVM there was less variance exhibited across the ten mixtures, moreover the variance were more uniform.

5.6 Conclusion

The ANNs implemented here have been shown in previous studies to be successful in classification of events from flow cytometry data. Two ANN implementations, the PRBF and MLP were trained using the QDEM FCM training set and compared to the performance of the SVM classifier in chapter 4. Rigorous parameter selection was applied in order to construct the optimum ANN. For the MLP, a five HLN configuration yielded the best performance (cv_{acc} = 96.72%, $train_{acc}$ = 96.95% and $test_{acc}$ = 96.12%). A PRBF with $\sigma = 2.5$ gave the best prediction of the dataset (cv_{acc} = 94.69%, and $test_{acc}$ = 94.38%).The SVM (cv_{acc} = 96.58%, $train_{acc}$ = 96.72% and $test_{acc}$ = 96.33%) is therefore the most suitable model for the classification of QDEMs from FCM data. The results of an external validation using multiplex QDEM test solutions further demonstrated the suitability of the SVM method. The SVM had a lower MC rate in each of the 10 tests than both the ANN classifiers and the variance for the SVM CCs (see Figure 45). Average SVM σ^2 = 31479, MLP σ^2 = 56698 and PRBF σ^2 = 37671.

The accuracy of the SVM is superior for the both the independent test set and multiplex test sets. Therefore the SVM is the optimum supervised learning technique to classify

events from the QDEM dataset. The model is highly accurate, sensitive and specific, outperforming ANNs. It has been shown previously that SVM outperforms the MLP for classification problems and underperforms with regression, although the differences are indeed small, the results presented here confirm this.

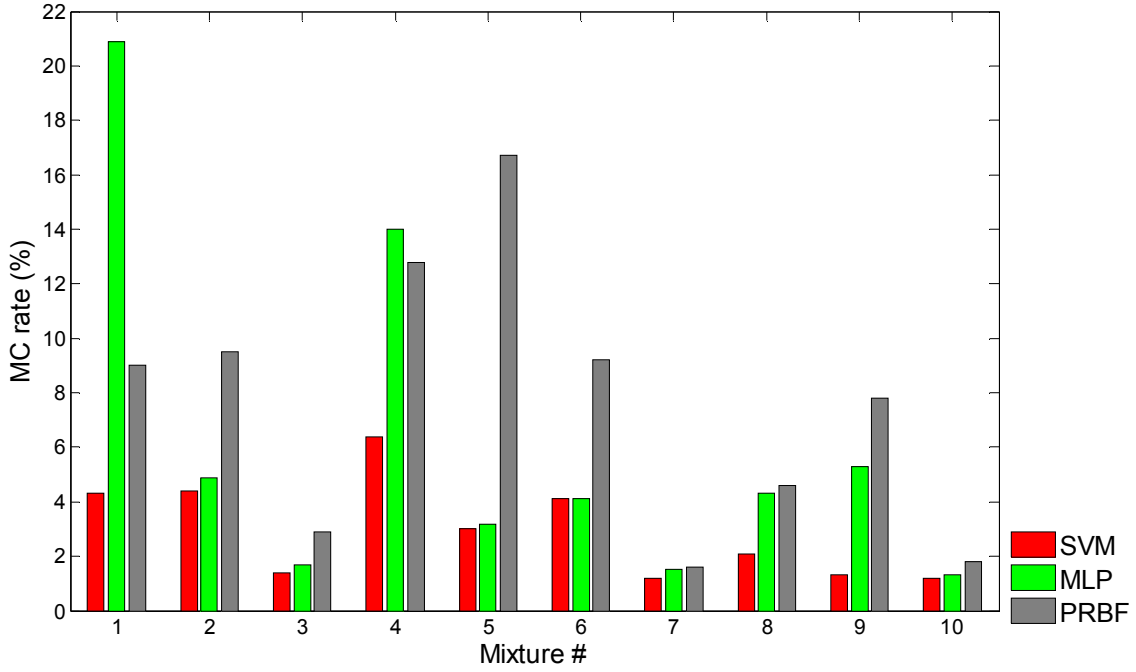

Figure 42 MC rates of the ten mixture tests for the supervised learning algorithms. The SVM has the lowest number of misclassifications in each test.

The main difference between the methods relates to model complexity, the MLP network usually consists of a small number of units in the hidden layer, the SVM incorporates a much larger number of SVs. The SVM formulation of the learning problem, (i.e. quadratic optimisation, greatly reduces the number of operations required thus reducing the training time [197]). The training and execution time of the SVMs were the most practical. The MLPs training time would prohibit flexibility in the laboratory and the execution time of PRBF was also time-consuming.

Chapter 6: Overall discussion and conclusions.

6.1 Overview

This chapter begins with an overall conclusion of the work described in this thesis. We begin with a discussion of the classification methods (section 6.2). As part of this project a user friendly software program was also developed to enable a flow cytometrist to apply the SVM classifier to QDEM recognition. The main functions of the program are outlined below (section 6.3). Finally an overall conclusion of this work is presented and recommendations for future work are outlined (section 6.4 and section 6.5).

6.2 General discussion

Increasing the multiplexing capacity of QDEM libraries to the levels suggested in the literature (~40,000 unique signatures) requires the utilisation of numerous emission wavelengths and discrete intensity levels. The first question asked in this thesis was if current means of QDEM identification were suitable for multicolour QDEMs analysed on a standard bench top flow cytometer. To this end MPG was evaluated with regard to its suitability to distinguish members of commercially available QDEMs from FCM data acquired on an EPICS XL with single laser excitation and four colour detection.

A 20-plex QDEM set was analysed using FCM with approximately 20,000 training events recorded. An external testing set of QDEM solutions was also prepared and analysed to provide a benchmark for the methods under examination here, 500 events for each QDEM in the solution were recorded. While the capacity of the library used was not large, the coding scheme complexity (4 emission wavelengths and 4 intensity levels) was greater than those previously described in the literature for QDEMs. The complex coding

scheme considered here should give a clear picture of how currently available data analysis methods would perform at higher levels of multiplexing.

A number of outliers were identified in each QDEM data set possibly arising from variations in bead manufacture, damage to the bead or variation in measurements. There is a degree of overspill between the fluorescent channels as the median fluorescent intensity was not uniform for each detector (Figure 16). The CoeffVs was also high for the microspheres analysed and provided a suitable dataset to rigorously test the classification methods.

Investigation of the suitability of a current encoded microsphere identification method was carried out. The method applied was an expert supervised gating technique, MPG. MPG in recent times has been applied successfully to such libraries (although the coding schemes described were less complex than for the QDEMs used here). MPG misclassified a large proportion of the multiplex solutions showing disappointing levels of false positive identifications resulting in average MC rate of 9.7% for the 10 mixtures (14.1% for mixtures 1-6). The most difficult to classify QDEMs in mixture 1 yielded a MC rate of ~30.6%. As stated previously the results for mixtures 7-10 should be treated with caution, while the classification accuracy increases, the increasing numbers of QDEMs in the solution mask the true performance of the model. The variance of correct classification may show that false positive classifications were present. To this end the variance of correct classification were calculated. MPG had the highest average variance across the external validation (Figure 45). The results could not be improved even after fine tuning of each QDEM region. Moreover multiple classifications were made on single

events; due to overlap between the gates (there were more classifications than events in the testing sets). Therefore the confidence in results obtained using this method was poor. There was no way to ensure the optimum gate for each population was obtained and the regions selected were based on the interpretation of the user. Therefore MPG is a subjective process relying on the skill of a particular user and as the number of QDEMs per assay increases would the number of plots to be considered increases non-linearly. MPG was also a time consuming method with ~1 hour required to set and tune the regions for each population.

The central aim of this thesis was to improve upon the classification accuracy of MPG for QDEM recognition through the use of supervised learning algorithms. Two of the most popular supervised algorithms for the discrimination of FCM subpopulations are SVMs and ANNs. Supervised learning techniques offer a novel solution to QDEM subpopulation identification. Multivariate machine learning algorithms have advantages over the MPG in that subjectivity is removed from the process and classification occurs in a multidimensional space where subtle relationships between detector signals are considered. SVMs have a good theoretical basis, allowing the multidimensional gating of subpopulations, moreover through the calculation of the maximal margin hyperplane the optimum gates can be found. ANN classifiers have also shown good potential FCM studies, the two most widely used ANN classifiers in the literature were utilised for QDEM classification A PRBF and MLP ANN were implemented and a comparison with the MPG and SVM model carried out for the QDEM dataset.

An outlier removal procedure was also developed to remove outlying events through setting an IQR threshold for each parameter, the classification accuracy was improved using this method. A total of 1,242 events (6.27% of total events acquired) were removed from the original training data improving the accuracy by 3.31% in the case of the SVM. As outlier removal was not included as part of the FCSexpress program, outlier filtered datasets were used only to construct the SVMs and ANNs.

In order to select the optimum model for the data set using SVMs and ANNs, a rigorous cross validation procedure was carried out for each learning system. An independent testing set was used to determine the generalisation error of each classifier. The cv_{acc}, $train_{acc}$ and $test_{acc}$ of each model (SVM, MLP, and PRBF) are shown below (Table 18). The classification accuracy of the SVM incorporating a linear kernel and C = 1 using the OVO multiclass design outperforms those of the ANNs (Table 8) with the best performance independent test set validation, cv_{acc} = 96.58%, $train_{acc}$ = 96.72% and $test_{acc}$ = 96.12%.. The MLP is the best ANN for the task. The optimum number of HLNs for the MLP was determined to be 5 through cross validation; cv_{acc} = 96.72%, $train_{acc}$ = 96.95% and $test_{acc}$ = 96.12%. The PRBF ANN (σ = 2.5) had the poorest performance of the three classifiers cv_{acc} = 94.69% and $test_{acc}$ = 94.38%. The SVM outperforms both ANN implementations although the difference between the SVM and MLP is small in independent testing.

Table 18 Comparison of supervised learning techniques for the identification of QDEMs from FCM data. The best classifier for the QDEM dataset is the SVM.

	cv_{acc} (%)	$train_{acc}$ (%)	$test_{acc}$ (%)
SVM	**96.58**	**96.72**	**96.33**
MLP	96.72	96.95	96.12
PRBF	94.69	N/A	94.38

As a further measure of confidence the sensitivity and specificity for each class was calculated on the test set predictions. The specificities for the three classifiers were comparable. The sensitivities for each model are shown below (Figure 43). For the most difficult microspheres to classify (QD0110, QD0111 and QD0101) the SVM again yielded the best average performance.

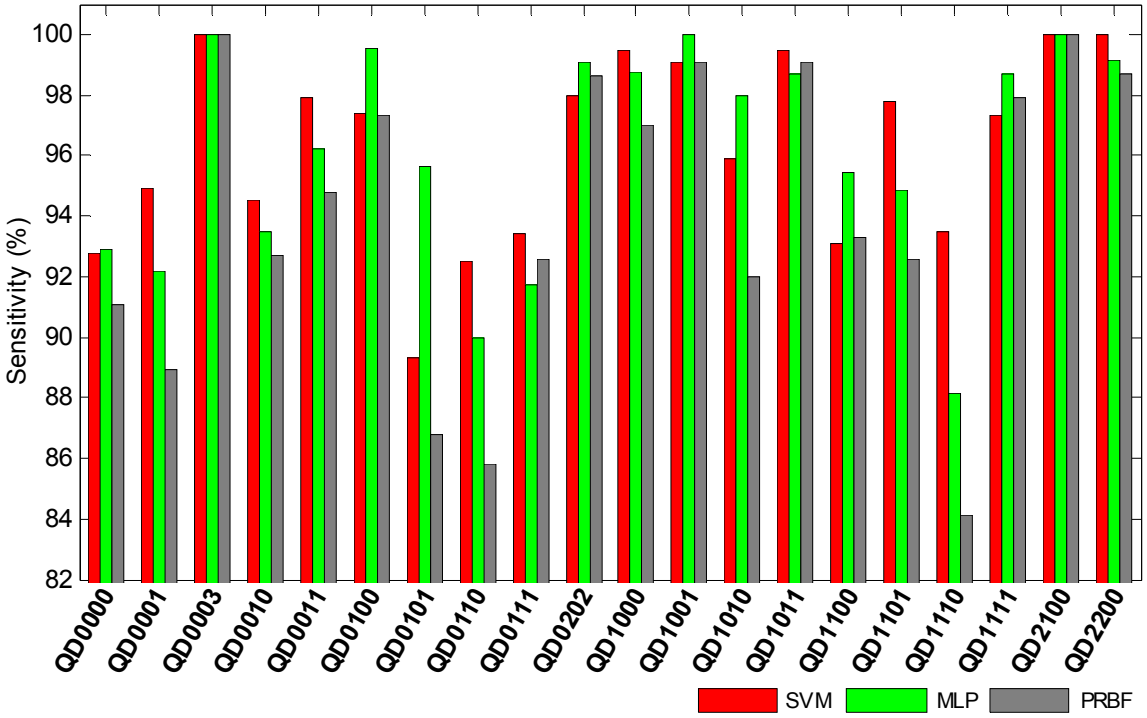

Figure 43 Sensitivities for the three classifiers. See section 4.3.4 for sensitivity calculation. MPG is not included as there is no independent test set validation.

To test the performance of the classifiers and compare the supervised algorithms with MPG, 10 QDEM mixtures were prepared using different numbers of QDEMs and analysed using FCM. The MC rate was calculated as there was no way of independently verifying the identities of the microspheres from the mixture solutions prior to analysis. The subpopulations present in the solution were known; hence the false positive results of each classifier are used to determine suitability.

All supervised learning algorithms were shown to return fewer false positives than the MPG method. The SVM showed excellent classification performance on these samples clearly outperforming MPG and both ANN methods (Table 19 and Figure 44). The MLP was the slightly more suitable ANN method outperforming the PRBF method by ~2%.

As stated previously the MC rate results should be treated with caution, as more QDEMs are included in the mixture. Hence the likely hood of a misclassified event being designated as QDEM known to be present. In future work it is essential that the classifications of SAT assay and SVM classification system be run in parallel with a standard detection platform e.g. microarray.

The variance was also calculated for classifications on QDEMs present in the mixture solutions (i.e. correct classifications) in each solution for each of the four classifiers (Figure 45). Calculation of the variance allows a further measure of performance of the classification techniques. Assuming that each of the testing solutions was homogeneous (rigorously agitated before aspiration to the flow cytometer), the most suitable classifier was identified as having the lowest MC rate and the lowest variance between the numbers of events assigned as correct. Although the QD1100 QDEM seemed to have a diminished stock concentration each classification paradigm was tested on an identical dataset, therefore this effect was negated.

Table 19 Comparison of the mixture misclassification rates and CC variances for each of the classification systems evaluated.

	Mixture #	MPG	SVM	MLP	PRBF
MC rate (%)	1-6	14.5	3.9	8.1	10.0
	All	9.7	2.9	6.1	7.5
CC variance (σ^2)	1-6	40448	29317	43151	29430
	All	63482	31479	56698	37671

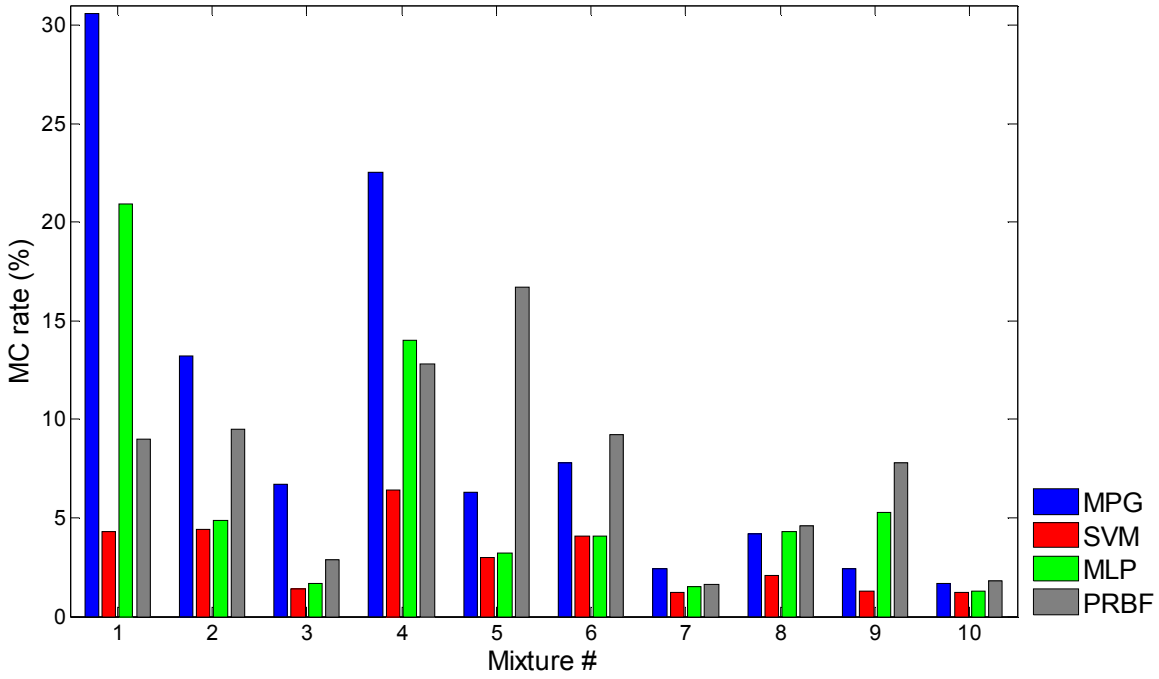

Figure 44 Comparison of the MC rate for the 10 multiplex test solutions. The SVM (red) has the lowest MC rate for all QDEM mixtures (2.9%).

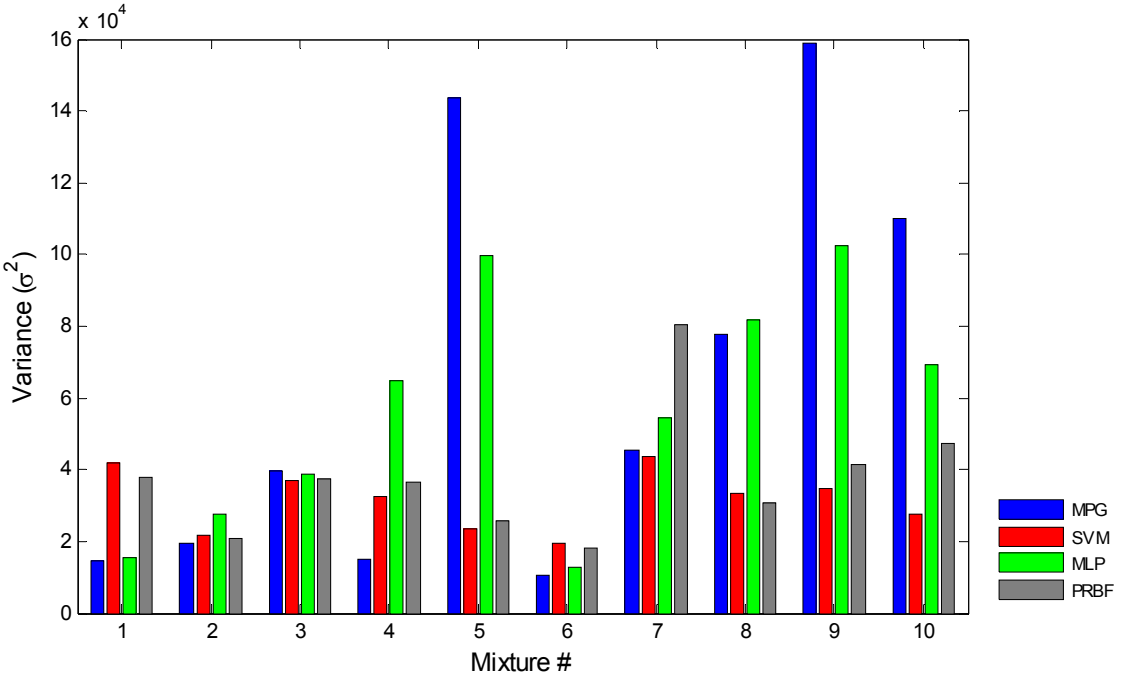

Figure 45 Variance of each multiplex mixture solution for the four different classification algorithms used. Assuming a homogenous mixture of QDEMs within the test solutions the variance of the included QDEMs is used an indicator of classification performance in the external validation. The SVM (red) demonstrates the lowest variance between the numbers of events detected in each mixture (average $\sigma^2 = 31479$).

MPG had the highest variance over the mixture solutions (average $\sigma^2 = 63482$) suggesting that FPs were present. The SVM (average $\sigma^2 = 31479$) showed a more balanced classification of the events expected with a homogeneous, ~50% lower than that of MPG (average $\sigma^2 = 63482$). Interestingly the PRBF variance (average $\sigma^2 = 37671$) was significantly lower than the MLP (average $\sigma^2 = 56698$).

The results of independent test set validation and analysis of the QDEMs show the SVM classifier to be the most suitable for the classification of QDEMs from FCM data outperforming both MPG and the ANNs. The success of the SVM over the ANN implementations for this task concurs with Moriss *et al.* who reported success with SVM for the discrimination of 20 phytoplankton species. Here a multiclass SVM outperformed single species RBF ANN and a large optimised RBF ANN for all species [152]. Although Quinn *et al.* reported that PRBF had the best performance for the classification of FCM events during an *in vitro* viability study, overcoming both the MLP and SVM learning algorithms [151]. Our work shows that in this case the SVM is superior to that of the ANNs for classification of QDEMs.

The effect of each of three classifiers when additional microspheres were added was determined to assess possible scale up issues. However there was no significant difference observed in the accuracy of each type of model with the addition of QDEMs for the results here; it is unclear if the classification accuracy would decrease beyond 20 QDEMs. The "scaling up" of RBF ANNs was also deemed to be more problematic for ANNs in comparison to SVM. The work of Boddy *et al*. points to SVM handling the scale of a number of classes to be handled much more efficiently by a SVM [152].

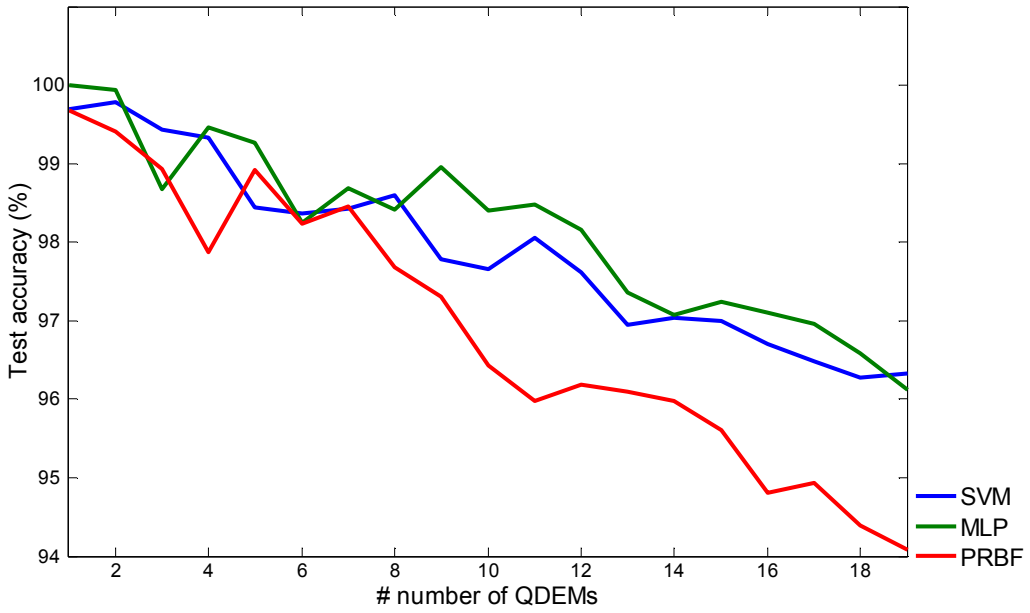

Figure 46 Effect of addition of QDEMs considered by the classifier on test set accuracy. The SVM and MLP decrease at a similar rate, future performance is unknown however the OVO SVM is well suited to offset these concerns.

The scale-up issue could be a potential limitation of the system although the theory of OVO SVMs should offset this. The creation of binary classifiers to discriminate against one another should be dependant on the complexity of the decision boundary required. Furthermore the performance of the RBF kernel SVM is encouraging, in that the performance was similar to that of the linear kernel SVM. If the complexity of class decision boundaries increases, a non-linear SVM could be employed to achieve classification in a kernel induced feature space e.g. RBF kernel.

Apart from possible scale-up issues, it is not yet clear at this stage if the current performance of the SVM can be improved. In theory it is possible that the SVM could exceed 99% accuracy, however accuracy is proportional to the quality of the microsphere manufacturing and encoding methods therefore increasing the precision of the FCM analysis (reduction of the CoeffV). Such a reduction in CoeffV may be required for

expansion of QDEM libraries. The high throughput nature of FCM also suggests spurious events are always likely to be present. The use of probability filtering of classification results removes the majority of these events . While the supervised learning methods have been shown to be successful perhaps the largest limitation of a supervised learning system is the application of these methods by laboratory users. The methods described in chapters 4 and 5 were implemented in the MATLAB environment restricting access to normal FCM users. To overcome this limitation a user friendly interface was designed in order to allow rapid and construction and evaluation of multiclass SVMs for the identification of QDEMs from SVM data. This software program forms a natural conclusion to the work described in this thesis.

6.3 FlowSVM: A software program for the SVM construction for the classification of QDEM from FCM data

6.3.1 Introduction

To allow laboratory users to construct and evaluate multiclass SVMs for QDEM subpopulation identification in flow cytometry a user friendly program, FlowSVM, was created. FlowSVM is a freely available standalone package developed in the MATLAB environment allowing standard data plotting and the development and evaluation of SVM classifiers for QDEM subpopulations. The following sections briefly describe the features of the program in two parts, firstly the standard data analysis module (section 6.3.2) allowing traditional FCM plotting and the module for the application of multiclass SVMs to QDEM classification (section 6.3.3).

6.3.2 FlowSVM: FCM data plotting tool

To allow visual inspection of the data prior to SVM training a tool to allow standard FCM plotting was developed (Figure 47). The FCM data directory must be chosen first, sample information contained in the HEADER portion of the FCS files is then extracted and displayed for each file. The FCM data is imported by selecting the relevant file from the listbox (Figure 47). Note: If the plotting tool is activated directly from the SVM manager (section 6.3.3), selected FCM data is transferred automatically. There are three types of plots available, standard non density histograms (univariate, bivariate and trivariate) and event density plots (scatter, contour and surface). Each FCS in the selected directory can be overlaid on a single plot with standard histogram plots - a useful feature for an initial indication of separation between QDEMs. A region selection tool is also included allowing only events within the selected area to be retained, sample statistics are recalculated for the selected region and new plots can be drawn. Standard plotting functions are also included such as 3D plot rotation, magnification, annotation and plot export.

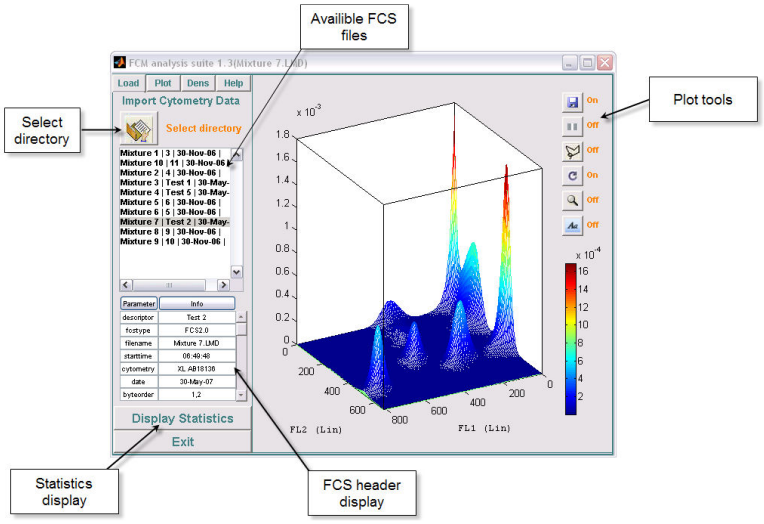

Figure 47 FlowSVM: Plotting tool interface. A surface plot of event density is shown.

Sample statistics are calculated for each dataset including the mean, median, standard deviation and the IQR. The number of outliers in each channel is also shown for each FCM channel. Boxplots can also be used to display all detector measurements simultaneously and outliers in the dataset.

6.3.3 FlowSVM: SVM management module

The main aim of the FlowSVM program was to allow laboratory users to construct and evaluate multiclass SVMs for the identification of QDEMs independently from MATLAB. The methodology described throughout chapter 4 is incorporated into the program. The main screen can be seen below (Figure 48), the various panels for each stage are selected from the top of the screen allowing data formatting, CV, training, testing and unknown QDEM prediction.

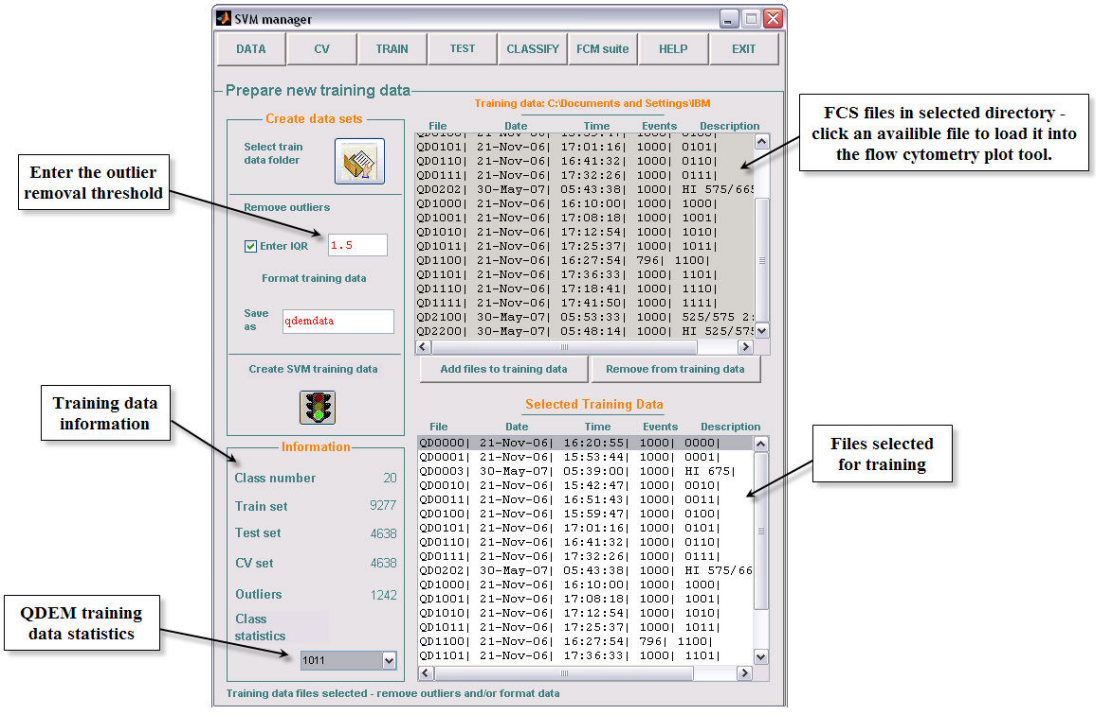

Figure 48 FlowSVM training data importation. Files in the current directory can be selected to form the training data. Outlier filtering is also carried out during the data formatting process.

The first stage in construction of an SVM for classification is the selection and formatting of training data. Once a directory has been specified the information contained in the HEADER is displayed. The user can then select the FCS files containing each class for SVM training. Selected data files are shown in the lower listbox (double clicking on a file in the upper listbox activates the plotting tool and transfers the selected training data - see section 6.3.2). Once data formatting is activated the training data is randomised, split into the training subsets and written to the LIBSVM format. The IQR cut-off for outlier removal can also be specified. The training data must be designated file name for data storage. An individual file is created for each training data subset and the events in each subset displayed to user along with the number of outliers removed. Standard statistics for each QDEM population can also be displayed for each class in the training data.

The four phases (parameter selection, training, testing and application) in SVM analysis are contained in separate panel within the program. Model selection using cross validation can be carried out by pressing the CV tab. Here the optimum parameters for the SVM can be determined for the selected *cv_set*. The four most popular kernels are implemented and the kernel specific parameters can be assigned. The number of folds must be entered for the CV procedure. Once the CV has completed the cv_{acc} is outputted for the selected parameters (Figure 49). If the cv_{acc} is unsatisfactory new parameters can be re-entered and the process repeated until the optimum model is located.

Following the selection of the optimum parameters SVM training can be carried out in the TRAIN panel. The training screen is very similar to that of parameter selection. Here

the parameters selected through CV can be applied to a training set selected from the data store. The constructed model is stored for further evaluation.

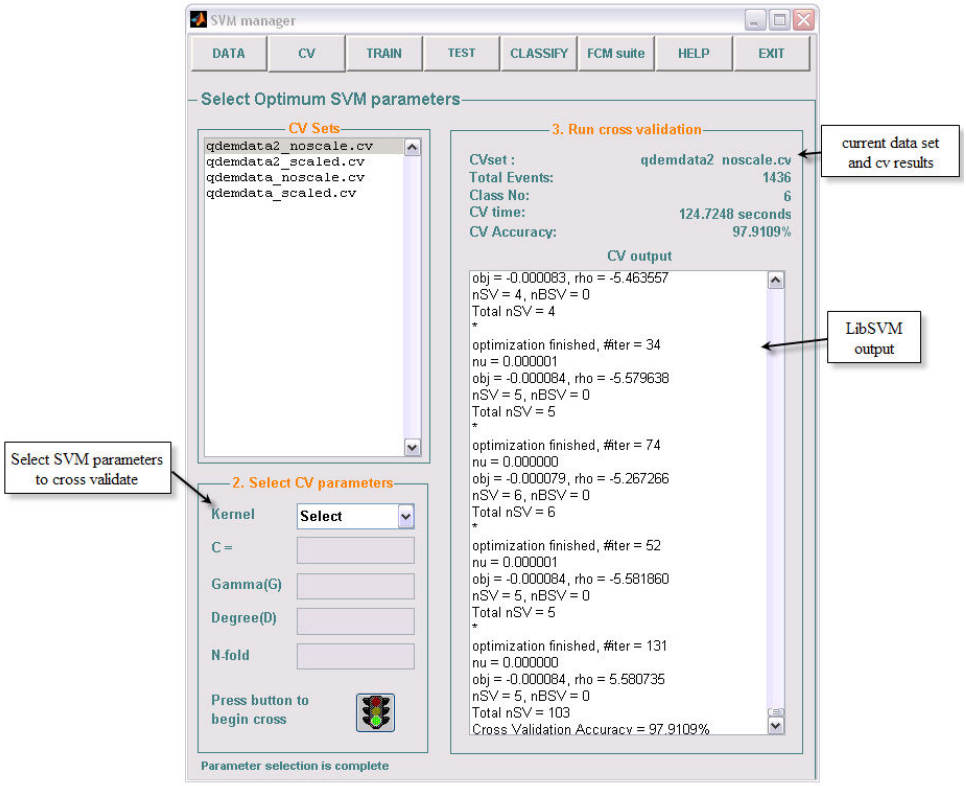

Figure 49 FlowSVM Parameter selection. CV is carried out on the selected dataset and the results returned to the user.

Complete independent test set validation of trained SVMs can be carried out in the TEST panel. The classification accuracy of corresponding testing sets for each model can be determined. Confusion matrices are also constructed and evaluated automatically and the sensitivity and specificity of each class outputted to the user. A bar chart of classification is presented to the user showing the extent of classifications across the test set. Therefore the user can efficiently determine the success of each SVM model on the data and maintain a record of each SVM constructed.

Validated classifiers can be applied to assay data in the CLASSIFY tab. Here the required SVM is selected along with the probability cut-off. An FCS file is then selected for presentation to the SVM. Following classification of the data set a plot of classified events for each class is displayed. The results of classification and the probability threshold applied are also recorded for further use.

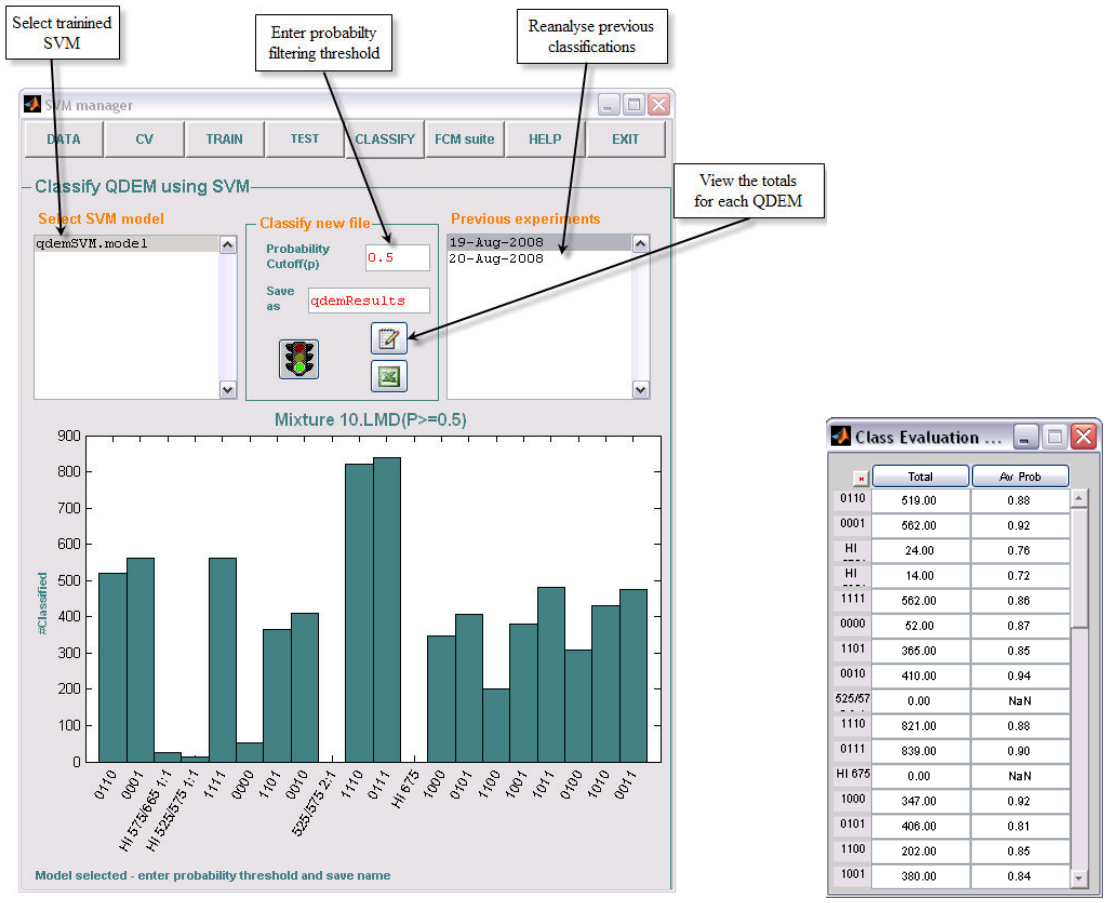

Figure 50 Prediction of QDEM SAT assays using the FlowSVM program. Trained models are selected for application to test files. The probability output cutoff points for classification can be specified and the results stored. A classification plot is presented. The total classifications are presented to the user.

It is hoped that this tool will make the SVM classifier more accessible to typical laboratory-based users. Future recommendations for possible extensions of this software are included in the next section.

Note: *The standalone program and source code for the program described above is freely available on the CD accompanying this thesis.*

6.4 Overall Conclusion

Suspension array technology has much potential in post genomic applications. Traditional methods of subpopulation identification methods have been shown to be limited for the complex encoding strategies possible with nanocyrstal optically encoded microspheres. An unmodified flow cytometer representative of equipment found in a variety of locations was used to acquire the QDEM data used in this thesis. Both a multiparameter gating and unsupervised clustering method were found to be deficient for the QDEM library analysed in this study. The aim of this work was to improve upon these methods using supervised learning techniques.

To this end two of the most popular learning paradigms, ANNs and SVMs were applied to the dataset. A 10-fold cross validation was used to select the optimum classifiers for each model type. Each model was then evaluated using internal and external validation. The multiclass SVM classification produced the classifier with the best classification rate in both independent test set validation (96.33%) and MC rate (2.94%) on the QDEM mixtures outperforming the ANNs and approaching that of the Luminex system (~2%). Additionally the training time of the SVM was rapid and classifications could be performed rapidly an important consideration for FCM. SVMs are well suited to this task and allowing the optimum gates to be located in a multidimensional space for each class. There is no reason why organic dye encoded microsphere could not be classified by the SVM although no such encoding scheme has been considered during this study.

A user friendly interface has been created to allow construction and evaluation of SVMs by laboratory users was developed for flow cytometrists. The program facilitates the conversion of FCS files into training data, parameter selection, training and independent test set validation. The resulting SVMs can be applied to unknown FCM in order to determine the identity of the microspheres present.

It is unclear how the SVM would perform when the encoding scheme is expanded. The OVO multiclass SVM should classify these microsphere with the similar results as those presented here, as the design of the classifier only considers any two classes at the same time. It is therefore likely that the intensity resolution between the encoding levels is the limiting factor in classification as opposed to the number of colours used or the SVM paradigm itself.

In conclusion the overall aims of this thesis have been met, an improved classifier for SAT using QDEM encoded microspheres has been developed using SVMs. SVMs outperform MPG and ANNs and have potential for the automated identification of QDEMs in expanded multiplexed assays for applications in genomics and proteomics. It is hoped that this work will contribute to the application of high throughput SAT assays using flow cytometry.

6.5 Recommendations for future work

While there is no doubt that SVM is a promising classifier for QDEMs, this potential needs to be built upon. The points below list the areas recommended for future work

- Further SVM evaluation is required at higher levels of multiplexing (increased numbers of unique QDEMs).

- Application and validation of the SVM QDEM classifier to biological problems, i.e. a SNP genotyping or gene expression analysis in parallel with microarrays is critical.

- Integration of the hybridisation signal within the SVM or possibly using the reporter channel as the recording trigger i.e. only hybridised events would be recorded negating the need for inclusion in the classification algorithm.

- Expansion of the FlowSVM software for increased number of unique microspheres and the development of a database for storage of experimental parameters, models and results.

- The integration of the SVM with flow cytometry acquisition software to allow online classification of events.

- Further development of assay chemistry, including the development of specific multiplex PCR protocols for applications such as SNP genotyping. Work is currently under way at Cranfield University toward the development of a multiplex bead assay for diabetes type II studies.

1. Lander ES, Linton LM, Birren B, Nusbaum C, Zody MC, Baldwin J, Devon K, Dewar K, Doyle M, FitzHugh W, et al: **Initial sequencing and analysis of the human genome.** *Nature* 2001, **409:**860-921.
2. Venter JC, Adams MD, Myers EW, Li PW, Mural RJ, Sutton GG, Smith HO, Yandell M, Evans CA, Holt RA, et al: **The sequence of the human genome.** *Science* 2001, **291:**1304.
3. Evans WE, Relling MV: **Pharmacogenomics: Translating functional genomics into rational therapeutics.** *Science* 1999, **286:**487-491.
4. Veenstra DL, Higashi MK, Phillips KA: **Assessing the cost-effectiveness of pharmacogenomics.** *Aaps Pharmsci* 2000, **2:**art. no.-29.
5. Nolan JP, Mandy FF: **Suspension array technology: New tools for gene and protein analysis.** *Cellular and Molecular Biology* 2001, **47:**1241-1256.
6. Nolan JP, Sklar LA: **Suspension array technology: evolution of the flat-array paradigm.** *Trends in Biotechnology* 2002, **20:**9-12.
7. Dunbar SA: **Applications of Luminex (R) xMAP (TM) technology for rapid, high-throughput multiplexed nucleic acid detection.** *Clinica Chimica Acta* 2006, **363:**71-82.
8. Tsuchihashi Z, Dracopoli NC: **Progress in high throughput SNP genotyping methods.** *The Parmacgenomics journal* 2002, **2:**103-110.
9. Xu HX, Sha MY, Wong EY, Uphoff J, Xu YH, Treadway JA, Truong A, O'Brien E, Asquith S, Stubbins M, et al: **Multiplexed SNP genotyping using the Qbead (TM) system: a quantum dot-encoded microsphere-based assay.** *Nucleic Acids Research* 2003, **31**.
10. De Rosa SC, Brenchley JM, Roederer M: **Beyond six colors: A new era in flow cytometry.** *Nature Medicine* 2003, **9:**112-117.
11. Wang H-Q, Liu T-C, Cao Y-C, Huang Z-L, Wang J-H, Li X-Q, Zhao Y-D: **A flow cytometric assay technology based on quantum dots-encoded beads.** *Analytica Chimica Acta* 2006, **580:**18-23.

12. Schena M, Shalon D, Davis RW, Brown DG: **Quantitative monitoring of gene expression patterns with a complementary DNA microarray.** *Science* 1995, **270:**467.
13. Hoheisel JD: **Microarray technology: beyond transcript profiling and genotype analysis.** *Nature Reviews Genetics* 2006, **7:**200-210.
14. Epstein JR, Biran I, Walt DR: **Fluorescence-based nucleic acid detection and microarrays.** *Analytica Chimica Acta* 2002, **469:**3-36.
15. Shepard JRE: **Polychromatic microarrays: Simultaneous multicolor array hybridization of eight samples.** *Analytical Chemistry* 2006, **78:**2478-2486.
16. Fulwyler MJ: **Method for detecting and separating antigen and antibodies in blood or other samples.** In *British patent 1561042*. UK; 1976.
17. Horan PK, Wheeless LL: **Quantitative Single Cell Analysis and Sorting.** *Science* 1977, **198:**149-157.
18. Fulton RJ, McDade RL, Smith PL, Kienker LJ, Kettman JR: **Advanced multiplexed analysis with the FlowMetrix(TM) system.** *Clinical Chemistry* 1997, **43:**1749-1756.
19. Nolan JP, Mandy F: **Multiplexed and microparticle-based analyses: Quantitative tools for the large-scale analysis of biological systems.** *Cytometry Part A* 2006, **69A:**318-325.
20. Fuja T, Hou S, Bryant P: **A multiplex microsphere bead assay for comparative RNA expression analysis using flow cytometry.** *Journal of Biotechnology* 2004, **108:**193-205.
21. Henry MR, Stevens PW, Sun J, Kelso DM: **Real-time measurements of DNA hybridization on microparticles with fluorescence resonance energy transfer.** *Analytical Biochemistry* 1999, **276:**204-214.
22. K.E.Meissner EH, R.P.Kruzelock, W.B.Spillman,Jr: **Quantum dot-taggd micropsheres for fluid based DNA microsarrays.** *physstatso* 2003, **0:**1355-1359.
23. Wilson R, Cossins AR, Spiller DG: **Encoded microcarriers for high-throughput multiplexed detection.** *Angewandte Chemie-International Edition* 2006, **45:**6104-6117.

24. Yu JD, Othman MI, Farjo R, Zareparsi S, MacNee SP, Yoshida S, Swaroop A: **Evaluation and optimization of procedures for target labeling and hybridization of cDNA microarrays.** *Molecular Vision* 2002, **8:**130-137.
25. Kellar KL, Iannone MA: **Multiplexed microsphere-based flow cytometric assays.** *Experimental Hematology* 2002, **30:**1227-1237.
26. Morgan E, Varro R, Sepulveda H, Ember JA, Apgar J, Wilson J, Lowe L, Chen R, Shivraj L, Agadir A, et al: **Cytometric bead array: a multiplexed assay platform with applications in various areas of biology.** *Clinical Immunology* 2004, **110:**252-266.
27. Tarnok A, Hambsch J, Chen R, Varro R: **Cytometric bead array to measure six cytokines in twenty-five microliters of serum.** *Clinical Chemistry* 2003, **49:**1000-1002.
28. Bellisario R, Colinas RJ, Pass KA: **Simultaneous measurement of thyroxine and thyrotropin from newborn dried blood-spot specimens using a multiplexed fluorescent microsphere immunoassay.** *Clinical Chemistry* 2000, **46:**1422-1424.
29. Yan XM, Zhong WW, Tang AJ, Schielke EG, Hang W, Nolan JP: **Multiplexed flow cytometric immunoassay for influenza virus detection and differentiation.** *Analytical Chemistry* 2005, **77:**7673-7678.
30. Fortina P, Kricka LJ, Surrey S, Grodzinski P: **Nanobiotechnology: the promise and reality of new approaches to molecular recognition.** *Trends in Biotechnology* 2005, **23:**168-173.
31. Chan WCW, Nie SM: **Quantum dot bioconjugates for ultrasensitive nonisotopic detection.** *Science* 1998, **281:**2016-2018.
32. Alivisatos AP: **Semiconductor nanocrystals: New materials through control of size.** *Abstracts of Papers of the American Chemical Society* 1998, **216:**U337-U337.
33. Ekimov AI, Efros AL, Onushchenko AA: **Quantum Size Effect in Semiconductor Microcrystals.** *Solid State Communications* 1985, **56:**921-924.
34. Medintz IL, Uyeda HT, Goldman ER, Mattoussi H: **Quantum dot bioconjugates for imaging, labelling and sensing.** *Nature Materials* 2005, **4:**435-446.

35. Yu WW, Peng XG: **Formation of high-quality CdS and other II-VI semiconductor nanocrystals in noncoordinating solvents: Tunable reactivity of monomers.** *Angewandte Chemie-International Edition* 2002, **41:**2368-2371.

36. Asokan S, Krueger KM, Alkhawaldeh A, Carreon AR, Mu ZZ, Colvin VL, Mantzaris NV, Wong MS: **The use of heat transfer fluids in the synthesis of high-quality CdSe quantum dots, core/shell quantum dots, and quantum rods.** *Nanotechnology* 2005, **16:**2000-2011.

37. Han MY, Gao XH, Su JZ, Nie S: **Quantum-dot-tagged microbeads for multiplexed optical coding of biomolecules.** *Nature Biotechnology* 2001, **19:**631-635.

38. Benecky MJ, Post DR, Schmitt SM, Kochar MS: **Detection of hepatitis B surface antigen in whole blood by coupled particle light scattering (Copalis(TM)).** *Clinical Chemistry* 1997, **43:**1764-1770.

39. Doering WE, Nie SM: **Spectroscopic tags using dye-embedded nanoparticies and surface-enhanced Raman scattering.** *Analytical Chemistry* 2003, **75:**6171-6176.

40. Jin RC, Cao YC, Thaxton CS, Mirkin CA: **Glass-bead-based parallel detection of DNA using composite Raman labels.** *Small* 2006, **2:**375-380.

41. Fenniri H, Ding LH, Ribbe AE, Zyrianov Y: **Barcoded resins: A new concept for polymer-supported combinatorial library self-deconvolution.** *Journal of the American Chemical Society* 2001, **123:**8151-8152.

42. Watson DA, Brown LO, Gaskill DF, Naivar M, Graves SW, Doorn SK, Nolan JP: **A flow cytometer for the measurement of Raman spectra.** *Cytometry Part A* 2008, **73A:**119-118.

43. Hett JJ: **Raman spectroscopy comes to flow cytometry.** *Cytometry Part A* 2008, **73A:**109-110.

44. Dejneka MJ, Streltsov A, Pal S, Frutos AG, Powell CL, Yost K, Yuen PK, Muller U, Lahiri J: **Rare earth-doped glass microbarcodes.** *Proceedings of the National Academy of Sciences of the United States of America* 2003, **100:**389-393.

45. Walton ID, Norton SM, Balasingham A, He L, Oviso DF, Gupta D, Raju PA, Natan MJ, Freeman RG: **Particles for multiplexed analysis in solution: Detection and identification of striped metallic particles using optical microscopy.** *Analytical Chemistry* 2002, **74:**2240-2247.

46. Moran EJ, Sarshar S, Cargill JF, Shahbaz MM, Lio A, Mjalli AMM, Armstrong RW: **Radio-Frequency Tag Encoded Combinatorial Library Method for the Discovery of Tripeptide-Substituted Cinnamic Acid Inhibitors of the Protein-Tyrosine-Phosphatase Ptp1B.** *Journal of the American Chemical Society* 1995, **117:**10787-10788.

47. Amsden B: **The production of uniformly sized polymer microspheres.** *Pharmaceutical Research* 1999, **16:**1140-1143.

48. Yi GR, Manoharan VN, Klein S, Brzezinska KR, Pine DJ, Lange FF, Yang SM: **Monodisperse micrometer-scale spherical assemblies of polymer particles.** *Advanced Materials* 2002, **14:**1137-1140.

49. Takeuchi S, Garstecki P, Weibel DB, Whitesides GM: **An axisymmetric flow-focusing microfluidic device.** *Advanced Materials* 2005, **17:**1067.

50. Freitas S, Merkle HP, Gander B: **Microencapsulation by solvent extraction/evaporation: reviewing the state of the art of microsphere preparation process technology.** *Journal of Controlled Release* 2005, **102:**313-332.

51. Martin-Banderas L, Rodriguez-Gil A, Cebolla A, Chavez S, Berdun-Alvarez T, Garcia JMF, Flores-Mosquera M, Ganan-Calvo AM: **Towards high-throughput production of uniformly encoded microparticles.** *Advanced Materials* 2006, **18:**559.

52. O'Brien P, Cummins SS, Darcy D, Dearden A, Masala O, Pickett NL, Ryley S, Sutherland AJ: **Quantum dot-labelled polymer beads by suspension polymerisation.** *Chemical Communications* 2003**:**2532-2533.

53. Wang DY, Rogach AL, Caruso F: **Semiconductor quantum dot-labeled microsphere bioconjugates prepared by stepwise self-assembly.** *Nano Letters* 2002, **2:**857-861.

54. Ma Q, Wang XY, Li YB, Shi YH, Su XG: **Multicolor quantum dot-encoded microspheres for the detection of biomolecules.** *Talanta* 2007, **72:**1446-1452.

55. Gao XH, Nie SM: **Quantum dot-encoded mesoporous beads with high brightness and uniformity: Rapid readout using flow cytometry.** *Analytical Chemistry* 2004, **76:**2406-2410.

56. Bradley M, Bruno N, Vincent B: **Distribution of CdSe quantum dots within swollen polystyrene microgel particles using confocal microscopy.** *Langmuir* 2005, **21:**2750-2753.

57. Cao YC, Huang ZL, Liu TC, Wang HQ, Zhu XX, Wang Z, Zhao YD, Liu MX, Luo QM: **Preparation of silica encapsulated quantum dot encoded beads for multiplex assay and its properties.** *Analytical Biochemistry* 2006, **351:**193-200.

58. Armstrong B, Stewart M, Mazumder A: **Suspension arrays for high throughput, multiplexed single nucleotide polymorphism genotyping.** *Cytometry* 2000, **40:**102-108.

59. Reeve L, Rew DA: **New technology in the analytical cell sciences: the laser scanning cytometer.** *European Journal of Surgical Oncology* 1997, **23:**445-450.

60. Darzynkiewicz Z, Bedner E, Li X, Gorczyca W, Melamed MR: **Laser-scanning cytometry: A new instrumentation with many applications.** *Experimental Cell Research* 1999, **249:**1-12.

61. Deptala A, Bedner E, Darzynkiewicz Z: **Unique analytical capabilities of laser scanning cytometry (LSC) that complement flow cytometry.** *Folia Histochemica Et Cytobiologica* 2001, **39:**87-89.

62. Rao RS, Visuri SR, McBride MT, Albala JS, Matthews DL, Coleman MA: **Comparison of multiplexed techniques for detection of bacterial and viral proteins.** *Journal of Proteome Research* 2004, **3:**736-742.

63. Vignali DAA: **Multiplexed particle-based flow cytometric assays.** *Journal of Immunological Methods* 2000, **243:**243-255.

64. Braeckmans K, De Smedt SC, Leblans M, Pauwels R, Demeester J: **Encoding microcarriers: Present and future technologies.** *Nature Reviews Drug Discovery* 2002, **1:**447-456.

65. Pickering JW, Martins TB, Greer RW, Schroder MC, Astill ME, Litwin CM, Hildreth SW, Hill HR: **A multiplexed fluorescent microsphere immunoassay for antibodies to pneumococcal capsular polysaccharides.** *American Journal of Clinical Pathology* 2002, **117:**589-596.

66. Smith JD, Rose ML: **Development of a Luminex based method to detect C4d binding by HLA antibodies.** *International Journal of Immunogenetics* 2007, **34:**290-290.

67. Lowe D, Hathaway M, Briggs D: **The high-dose hook effect in the detection and monitoring of HLA specific antibody by Luminex assay.** *International Journal of Immunogenetics* 2007, **34:**288-288.

68. Powell K, Darke C: **ELISA, Luminex (R) and flow cytometry testing of CDC-defined IgM HLA antibodies.** *International Journal of Immunogenetics* 2007, **34:**299-299.

69. Funding M, Hansen TK, Gjedsted J, Ehlers N: **Simultaneous quantification of 17 immune mediators in aqueous humour from patients with corneal rejection.** *Acta Ophthalmologica Scandinavica* 2006, **84:**759-765.

70. Hoffmann TK, Sonkoly E, Homey B, Scheckenbach K, Gwosdz C, Bas M, Chaker A, Schirlau K, Whiteside TL: **Aberrant cytokine expression in serum of patients with adenoid cystic carcinoma and squamous cell carcinoma of the head and neck.** *Head and Neck-Journal for the Sciences and Specialties of the Head and Neck* 2007, **29:**472-478.

71. Dehqanzada ZA, Storrer CE, Hueman MT, Foley R, Harris K, Jama Y, Shriver CD, Ponniah S, Peoples GE: **Assessing serum cytokine profiles in breast cancer patients receiving a HER2/neu vaccine using Luminex (R) technology.** *Annals of Surgical Oncology* 2005, **12:**S47-S48.

72. Bobrowski WF, McDuffie JE, Sobocinski G, Chupka J, Olle E, Bowman A, Albassam M: **Comparative methods for multiplex analysis of cytokine protein expression in plasma of lipopolysaccharide-treated mice.** *Cytokine* 2005, **32:**194-198.

73. Proft T, Schrage B, Fraser JD: **The cytokine response to streptococcal Superantigens varies between individual toxins and between individuals: Implications for the pathogenesis of group A streptococcal diseases.** *Journal of Interferon and Cytokine Research* 2007, **27:**553-557.

74. Killebrew DA, Shikuma CM, Gerschenson M: **Luminex cytokine expression array in subcutaneous fat adipocytes, preadipocytes and macrophages in HIV-lipoatrophic patients.** *Antiviral Therapy* 2006, **11:**L25-L26.

75. Yurkovetsky ZR, Kirkwood JM, Edington HD, Marrangoni AM, Velikokhatnaya L, Winans MT, Gorelik E, Lokshin AE: **Multiplex analysis of serum cytokines in melanoma patients treated with interferon-alpha 2b.** *Clinical Cancer Research* 2007, **13:**2422-2428.

76. Schmitt M, Bravo IG, Snijders PJF, Gissmann L, Pawlita M, Waterboer T: **Bead-based multiplex genotyping of human papillomaviruses.** *Journal of Clinical Microbiology* 2006, **44:**504-512.

77. Naciff JM, Richardson BD, Oliver KG, Jump ML, Torontali SM, Juhlin KD, Carr GJ, Paine JR, Tiesman JA, Daston GP: **Design of a microsphere-based high-throughput gene expression assay to determine estrogenic potential.** *Environmental Health Perspectives* 2005, **113:**1164-1171.

78. Jiang HL, Zhu HH, Zhou LF, Chen F, Chen Z: **Genotyping of human papillomavirus in cervical lesions by L1 consensus PCR and the Luminex xMAP system.** *Journal of Medical Microbiology* 2006, **55:**715-720.

79. Flagella M, Bui S, Zheng Z, Nguyen CT, Zhang AG, Pastor L, Ma YQ, Yang W, Crawford KL, McMaster GK, et al: **A multiplex branched DNA assay for parallel quantitative gene expression profiling.** *Analytical Biochemistry* 2006, **352:**50-60.

80. Deregt D, Gilbert SA, Dudas S, Pasick J, Baxi S, Burton KM, Baxi MK: **Multiplex DNA suspension microarray for simultaneous detection and differentiation of classical swine fever virus and other pestiviruses.** *Journal of Virological Methods* 2006, **136:**17-23.

81. Li ZP, Kambara H: **Single nucleotide polymorphism analysis based on minisequencing coupled with a fluorescence microsphere technology.** *Journal of Nanoscience and Nanotechnology* 2005, **5:**1256-1260.

82. Brown JT, Lahey C, Laosinchai-Wolf W, Hadd AG: **Polymorphisms in the glucocerebrosidase gene and pseudogene urge caution in clinical analysis of Gaucher disease allele c.1448T > C (L444P).** *Bmc Medical Genetics* 2006, **7:**-.

83. Nam JM, Thaxton CS, Mirkin CA: **Nanoparticle-based bio-bar codes for the ultrasensitive detection of proteins.** *Science* 2003, **301:**1884-1886.

84. Cooper DN, Smith BA, Cooke HJ, Niemann S, Schmidtke J: **An Estimate of Unique DNA-Sequence Heterozygosity in the Human Genome.** *Human Genetics* 1985, **69:**201-205.

85. Hiratsuka M, Sasaki T, Mizugaki M: **Genetic testing for pharmacogenetics and its clinical application in drug therapy.** *Clinica Chimica Acta* 2006, **363:**177-186.

86. Hayashi K, Hashimoto N, Daigen M, Ashikawa I: **Development of PCR-based SNP markers for rice blast resistance genes at the Piz locus.** *Theoretical and Applied Genetics* 2004, **108:**1212-1220.

87. Feltus FA, Wan J, Schulze SR, Estill JC, Jiang N, Paterson AH: **An SNP resource for rice genetics and breeding based on subspecies Indica and Japonica genome alignments.** *Genome Research* 2004, **14:**1812-1819.

88. Chen LM, Perlina A, Lee CJ: **Positive selection detection in 40,000 human immunodeficiency virus (HIV) type 1 sequences automatically identifies drug resistance and positive fitness mutations in HIV protease and reverse transcriptase.** *Journal of Virology* 2004, **78:**3722-3732.

89. Leeder JS: **Pharmacogenetics and pharmacogenomics.** *Pediatric Clinics of North America* 2001, **48:**765-+.

90. Marshall E: **Genomics - Drug firms to create public database of genetic mutations.** *Science* 1999, **284:**406-407.

91. Mollevi DG, Serrano T, Ginesta MM, Valls J, Torras J, Navarro M, Ramos E, Germa JR, Jaurrieta E, Moreno V, et al: **Mutations in TP53 are a prognostic**

factor in colorectal hepatic metastases undergoing surgical resection. *Carcinogenesis* 2007, **28:**1241-1246.

92. Castro MG, Rodriguez-Pascual F, Magan-Marchal N, Reguero JR, Alonso-Montes C, Moris C, Alvarez V, Lamas S, Coto E: **Screening of the endothelin1 gene (EDN1) in a cohort of patients with essential left ventricular hypertrophy.** *Annals of Human Genetics* 2007, **71:**601-610.
93. Yoo NJ, Soung YH, Lee SH, Jeong EG, Lee SH: **Mutational analysis of caspase-14 gene in common carcinomas.** *Pathology* 2007, **39:**330-333.
94. Bozzi A, Pereira PPN, Reis BS, Goulart MI, Pereira MCN, Pedroso EP, Leite MF, Goes AM: **Interleukin-10 and tumor necrosis factor-alpha single nucleotide gene polymorphism frequency in paracoccidioidomycosis.** *Human Immunology* 2006, **67:**931-939.
95. Hammerschmied CG, Stoehr R, Walter B, Wieland WF, Hartmann A, Blaszyk H, Denzinger S: **Role of the STK15 Phe31Ile polymorphism in renal cell carcinoma.** *Oncology Reports* 2007, **17:**3-7.
96. Saiki RK, Walsh PS, Levenson CH, Erlich HA: **Genetic-Analysis of Amplified DNA with Immobilized Sequence-Specific Oligonucleotide Probes.** *Proceedings of the National Academy of Sciences of the United States of America* 1989, **86:**6230-6234.
97. Macdonald SJ, Pastinen T, Genissel A, Cornforth TW, Long AD: **A low-cost open-source SNP genotyping platform for association mapping applications.** *Genome Biology* 2005, **6**.
98. Cai H, White PS, Torney D, Deshpande A, Wang ZL, Marrone B, Nolan JP: **Flow cytometry-based minisequencing: A new platform for high-throughput single-nucleotide polymorphism scoring.** *Genomics* 2000, **66:**135-143.
99. Sundaresan BC, Xu M, Davis-Fleischer K, Phillips M, Bell PA, Boyce-Jacino M: **Bench-top genotyping using a 96 strip-well primer extension SNP-IT (TM) assay.** *American Journal of Human Genetics* 2001, **69:**460-460.
100. Ross P, Hall L, Smirnov I, Haff L: **High level multiplex genotyping by MALDI-TOF mass spectrometry.** *Nature Biotechnology* 1998, **16:**1347-1351.

101. Cronin MT, Frueh F, Pho M, Dutta D, Brennan TM: **Applying rapid DNA microarray optimization capability to SNP screening and genotyping.** *American Journal of Human Genetics* 1999, **65:**A224-a224.

102. Flavell AJ, Bolshakov VN, Booth A, Jing R, Russell J, Ellis THN, Isaac P: **A microarray-based high throughput molecular marker genotyping method: the tagged microarray marker (TAM) approach.** *Nucleic Acids Research* 2003, **31**.

103. Ye F, Li MS, Taylor JD, Nguyen Q, Colton HM, Casey WM, Wagner M, Weiner MP, Chen JW: **Fluorescent microsphere-based readout technology for multiplexed human single nucleotide polymorphism analysis and bacterial identification.** *Human Mutation* 2001, **17:**305-316.

104. Chen JW, Iannone MA, Li MS, Taylor JD, Rivers P, Nelsen AJ, Slentz-Kesler KA, Roses A, Weiner MP: **A microsphere-based assay for multiplexed single nucleotide polymorphism analysis using single base chain extension.** *Genome Research* 2000, **10:**549-557.

105. Rockenbauer E, Petersen K, Vogel U, Bolund L, Kolvraa S, Nielsen KV, Nexo BA: **SNP genotyping using microsphere-linked PNA and flow cytometric detection.** *Cytometry Part A* 2005, **64A:**80-86.

106. Deshpande A, Nolan JP, White PS, Valdez YE, Hunt WC, Peyton CL, Wheeler CM: **TNF-alpha promoter polymorphisms and susceptibility to human papillomavirus 16-associated cervical cancer.** *Journal of Infectious Diseases* 2005, **191:**969-976.

107. Yang L, Tran DK, Wang X: **BADGE, BeadsArray for the Detection of Gene Expression, a high-throughput diagnostic bioassay.** *Genome Research* 2001, **11:**1888-1898.

108. Eastman PS, Ruan WM, Doctolero M, Nuttall R, De Feo G, Park JS, Chu JSF, Cooke P, Gray JW, Li S, Chen FQF: **Qdot nanobarcodes for multiplexed gene expression analysis.** *Nano Letters* 2006, **6:**1059-1064.

109. Nielsen UB, Geierstanger BH: **Multiplexed sandwich assays in microarray format.** *Journal of Immunological Methods* 2004, **290:**107-120.

110. Carson RT, Vignali DAA: **Simultaneous quantitation of 15 cytokines using a multiplexed flow cytometric assay.** *Journal of Immunological Methods* 1999, **227:**41-52.

111. Moss DM, Montgomery JM, Newland SV, Priest JW, Lammie PJ: **Detection of Cryptosporidium antibodies in sera and oral fluids using multiplex bead assay.** *Journal of Parasitology* 2004, **90:**397-404.

112. Mchugh TM, Miner RC, Logan LH, Stites DP: **Simultaneous Detection of Antibodies to Cytomegalo-Virus and Herpes-Simplex Virus by Using Flow-Cytometry and a Microsphere-Based Fluorescence Immunoassay.** *Journal of Clinical Microbiology* 1988, **26:**1957-1961.

113. Adams EW, Ueberfeld J, Ratner DM, O'Keefe BR, Walt DR, Seeberger PH: **Encoded fiber-optic microsphere arrays for probing protein-carbohydrate interactions.** *Angewandte Chemie-International Edition* 2003, **42:**5317-5320.

114. Chapman GV: **Instrumentation for flow cytometry** *JImmuno meth* 2000, **3**.

115. Nunez R: **Flow Cytometery: Principals and instrumentation.** *Curr Issues Mol Biol* 2001, **2:**39-45.

116. Bogh LDD, T.A. : **Flow cytometry instrumentation in research and clinical laboratories** *ClinLab Sci* 1993, **6:**167-173.

117. Lowe MS, A., Zhang,Y.Z., and Getts,R. : **Multiplexed, particle-based detection of DNA using flow cytometry with 3DN dendrimers for signam amplification** *Cytometry A* 2004, **60:**135-144.

118. Mycoy JP, Jr and Carey, J.L. : **Recent advances in flow cytometric techniques for cancer detection and prognosis.** *ImmunolSer* 1990, **53:**171-187.

119. Poletav AI, Gnuchev,N.V.,and Zelenin,A.V. : **Flow cytometry and cell sorting:currnet state and prosects for use in molecular biology.** 1987, **21:**23-27.

120. Yasa MH, Bektas,A., Yukselen,V., Akbulut,H., Camci,C., and Ormeci,N.: **DNA analysis and DNA ploidy in gastric cancer and gastric precancerous lesions.** *International Journal of Clinical Practice* 2005, **59:**1029-1033.

121. Shapiro HM: *Practical flow cytometry.* Wiley-Liss; 2003.

122. Subira D, Gorgolas M, Castanon S, Serrano C, Roman A, Rivas F, Thomas JF: **Advantages of flow cytometry immunophenotyping for the diagnosis of central nervous system non-Hodgkin's lymphoma in AIDS patients.** *Hiv Medicine* 2005, **6:**21-26.

123. Bertuzzi A, Gandolfi A, Germani A, Spano M, Starace G, Vitelli R: **Analysis of DNA-Synthesis Rate of Cultured-Cells from Flow Cytometric Data.** *Cytometry* 1984, **5:**619-628.

124. Kelley KA, McDowell JL: **Practical considerations for the selection and use of optical filters in flow cytometry.** *Cytometry* 1988, **9:**277-280.

125. V.Watson J: *Flow Cytomtetry Data Analysis: Basic concepts and statistics.* Cambridge university press; 1992.

126. .

127. Snow C: **Flow cytometer electronics.** *Cytometry Part A* 2004, **57A:**63-69.

128. Dean PN, Bagwell CB, Lindmo T, Murphy RF, Salzman GC: **Introduction to Flow-Cytometry Data File Standard.** *Cytometry* 1990, **11:**321-322.

129. [Anon]: **Data File Standard for Flow-Cytometry - Data File Standards Committee of the Society for Analytical Cytology.** *Cytometry* 1990, **11:**323-332.

130. Herzenberg LA, Tung J, Moore WA, Herzenberg LA, Parks DR: **Interpreting flow cytometry data: a guide for the perplexed.** *Nature Immunology* 2006, **7:**681-685.

131. Camilla C, Mely L, Magnan A, Casano B, Prato S, Debono S, Montero F, Defoort JP, Martin M, Fert V: **Flow cytometric microsphere-based immunoassay: Analysis of secreted ctytokines in whole-blood samples from asthmatics.** *Clinical and Diagnostic Laboratory Immunology* 2001, **8:**776-784.

132. Keij JF, Steinkamp JA: **Flow cytometric characterization and classification of multiple dual-color fluorescent microspheres using fluorescence lifetime.** *Cytometry* 1998, **33:**318-323.

133. Yao G, Wang L, Wu YR, Smith J, Xu JS, Zhao WJ, Lee EJ, Tan WH: **FloDots: luminescent nanoparticles.** *Analytical and Bioanalytical Chemistry* 2006, **385:**518-524.

134. Bhaskar H, Hoyle DC, Singh S: **Machine learning in bioinformatics: A brief survey and recommendations for practitioners.** *Computers in Biology and Medicine* 2006, **36:**1104-1125.

135. Harz M, Rosch P, Peschke KD, Ronneberger O, Burkhardt H, Popp J: **Micro-Raman spectroscopic identification of bacterial cells of the genus Staphylococcus and dependence on their cultivation conditions.** *Analyst* 2005, **130:**1543-1550.

136. Christianini NS-T, John; : *An Introduction to Support Vector Machines and Other Kernel-based Learning Methods.* Cambridge Universtiy Press; 2000.

137. Vladimir NV: *The nature of statistical learning theory.* Springer-Verlag New York, Inc.; 1995.

138. Burges C: **A Tutorial on Support Vector Machines for Pattern Recognition.** *Data Mining and Knowledge Discovery* 1998, **2:**121-167.

139. Minsky ML, Papert SA: *Perceptrons.* Expanded Edition 1990 edn: MIT Press; 1969.

140. Bredensteiner EJ, Bennett KP: **Multicategory classification by support vector machines.** *Computational Optimization and Applications* 1999, **12:**53-79.

141. Weston J, Watkins C: **Multi-class support vector machines.** *Technical Report CSD-TR-98-04 , Royal Holloway, University of London,* 1998.

142. Tsujinishi D, Abe S: **Fuzzy least squares support vector machines for multiclass problems.** *Neural Networks* 2003, **16:**785-792.

143. ???: **Multiclass support vector machines.** 2008.

144. Hastie T, Tibshirani R: **Classification by pairwise coupling.** *Annals of Statistics* 1998, **26:**451-471.

145. Hsu CW, Lin CJ: **A comparison of methods for multiclass support vector machines.** *Ieee Transactions on Neural Networks* 2002, **13:**415-425.

146. Lin CHaCLHaC: **A comparison of methods for multi-class support vector machines.** 2001.

147. Melgani F, Bruzzone L: **Classification of hyperspectral remote sensing images with support vector machines.** *Ieee Transactions on Geoscience and Remote Sensing* 2004, **42:**1778-1790.

148. Liu Y, Zheng YF: **One-against-all multi-class SVM classification using reliability measures.** In *IEEE International Joint Conference on Neural Networks*; *31/08/05*. 2005: 849-854.

149. Cualing HD: **Automated analysis in flow cytometry.** *Cytometry* 2000, **42:**110-113.

150. Adjouadi M, Zong N, Ayala M: **Multidimensional pattern recognition and classification of white blood cells using support vector machines.** *Particle & Particle Systems Characterization* 2005, **22:**107-118.

151. Quinn J, Fisher PW, Capocasale RJ, Achuthanandam R, Kam M, Bugelski PJ, Hrebien L: **A statistical pattern recognition approach for determining cellular viability and lineage phenotype in cultured cells and murine bone marrow.** *Cytometry Part A* 2007, **71A:**612-624.

152. Morris CW, Autret A, Boddy L: **Support vector machines for identifying organisms - a comparison with strongly partitioned radial basis function networks.** *Ecological Modelling* 2001, **146:**57-67.

153. Toedling J, Rhein P, Ratei R, Karawajew L, Spang R: **Automated in-silico detection of cell populations in flow cytometry readouts and its application to leukemia disease monitoring.** *Bmc Bioinformatics* 2006, **7:**-.

154. J.Tukey: *Exploratory Data Analysis.* Addison-Wesely; 1977.

155. Lin C-CCaC-J: **LIBSVM: a library for support vector machines.**

156. Ting-Fan W, Chih-Jen L, Ruby CW: **Probability Estimates for Multi-class Classification by Pairwise Coupling.** *J Mach Learn Res* 2004, **5:**975-1005.

157. Breiman L: **Heuristics of instability and stabilization in model selection.** *Annals of Statistics* 1996, **24:**2350-2383.

158. Goutte C: **Note on free lunches and cross-validation.** *Neural Computation* 1997, **9:**1245-1249.

159. Frank RE, Massy WF, Morrison DG: **Bias in multiple discriminate analysis.** *Journal of Marketing Research* 1965, **2:**250-258.

160. Rocco SCM, Moreno JA: **System reliability evaluation using Monte Carlo & support vector machine.** *Annual Reliability and Maintainability Symposium, 2003 Proceedings* 2003**:**482-486.

161. Hua SJ, Sun ZR: **Support vector machine approach for protein subcellular localization prediction.** *Bioinformatics* 2001, **17:**721-728.

162. Keerthi SS, Lin CJ: **Asymptotic behaviors of support vector machines with Gaussian kernel.** *Neural Computation* 2003, **15:**1667-1689.

163. Winters-Hilt S, Yelundur A, McChesney C, Landry M: **Support Vector Machine implementations for classification & clustering.** *Bmc Bioinformatics* 2006, **7:**-.

164. Mayoraz E, Alpaydin E: **Support vector machines for multi-class classification.** *Engineering Applications of Bio-Inspired Artificial Neural Networks, Vol Ii* 1999, **1607:**833-842.

165. Coporation L: *Luminex 200 specifications.* 2005.

166. Aleksander I: **The Handbook of Brain Theory and Neural Networks - Arbib,Ma.** *Nature* 1995, **376:**564-564.

167. Jain AK, Mao JC, Mohiuddin KM: **Artificial neural networks: A tutorial.** *Computer* 1996, **29:**31-&.

168. Mcculloch WS, Pitts W: **A Logical Calculus of the Ideas Immanent in Nervous Activity (Reprinted from Bulletin of Mathematical Biophysics, Vol 5, Pg 115-133, 1943).** *Bulletin of Mathematical Biology* 1990, **52:**99-115.

169. Rosenblatt F: **The Perceptron - a Probabilistic Model for Information-Storage and Organization in the Brain.** *Psychological Review* 1958, **65:**386-408.

170. Hopfield JJ: **Neural Networks and Physical Systems with Emergent Collective Computational Abilities.** *Proceedings of the National Academy of Sciences of the United States of America-Biological Sciences* 1982, **79:**2554-2558.

171. Werbos PJ: **Generalization of Backpropagation with Application to a Recurrent Gas Market Model.** *Neural Networks* 1988, **1:**339-356.

172. Yao X, Liu Y: **Neural Networks for Breast Cancer Diagnosis.** *Proceedings of the 1999 Congress on Evolutionary Computation* 1999, **3:**1767.

173. Somervuo P, Kohonen T: **Self-organizing maps and learning vector quantization for feature sequences.** *Neural Processing Letters* 1999, **10:**151-159.

174. Boddy L, Morris CW, Wilkins MF, Tarran GA, Burkill PH: **Neural-Network Analysis of Flow Cytometric Data for 40 Marine-Phytoplankton Species.** *Cytometry* 1994, **15:**283-293.

175. Jonker R, Groben R, Tarran G, Medlin L, Wilkins M, Garcia L, Zabala L, Boddy L: **Automated identification and characterisation of microbial populations using flow cytometry: the AIMS project.** *Scientia Marina* 2000, **64:**225-234.

176. Wilkins MF, Boddy L, Morris CW, Jonker RR: **Identification of phytoplankton from flow cytometry data by using radial basis function neural networks.** *Applied and Environmental Microbiology* 1999, **65:**4404-4410.

177. Smits JRM, Breedveld LW, Derksen MWJ, Kateman G, Balfoort HW, Snoek J, Hofstraat JW: **Pattern-Classification with Artificial Neural Networks - Classification of Algae, Based Upon Flow Cytometer Data.** *Analytica Chimica Acta* 1992, **258:**11-25.

178. Morris CW, Boddy L, Allman R: **Identification of Basidiomycete Spores by Neural Network Analysis of Flow-Cytometry Data.** *Mycological Research* 1992, **96:**697-701.

179. Boddy L, Wilkins MF, Morris CW: **Pattern recognition in flow cytometry.** *Cytometry* 2001, **44:**195-209.

180. Kothari R, Cualing H, Balachander T: **Neural network analysis of flow cytometry immunophenotype data.** *Ieee Transactions on Biomedical Engineering* 1996, **43:**803-810.

181. Ravdin PM, Clark GM, Hough JJ, Owens MA, Mcguire WL: **Neural Network Analysis of DNA Flow-Cytometry Histograms.** *Cytometry* 1993, **14:**74-80.

182. Haykin S: *Neural Networks A Comprehensive Foundation* Prentice-Hall; 1998.

183. Hassoun MH: *Fundamentals of artificial neural networks.* MIT Press; 1995.

184. Rumelhart DE, Hinton GE, Williams RJ: **Learning Representations by Back-Propagating Errors.** *Nature* 1986, **323:**533-536.

185. Sejnowski TJ, Kienker PK, Hinton GE: **Learning Symmetry Groups with Hidden Units - Beyond the Perceptron.** *Physica D* 1986, **22:**260-275.

186. Broomhead DS, D L: **Multivariate functional interpolation and adaptive networks.** *Complex System 2,* 1988**:**321-355.

187. Tipping ME, Lowe D: **Shadow targets: A novel algorithm for topographic projections by radial basis functions.** *Neurocomputing* 1998, **19:**211-222.

188. Roy A, Govil S, Miranda R: **An Algorithm to Generate Radial Basis Function (Rbf)-Like Nets for Classification Problems.** *Neural Networks* 1995, **8:**179-201.

189. Moody J, Darken C: **Fast learning in networks of locally tuned processing units.** *Nueral Computation* 1989, **1:**281-294.

190. Musavi MT, Ahmed W, Chan KH, Faris KB, Hummels DM: **On the Training of Radial Basis Function Classifiers.** *Neural Networks* 1992, **5:**595-603.

191. Blue JL, Candela GT, Grother PJ, Chellappa R, Wilson CL: **Evaluation of Pattern Classifiers for Fingerprint and Ocr Applications.** *Pattern Recognition* 1994, **27:**485-501.

192. Wasserman PD: *Advanced Methods in Neural Computing.* New York: Van Nostrand Reinhold; 1993.

193. Denmark TUo: **ANN:DTU Toolbox.** 2002.

194. Hintz-Madsen M, Hansen LK, Larsen J, Pedersen MW, Larsen M: **Neural classifier construction using regularization, pruning and test error estimation.** *Neural Networks* 1998, **11:**1659-1670.

195. MathWorks: *MATLAB: User Manual 7.3.*

196. Arribas JI, Cid-Sueiro J: **A model selection algorithm for a Posteriori probability estimation with neural networks.** *Ieee Transactions on Neural Networks* 2005, **16:**799-809.

197. Osowski S, Siwek K, Markiewicz T: **MLP and SVM networks - a comparative study.** In *6th Nordic Signal Processing Symposium; Espoo, Finland*. 2004

198. Roederer M, Hardy RR: **Frequency difference gating: A multivariate method for identifying subsets that differ between samples.** *Cytometry* 2002**:**134-135.

199. Mario Roederer WM, Adam Treister, Richard R. Hardy, and Leonore A. Herzenberg **Probability Binning Comparison: A metric for Quantitating Multivariate Distribution Differences** *Cytometry* 2001, **45:**47-55.

200. Roederer M, Hardy RR: **Frequency difference gating: A multivariate method for identifying subsets that differ between samples.** *Cytometry* 2001, **45:**56-64.

Appendix 1: Frequency difference gating and probability binning.

Clustering algorithms can be used to identify subsets of cells in FCM data based on different characteristics of that data. The second standard classification method evaluated for the QDEM library was an unsupervised clustering method called frequency difference gating first described by Roeder *et al* [198]. The technique has overcome previous limitations including the computational expense of such algorithms and integration of domain specific knowledge and is implemented as part of the Flojo software suite (Tree Star, San Carlos, CA). A possible advantage of this method is that no training data is required for subpopulation identification. Decisions are based solely on the multiplexing test set distributions and no underlying assumptions are made. The similarity and dissimilarity of samples can be identified and the data can be gated on events in one sample that are different from a control even if the differences are not visible on bivariate plots. A variation of the chi-squared statistic was extended to a multivariate space. The normalised chi-squared value for the *i*th bin is calculated as:

$$\chi'^2 = \sum_{i=1}^{\#bins} \frac{\left(c_i^n - s_i^n\right)^2}{\left(c_i^n + s_i^n\right)} \qquad \textbf{(3.1)}$$

$$c_i^n = \frac{c_i}{E^c} \text{ and } s_i^n = \frac{s_i}{E^s}$$

Where c_i and s_i are the number of control and test samples falling into bin *i*. E^c and E^s are the total events in the control and test samples. In the case of samples where no control is possible or logical (in our case), the control is the combination of the test sample events. Each sample is then compared to the combined test control. The algorithm has been successfully applied to the differentiation of HIV+ and HIV- samples and mouse B cells [199].

The probability binning method described above can also be used to generate so-called "frequency difference gates". Frequency difference gating constructs gates in multivariate space where there is a difference in frequency between multivariate distributions (determined using probability binning comparison). A possible limitation of this method is that small differences in staining intensity can result in incorrect classifications of the data; therefore robust calibration is required for measurements [200].

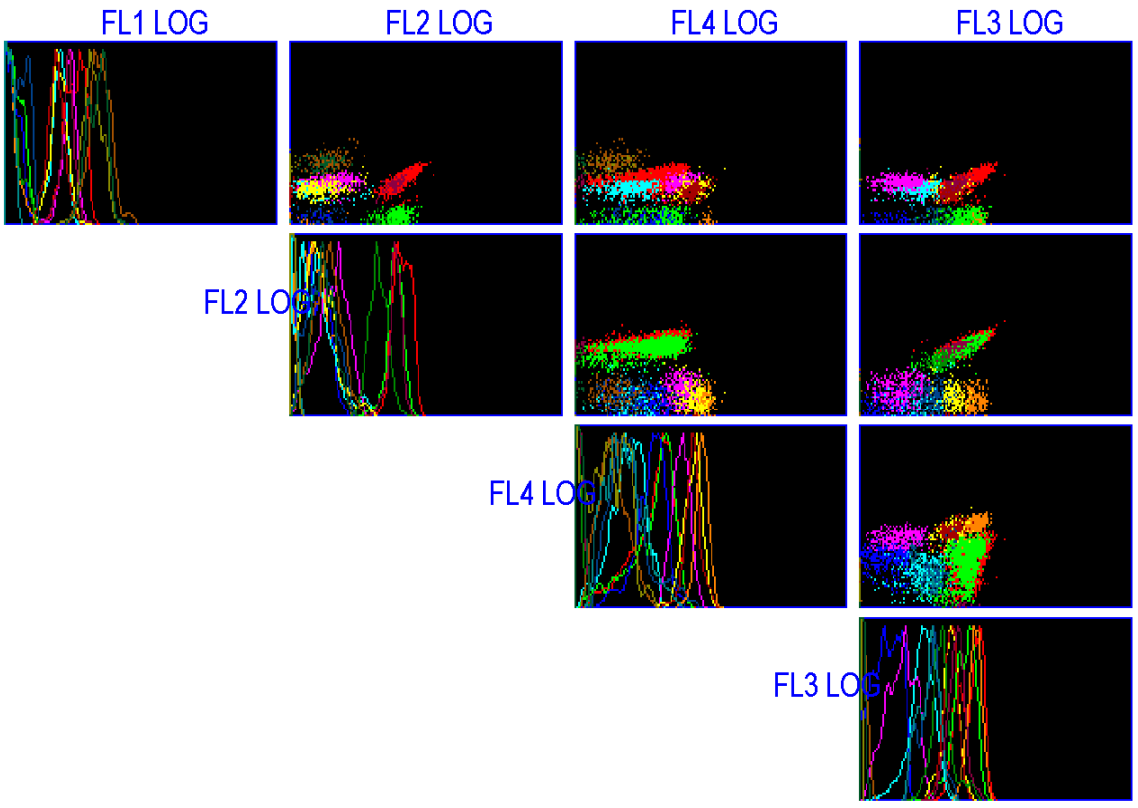

Figure 51 Clustering of the Multiplex test 10 using the probability binning clustering method described by Roederer *et al.* The 15 clusters containing the most events were frequency difference gated using the Flojo software suite. While the algorithm has indeed identified a number of subpopulations in the data it is difficult to conclude which cluster pertains to a QDEM. Therefore a tabular output is also provided (Table 20).

The clustering algorithm was applied to the 10 FCM datasets (Table 20 and Figure 51). The remaining nine multiplex tests can be found in the CD appendix accompanying this

thesis. As can be seen from the multiplex results (test 10) it is difficult to reliably assign identity to the QDEM subpopulations. For the 15 clusters containing the most events, the biggest cluster contains more than 1900 events while the lowest cluster contains only 93 events. We would expect there to be a greater balance between microsphere classes (as equal amounts of the stock solution were added to each multiplex solution). It is possible that more events were acquired for certain QDEM classes however this imbalance in class detection was not observed during the MPG analysis.

Table 20 Flojo clustering results. The test solutions were clustered using probability binning comparison and frequency difference gating applied. The results for multiplex test 10 are shown. The top 15 cluster designations were also plotted (Figure 51). It is difficult from these results to identify the QDEMs correctly. The output of the Flojo algorithm was deemed to be unsuitable for the discrimination of the QDEMs from FCM data.

Events	Name	FL1	FL2	FL3	FL4	QDEM
7500	Parent					
1901	Cluster 1	+	++	++	+	1221
1897	Cluster 2	—	+	+	+	0111
565	Cluster 3	—	—	—	+	0001
493	Cluster 4	—	—	++	++	0022
405	Cluster 5	+	—	+	—	1010
383	Cluster 6	+	—	—	+	1001
248	Cluster 7	+	—	+	++	1012
238	Cluster 8	—	—	+	++	0012
228	Cluster 9	—	+	+	—	0110
215	Cluster 10	—	—	+	+	0011
160	Cluster 11	+	—	—	—	1000
123	Cluster 12	—	—	+	—	0010
111	Cluster 13	+	+	+	—	1110
99	Cluster 14	+	—	—	—	1000
93	Cluster 15	+	—	—	—	1000

The second deficiency of the method is that the actual identification of the class is subjective. Shown above is the output of the analysis, here the fluorescent parameters are shown where a ranking scheme is used to define the parameters that distinguish the microspheres (Table 20). It can be seen that the identification of the microspheres

becomes subjective relying on the cluster plot and the user interpretation of the results shown below.

This point is outlined by Roderer *et al.* who state that frequency difference gating is meant to identify subsets in multidimensional space. Confident identification of multiple populations using this method was impossible. It is likely that this algorithm works best when a control population is provided. The paper describing this algorithm presented an example of HIV analysis where a test was provided with excellent results. In our case as mentioned above a control" set is not applicable. Therefore the Flojo clustering method, while having a distinct advantage (in that no training set is required) is not suitable for the identification of QDEMs from the datasets provided. It is expected that by increasing the number of unique microspheres that the performance of the algorithm would decrease.

In conclusion, each of the ten QDEM mixtures were analysed using this method, however results were poor. It was difficult to determine the identity of each cluster; moreover there was a large discrepancy between the numbers of events in each cluster when compared to the quantities inputted in each QDEM solution. As each QDEM solution was added to the test solution in equal concentration (except for QD1100) the results obtained highlight the deficiency of this method for classification of the QDEMs within the test solutions. Therefore the MPG results provided the benchmark for current QDEM identification techniques.

Appendix 2: Confusion Matrices.

SVM confusion Matrix

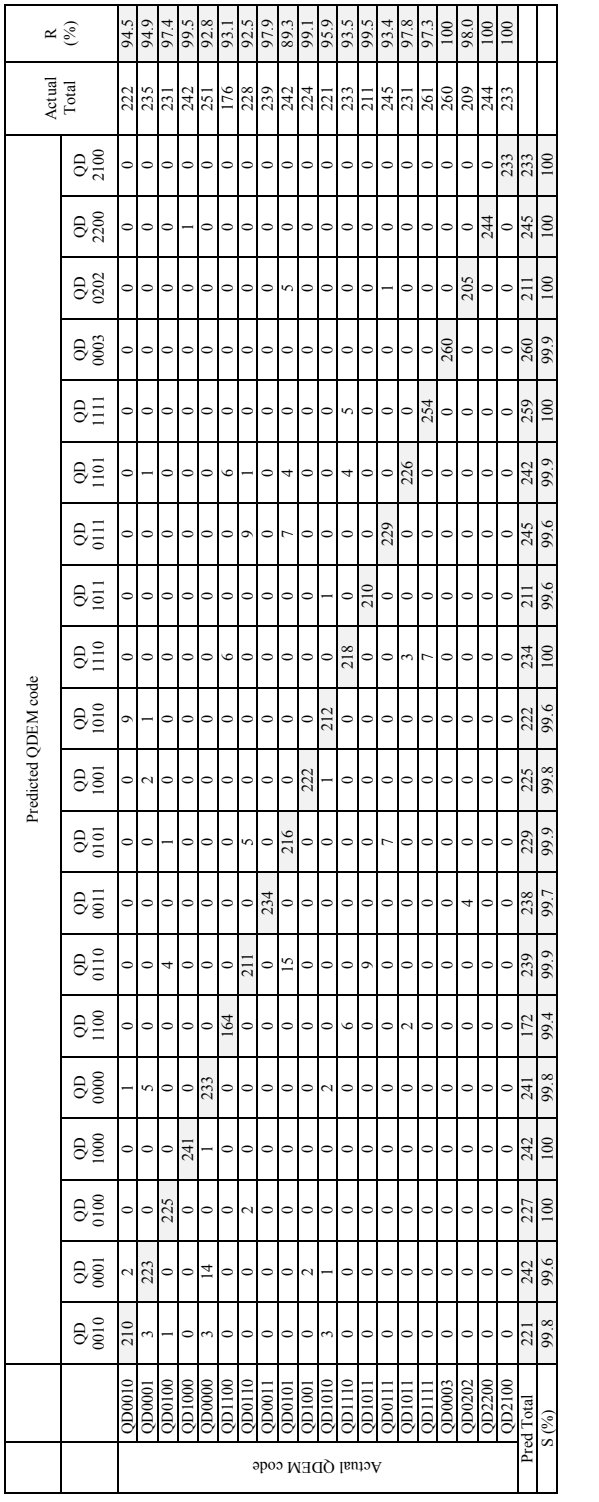

		Predicted QDEM code																			Actual Total	R (%)
		QD 0010	QD 0001	QD 0100	QD 1000	QD 0000	QD 1100	QD 0110	QD 0011	QD 0101	QD 1001	QD 1010	QD 1110	QD 1011	QD 0111	QD 1101	QD 1111	QD 0003	QD 0202	QD 2200	QD 2100	
Actual QDEM code	QD0010	210	2	0	0	1	0	0	0	0	0	9	0	0	0	0	0	0	0	0	0	222	94.5
	QD0001	3	223	0	0	5	0	0	0	0	2	1	0	0	0	1	0	0	0	0	0	235	94.9
	QD0100	1	0	225	0	0	0	4	0	1	0	0	0	0	0	0	0	0	0	0	0	231	97.4
	QD1000	0	0	0	241	0	0	0	0	0	0	0	0	0	0	0	0	0	0	1	0	242	99.5
	QD0000	3	14	0	1	233	0	0	0	0	0	0	0	0	0	0	0	0	0	0	0	251	92.8
	QD1100	0	0	0	0	0	164	0	0	0	0	0	6	0	0	6	0	0	0	0	0	176	93.1
	QD0110	0	0	2	0	0	0	211	0	5	0	0	0	0	9	1	0	0	0	0	0	228	92.5
	QD0011	0	0	0	0	0	0	0	234	0	0	0	0	0	0	0	0	0	0	0	0	239	97.9
	QD0101	0	0	0	0	0	0	15	0	216	0	0	0	0	7	4	0	0	5	0	0	242	89.3
	QD1001	0	2	0	0	0	0	0	0	0	222	0	0	0	0	0	0	0	0	0	0	224	99.1
	QD1010	3	1	0	0	2	0	0	0	0	1	212	0	1	0	0	0	0	0	0	0	221	95.9
	QD1110	0	0	0	0	0	6	0	0	0	0	0	218	0	0	4	5	0	0	0	0	233	93.5
	QD1011	0	0	0	0	0	0	9	0	0	0	0	0	210	0	0	0	0	0	0	0	211	99.5
	QD0111	0	0	0	0	0	0	0	0	7	0	0	0	0	229	0	0	0	1	0	0	245	93.4
	QD1011	0	0	0	0	0	2	0	0	0	0	0	3	0	0	226	0	0	0	0	0	231	97.8
	QD1111	0	0	0	0	0	0	0	0	0	0	0	7	0	0	0	254	0	0	0	0	261	97.3
	QD0003	0	0	0	0	0	0	0	0	0	0	0	0	0	0	0	0	260	0	0	0	260	100
	QD0202	0	0	0	0	0	0	0	4	0	0	0	0	0	0	0	0	0	205	0	0	209	98.0
	QD2200	0	0	0	0	0	0	0	0	0	0	0	0	0	0	0	0	0	0	244	0	244	100
	QD2100	0	0	0	0	0	0	0	0	0	0	0	0	0	0	0	0	0	0	0	233	233	100
Pred Total		221	242	227	242	241	172	239	238	229	225	222	234	211	245	242	259	260	211	245	233		
S (%)		99.8	99.6	100	100	99.8	99.4	99.9	99.7	99.9	99.8	99.6	100	99.6	99.6	99.9	100	99.9	100	100	100		

MLP confusion Matrix

		Predicted QDEM code																			Actual Total	R(%)
		QD 0010	QD 0001	QD 0100	QD 1000	QD 0000	QD 1100	QD 0110	QD 0011	QD 0101	QD 1001	QD 1010	QD 1110	QD 1011	QD 0111	QD 1101	QD 1111	QD 0003	QD 0202	QD 2200	QD 2100		
Actual QDEM code	QD0010	228	2	3	0	3	1	0	0	0	0	0	9	0	0	0	0	0	0	0	0	246	92.7
	QD0001	8	193	0	0	12	0	0	0	0	0	4	0	0	0	0	0	0	0	0	0	217	88.9
	QD0100	0	0	216	0	0	1	5	0	0	0	0	0	0	0	0	0	0	0	0	0	222	97.3
	QD1000	4	0	0	230	0	0	0	0	0	0	0	0	0	0	0	0	0	0	3	0	237	97.0
	QD0000	8	12	0	2	245	0	0	0	0	0	1	0	0	0	1	0	0	0	0	0	269	91.1
	QD1100	0	0	0	0	0	162	0	0	0	0	0	8	0	0	5	0	0	0	0	0	175	92.6
	QD0110	0	0	1	0	0	0	188	0	16	0	0	0	0	14	0	0	0	0	0	0	219	85.8
	QD0011	1	0	0	0	0	0	0	253	0	0	0	0	0	0	0	0	0	13	0	0	267	94.8
	QD0101	0	0	0	0	0	0	14	0	217	0	0	0	0	16	2	1	0	0	0	0	250	86.8
	QD1001	1	1	0	0	0	0	0	0	0	220	0	0	0	0	0	0	0	0	0	0	222	99.1
	QD1010	17	0	0	1	0	0	0	0	0	1	231	0	1	0	0	0	0	0	0	0	251	92.0
	QD1110	0	0	0	0	0	11	0	0	0	0	0	185	0	0	14	10	0	0	0	0	220	84.1
	QD1011	1	0	0	0	0	0	0	0	0	0	0	0	230	0	0	0	0	1	0	0	232	99.1
	QD0111	0	0	0	0	0	0	9	0	9	0	0	0	0	224	0	0	0	0	0	0	242	92.6
	QD1011	0	0	0	0	0	2	0	0	2	0	0	7	0	0	224	5	0	0	0	0	240	93.3
	QD1111	0	0	0	0	0	0	0	0	0	0	0	5	0	0	0	228	0	0	0	0	233	97.9
	QD0003	0	0	0	0	0	0	0	0	0	0	0	0	0	0	0	0	236	0	0	0	236	100.0
	QD0202	0	0	0	0	0	0	0	2	0	0	0	0	1	0	0	0	0	214	0	0	217	98.6
	QD2200	2	0	0	1	0	0	0	0	0	0	0	0	0	0	0	0	0	0	227	0	230	98.7
	QD2100	0	0	0	0	0	0	0	0	0	0	0	0	0	0	0	0	0	0	0	213	213	100.0
Pred Total		270	208	220	234	260	177	216	255	244	221	245	205	232	254	246	244	236	228	230	213		
S (%)		99.0	99.7	99.9	99.9	99.7	99.7	99.4	100.0	99.4	100.0	99.7	99.5	100.0	99.3	99.5	99.6	100.0	99.7	99.9	100.0		

PRBF confusion Matrix

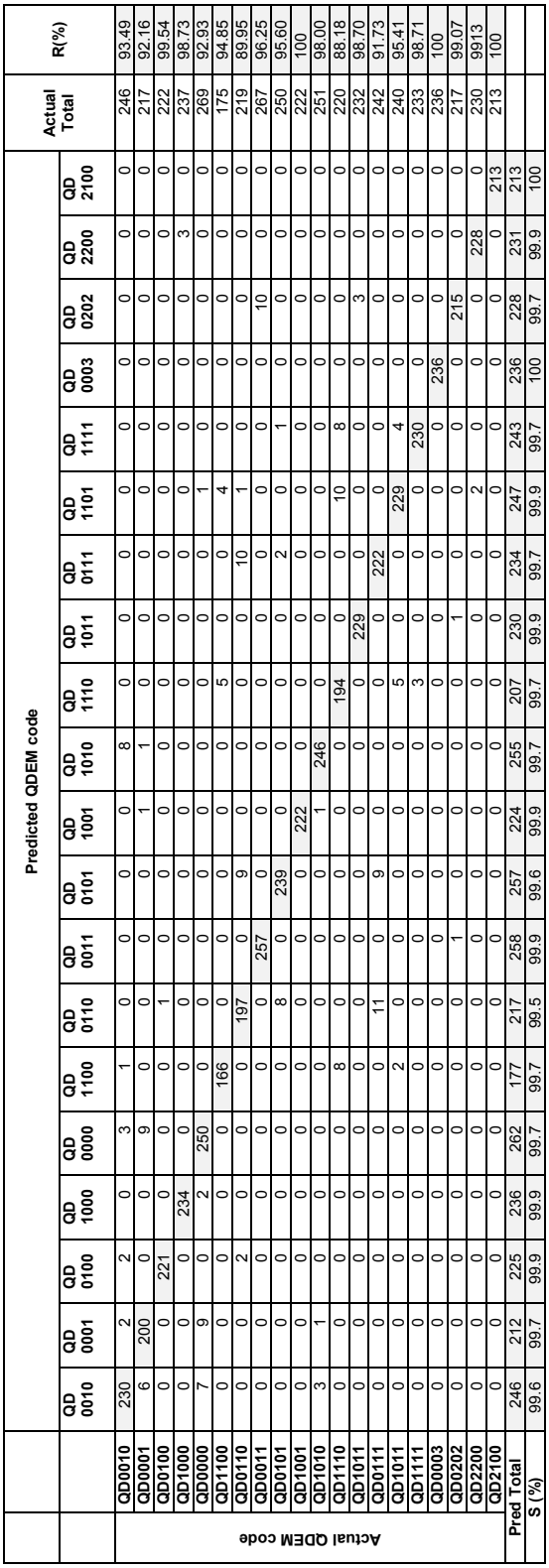

Actual QDEM code		Predicted QDEM code																	Actual Total	R(%)
		QD 0010	QD 0001	QD 0100	QD 1000	QD 0000	QD 1100	QD 0110	QD 0011	QD 0101	QD 1001	QD 1010	QD 1110	QD 1011	QD 0111	QD 1101	QD 1111	QD 0003	QD 0202	QD 2200	QD 2100		
	QD0010	230	2	2	0	3	1	0	0	0	0	8	0	0	0	0	0	0	0	0	0	246	93.49
	QD0001	6	200	0	0	9	0	0	0	0	1	1	0	0	0	0	0	0	0	0	0	217	92.16
	QD0100	0	0	221	0	0	0	1	0	0	0	0	0	0	0	0	0	0	0	0	0	222	99.54
	QD1000	0	0	0	234	0	0	0	0	0	0	0	0	0	0	0	0	0	0	3	0	237	98.73
	QD0000	7	9	0	2	250	0	0	0	0	0	0	0	0	0	1	0	0	0	0	0	269	92.93
	QD1100	0	0	0	0	0	166	0	0	0	0	0	5	0	0	4	0	0	0	0	0	175	94.85
	QD0110	0	0	2	0	0	0	197	0	9	0	0	0	0	10	1	0	0	0	0	0	219	89.95
	QD0011	0	0	0	0	0	0	0	257	0	0	0	0	0	2	0	1	0	10	0	0	267	96.25
	QD0101	0	0	0	0	0	0	8	0	239	0	0	0	0	0	0	0	0	0	0	0	250	95.60
	QD1001	0	0	0	0	0	0	0	0	0	222	0	0	0	0	0	0	0	0	0	0	222	100
	QD1010	3	1	0	0	0	0	0	0	0	1	246	0	0	0	0	0	0	0	0	0	251	98.00
	QD1110	0	0	0	0	0	8	0	0	0	0	0	194	0	0	10	8	0	0	0	0	220	88.18
	QD1011	0	0	0	0	0	0	0	0	0	0	0	0	229	0	0	0	0	3	0	0	232	98.70
	QD0111	0	0	0	0	0	0	11	0	9	0	0	0	0	222	0	0	0	0	0	0	242	91.73
	QD1011	0	0	0	0	0	2	0	0	0	0	0	5	0	0	229	4	0	0	0	0	240	95.41
	QD1111	0	0	0	0	0	0	0	0	0	0	0	3	0	0	0	230	0	0	0	0	233	98.71
	QD0003	0	0	0	0	0	0	0	0	0	0	0	0	0	0	0	0	236	0	0	0	236	100
	QD0202	0	0	0	0	0	0	0	1	0	0	0	0	1	0	0	0	0	215	0	0	217	99.07
	QD2200	0	0	0	0	0	0	0	0	0	0	0	0	0	0	2	0	0	0	228	0	230	9913
	QD2100	0	0	0	0	0	0	0	0	0	0	0	0	0	0	0	0	0	0	0	213	213	100
Pred Total		246	212	225	236	262	177	217	258	257	224	255	207	230	234	247	243	236	228	231	213		
S (%)		99.6	99.7	99.9	99.9	99.7	99.7	99.5	99.9	99.6	99.9	99.7	99.7	99.9	99.7	99.9	99.7	100	99.7	99.9	100		

Appendix 3: QDEM specifications

Product data sheet

MultiPlexBeads™

Authorized for research use only

Contents

The vial(s) contains carboxyl-functionalized, 5 μm acrylic beads encoded with fluorescent, composition-tuneable nanocyrstals. Blank beads are not encoded with nanocyrstals. There are approximately 1.46 x 10^7 beads per mg. The beads are shipped in deionised water with 0.01% sodium azides.

Instructions

The beads should be stored between 2 and 25 ºC in the dark. Beads may be centrifuged (1000 G, 5 minutes) to change solvent if desired. If beads aggregate, follow directions below to disperse. Binding ligands to surface carboxylic acids can be accomplished with EDC in TBS in a pH range of 6.5 - 8.0 by following our recommended Protein Binding Protocol.

Bead dispersion protocol

1) Vortex, 10 seconds
2) Shake vigorously by hand, 5 seconds
3) Sonicate, 20 seconds (vortex 50 seconds if sonicator not available)
4) Repeat three times

Material safety data sheet

Chemical Product

Acrylic beads that encapsulate semiconductor nanocyrstals, are stored in tris-buffered saline, and have -COOH groups or UltraAvidin (Leinco Technologies) on its surface.

Composition, Information on Ingredients

Name	CAS #	% by weight
Water	7732-18-5	97.0-98.5
Polystyrene	9003-70-7	0.5-2.0
Sodium Chloride	7647-14-5	0.8
Tris (Hydroxymethyl) Aminomethane Free Base	77-86-1	.11
Tris (Hydroxymethyl) Aminomethane Hydrochloride Salt	1185-53-1	.02
Potassium chloride	7447-40-7	.02
Divinyl benzene	1321-74-0	.01
Sodium Azide	26628-22-8	0.01
BSA	9048-46-8	0-1
Avidin	1405-69-2	0-0.01
CdSe	1306-24-7	<0.001

Section 3 - Hazards Identification
Appearance: Opaque liquid. CAUTION! The toxicological properties of this material have not been fully investigated. May cause eye and skin irritation. May cause respiratory and digestive tract irritation.

Target Organs: None known.

Potential Health Effects
Eye: May cause eye irritation. The toxicological properties of this material have not been fully investigated.
Skin: May cause skin irritation. The toxicological properties of this material have not been fully investigated.
Ingestion: May cause gastrointestinal irritation with nausea, vomiting and diarrhea. The toxicological properties of this substance have not been fully investigated.
Inhalation: May cause respiratory tract irritation. The toxicological properties of this substance have not been fully investigated.
Chronic: No information found.

Section 4 - First Aid Measures

Eyes: Flush eyes with plenty of water for at least 15 minutes, occasionally lifting The upper and lower eyelids. Get medical aid immediately.

Skin: Get medical aid. Flush skin with plenty of water for at least 15 minutes while removing contaminated clothing and shoes. Wash clothing before reuse.

Ingestion: If victim is conscious and alert, give 2-4 cupfuls of milk or water. Never give anything by mouth to an unconscious person. Get medical aid immediately.

Inhalation: Remove from exposure and move to fresh air immediately. If not breathing, give artificial respiration. If breathing is difficult, give oxygen. Get medical aid.

Physician: Treat symptomatically and supportively.

Section 5 - Firefighting Measures
Not a fire hazard.

Section 6 - Accidental Release Measures
Wear NIOSH approved chemical safety gloves, goggles, and rubber boots. Sweep up product and place in a sealed bag. Hold for disposal. Avoid generating dusty conditions. Provide ventilation.

Section 7 - Handling and Storage
Store in a dark, cool (2 - 25 ºC) place. Gentle sonication to disperse beads in solution is recommended prior to use. Beads may be centrifuged to change solvent if desired.

Section 8 - Engineering Controls & Personal Protective Equipment
Engineering Controls
Use adequate ventilation to keep airborne concentrations low.

Personal Protective Equipment
Eyes: Wear appropriate protective eyeglasses or chemical safety goggles as described by OSHA's eye and face protection regulations in 29 CFR 1910.133 or European Standard EN166.

Skin: Wear appropriate protective gloves to prevent skin exposure. Clothing: Wear appropriate protective clothing to prevent skin exposure.

Respirators: Follow the OSHA respirator regulations found in 29 CFR 1910.134 or European Standard EN 149. Use a NIOSH or European Standard EN 149 approved respirator when necessary.

Appendix 4: CD contents

- **FCM data – flow cytometry data used in the thesis**
  - *Training data* – for construction of classifiers.
  - *Mixture data* – for external validation.

- **FlowSVM**
  - *MATLAB code* – GUI m-files.
  - *Standalon*e – compiled version.

- **General m-files**
  - *classifierEval.m* – calculation of performance measures from confusion matrix.
  - *constructConfusion.m* – construction of confusion matrix from the results of independent testing
  - *medoutlierfilt.m* – outlier filtering using IQR.

- **MLP construction**
  - *nc_muliclass toolbox* – DTU ANN toolbox.
  - *mlpconstruction.m* – construct n-node MLP.
  - *mlpPrediciton.m* – determine unknown QDEMs.
  - *mlpXval.m* – MLP cross validation.

- **MPG construction**
  - *QDEM multiparameter gating.fey* – multiparameter gating set-up for FCSExpress.

- **PRBF construction**
  - *prbfconstruction.m* – script for the construction and evaluation of a PRBF.
  - *prbfXval.m* – function selection of the optimal smoothing factor for a PRBF.

- **SVM construction**
  - *svmconstruction.m* – script for the construction and evaluation of a SVM.
  - *svmlread.m*– read the LIBSVM sparse density format.
  - *svmlwrite.m* – write to LIBSVM sparse density format.
  - *svmpredict.exe* – LIBSVM executable for classification.
  - *svmtrain.exe* – LIBSVM executable for training.

- **Thesis**

Note: *In order to run the m-files on the CD the MATLAB path must be set to the CD to include subfolders. To run the FlowSVM program without either MATLAB or the MATLAB MCR must be installed on the machine.*